Active Site for Propene Metathesis in Silica-Supported Molybdenum Oxide Catalysts

vorgelegt von
Master of Engineering
Kazuhiko Amakawa
aus Yokohama, Japan

von der Fakultät II - Mathematik und Naturwissenschaften
der Technischen Universität Berlin
zur Erlangung des akademischen Grades
Doktor der Naturwissenschaften
- Dr. rer. nat. -
genehmigte Dissertation

Promotionsausschuss:

Vorsitzender: Prof. Dr. Peter Hildebrandt
Berichter/Gutachter: Prof. Dr. Robert Schlögl (FHI der MPG)
Berichter/Gutachter: Prof. Dr. Reinhard Schomäcker
Berichter/Gutachter: Prof. Dr. Christian Limberg (HU Berlin)

Tag der wissenschaftlichen Aussprache: 21.06.2013

Berlin, 2013
D83

Acknowledgement

First and foremost I would like to express my thanks and deep respect to Professor Dr. Robert Schlögl who has been hosting me at his Department of Inorganic Chemistry at the Fritz Haber Institute of the Max Planck Society. Your profound intellect and enormous knowledge has been enlightening and leading me to a deeper level of thinking.

I would also like to deeply thank my supervisor, Dr. Annette Trunschke, for her continuous support and multiple discussions. Her curiosity and pursuing mind as a native scientist has been always stimulating and driving me.

In the organization and defense of my thesis at the Technical University of Berlin, I thank Professor Dr. Reinhard Schomäcker for hosting me as an external student. I am very grateful to Professor Dr. Peter Hildebrandt and Professor Dr. Christian Limberg at Humboldt University of Berlin and for agreeing to be part of my examining committee.

A number of colleagues in the Department of Inorganic Chemistry contributed in performing experiments, calculations, technical assistance and discussions. I would like to acknowledge the following people (in no particular order): Jutta Kröhnert (IR), Dr. Sabine Wrabetz (microcalorimetry), Dr. Michael Hävecker (NEXAFS), Dr. Chunsheng Guo (theory), Dr. Lili Sun (theory), Professor Dr. Klaus Hermann (theory), Dr. Genka Tzolova-Müller (UV-vis), Maike Hashagen (experimental assistance), Dr. Frank Girgsdies (XRD), Gisela Weinberg (SEM-EDX), Dr. Tom Cotter (Raman and discussion), Pierre Schwach (Photoluminescence), Edith Kitzelmann (XRD, TG), Gisela Lorenz (N_2 physisorption), Achim Klein-Hoffmann (XRF), Dr. Neil G. Hamilton (IR), Dr. Andrey Tarasov (TG), Siegfried Engelschalt (catalytic setup), Dr. Raoul Naumann d'Alnoncourt (catalytic setup), Dr. Benjamin Frank (discussion), Dr. Oleksiy Khavryuchenko (discussion), Till Wolfram (discussion), Dr. Jörg Thielemann (discussion) and Dr. Yury V. Kol'enko (discussion). I also thank my officemates Dr. Detre Teschner, Ramzi Farra, Pia Kjær Nielsen and Dr. Tulio Rocha for the warm atmosphere and inspiring chat, and the members of "Reactivity group" for valuable discussions and encouraging. Dr. Axel Knop-Gericke is acknowledged for supervising me during the initial period of the research stay at the FHI. I thank Dr. Malte Behrens for his kind contact before joining the FHI, which enabled me to catch the great opportunity to stay here.

I thank Professor Dr. Israel E. Wachs at Lehigh University (USA) for the fruitful discussion and organizing the UV-Raman and Mo K-edge XAFS experiments. I thank Soe Lwin and Chieu Vuong T. Nguyen at Lehigh University for performing the UV-Raman experiments, and Professor Dr. Anatoly I. Frenkel and Dr. Anitha Patlolla at Yeshiva University (USA) for performing the Mo K-edge XAFS study. Felix Hemmann and Professor Dr. Christian Jäger at BAM Federal Institute for Materials Research and Testing are acknowledged for performing the ^{1}H-NMR study.

Mitsubishi Gas Chemical Co. Inc. is gratefully acknowledged for a fellowship and supporting my research activity at the FHI. Especially, I thank Dr. Jun Yoshihara from Mitsubishi Gas Chemical for his continuous support.

Finally I thank my dearest wife Sachiko, my son Dai, and my daughter Aika for their support, patience, unceasing encouragement and love.

Berlin, den 26.06.2013

Eidesstattliche Versicherung

Hiermit versichere ich, Kazuhiko Amakawa, dass die vorgelegte Dissertation von mir selbstständig angefertigt wurde und alle von mir genutzten Hilfsmittel und Hilfen angegeben wurden, insbesondere habe ich die wörtlich oder dem Sinne nach anderen Veröffentlichungen entnommenen Stelle kenntlich gemacht. Im Folgenden erfolgt auch eine Liste der verwendeten Originalquellen.

Die Arbeit ist in Zusammenarbeit mit anderen Wissenschaftler(inne)n (Dr. Annette Trunschke, Dr. Sabine Wrabetz, Jutta Kröhnert, Dr. Genka Tzolova-Müller, Dr. Benjamin Frank, Felix Hemmann, Prof. Christian Jäger, Dr. Lili Sun, Dr. Chunsheng Guo, Dr. Michael Hävecker, Prof. Israel E. Wachs, Soe Lwin, Prof. Anatoly I. Frenkel, Dr. Anitha Patlolla, Prof. Klaus Hermann und Prof. Robert Schlögl) entstanden, deren Namen in der Dissertation angegeben sind. Inhalte der Dissertation wurden und werden nicht in gleicher oder abgewandelter Form für anderweitige Promotionen genutzt.

(1) Dumesic, J. A.; Huber, G. W.; Boudart, M. In *Handbook of Heterogeneous Catalysis 2nd ed.*; Wiley-VCH: Weinheim, 2008; pp. 1–15.
(2) Chauvin, Y. *Angew. Chem. Int. Ed.* **2006**, *45*, 3740–3747.
(3) Handzlik, J.; Ogonowski, J. *Catal. Lett.* **2003**, *88*, 119–122.
(4) Ding, J.; Hua, W. *Chem. Eng. Technol.* **2013**, *36*, 83–90.
(5) Mol, J. C.; Leeuwen, P. W. N. M. *Metathesis of Alkens in “Handbook of Heterogeneous Catalysis”*; 2nd ed.; Wiley-VCH,: Weinheim, 2008.
(6) Schrock, R. R. *Acc. Chem. Res.* **1986**, *19*, 342–348.
(7) Schrock, R. R. *Angew. Chem. Int. Ed.* **2006**, *45*, 3748–3759.
(8) Schrock, R. R.; Hoveyda, A. H. *Angew. Chem. Int. Ed.* **2003**, *42*, 4592–4633.
(9) Feher, F. J.; Tajima, T. L. *J. Am. Chem. Soc.* **1994**, *116*, 2145–2146.
(10) Blanc, F.; Rendon, N.; Berthoud, R.; Basset, J.-M.; Coperet, C.; Tonzetich, Z. J.; Schrock, R. R. *Dalton Trans.* **2008**, 3156–3158.
(11) Blanc, F.; Thivolle-Cazat, J.; Basset, J.-M.; Copéret, C.; Hock, A. S.; Tonzetich, Z. J.; Schrock, R. R. *J. Am. Chem. Soc.* **2007**, *129*, 1044–1045.
(12) Vikulov, K. A.; Shelimov, B. N.; Kazansky, V. B. *J. Mol. Catal.* **1991**, *65*, 393–402.
(13) Iwasawa, Y.; Ichinose, H.; Ogasawara, S.; Soma, M. *J. Chem. Soc., Faraday Trans. 1* **1981**, *77*, 1763–1777.
(14) Anpo, M.; Kondo, M.; Kubokawa, Y.; Louis, C.; Che, M. *J. Chem. Soc., Faraday Trans. 1:* **1988**, *84*, 2771–2782.
(15) Rappe, A. K.; Goddard, W. A. *J. Am. Chem. Soc.* **1982**, *104*, 448–456.
(16) Wengrovius, J. H.; Schrock, R. R.; Churchill, M. R.; Missert, J. R.; Youngs, W. J. *J. Am. Chem. Soc.* **1980**, *102*, 4515–4516.
(17) Kress, J. R. M.; Russell, M. J. M.; Wesolek, M. G.; Osborn, J. A. *J. Chem. Soc., Chem. Commun.* **1980**, 431–432.
(18) Mazoyer, E.; Merle, N.; Mallmann, A. de; Basset, J.-M.; Berrier, E.; Delevoye, L.; Paul, J.-F.; Nicholas, C. P.; Gauvin, R. M.; Taoufik, M. *Chem. Commun.* **2010**, *46*, 8944–8946.
(19) Solans-Monfort, X.; Copéret, C.; Eisenstein, O. *Organometallics* **2012**, *31*, 6812–6822.
(20) Mol, J. *J. Mol. Catal. A: Chem.* **2004**, *213*, 39–45.
(21) Debecker, D. P.; Stoyanova, M.; Colbeau-Justin, F.; Rodemerck, U.; Boissière, C.; Gaigneaux, E. M.; Sanchez, C. *Angew. Chem. Int. Ed.* **2012**, *51*, 2129–2131.
(22) Debecker, D. P.; Bouchmella, K.; Stoyanova, M.; Rodemerck, U.; Gaigneaux, E. M.; Mutin, P. H. *Catal. Sci. Technol.* **2011**.
(23) Debecker, D. P.; Schimmoeller, B.; Stoyanova, M.; Poleunis, C.; Bertrand, P.; Rodemerck, U.; Gaigneaux, E. M. *J. Catal.* **2011**, *277*, 154–163.
(24) Debecker, D. P.; Stoyanova, M.; Rodemerck, U.; Gaigneaux, E. M. *J. Mol. Catal. A: Chem.* **2011**, *340*, 65–76.
(25) Debecker, D.; Bouchmella, K.; Poleunis, C.; Eloy, P.; Bertrand, P.; Gaigneaux, E.; Mutin, P. *Chem. Mater.* **2009**, *21*, 2817–2824.

(26) Boer, M.; Dillen, A. J.; Koningsberger, D. C.; Geus, J. W.; Vuurman, M. A.; Wachs, I. E. *Catal. Lett.* **1991**, *11*, 227–239.
(27) Howman, E. J.; Mgcrath, B. P.; Williams, K. V. Catalyst regeneration process. British Patent 1,144,085, March 5, **1969**.
(28) Salameh, A.; Copéret, C.; Basset, J.-M.; Böhm, V. P. W.; Röper, M. *Adv. Synth. Catal.* **2007**, *349*, 238–242.
(29) Chauvin, Y.; Commereuc, D. *J. Chem. Soc., Chem. Commun.* **1992**, 462–464.
(30) Iwasawa, Y.; Hamamura, H. *J. Chem. Soc., Chem. Commun.* **1983**, 130–132.
(31) Iwasawa, Y.; Kubo, H.; Hamamura, H. *J. Mol. Catal.* **1985**, *28*, 191–208.
(32) McCoy, J. R.; Farona, M. F. *J. Mol. Catal.* **1991**, *66*, 51–58.
(33) Farona, M. F.; Tucker, R. L. *J. Mol. Catal.* **1980**, *8*, 85–90.
(34) Grubbs, R. H.; Swetnick, S. J. *J. Mol. Catal.* **1980**, *8*, 25–36.
(35) Laverty, D. T.; Rooney, J. J.; Stewart, A. *J. Catal.* **1976**, *45*, 110–113.
(36) Grünert, W.; Stakheev, A. Y.; Feldhaus, R.; Anders, K.; Shpiro, E. S.; Minachev, K. M. *J. Catal.* **1992**, *135*, 287–299.
(37) Chen, X.; Zhang, X.; Chen, P. *Angew. Chem. Int. Ed.* **2003**, *42*, 3798–3801.
(38) Basrur, A. G.; Patwardhan, S. R.; Was, S. N. *J. Catal.* **1991**, *127*, 86–95.
(39) ECHIGOYA, E.; NAKAMURA, R. *NIPPON KAGAKU KAISHI* **1972**, 500–&.
(40) Engelhardt, J. *Journal of Molecular Catalysis* **1980**, *8*, 119–125.
(41) Shelimov, B. N.; Elev, L. V.; Kazansky, V. B. *Journal of Catalysis* **1986**, *98*, 70–81.
(42) MOL, J. *CATALYSIS LETTERS* **1994**, *23*, 113–118.
(43) Vikulov, K. A.; Shelimov, B. N.; Kazansky, V. B. *J. Mol. Catal.* **1992**, *72*, 1–11.
(44) Vikulov, K. A.; Elev, I. V.; Shelimov, B. N.; Kazansky, V. B. *J. Mol. Catal.* **1989**, *55*, 126–145.
(45) Shelimov, B. N.; Elev, I. V.; Kazansky, V. B. *J. Mol. Catal.* **1988**, *46*, 187–200.
(46) Vikulov, K. A.; Shelimov, B. N.; Kazansky, V. B.; Mol, J. C. *J. Mol. Catal.* **1994**, *90*, 61–67.
(47) Anpo, M.; Tanahashi, I.; Kubokawa, Y. *J. Chem. Soc., Faraday Trans. 1:* **1982**, *78*, 2121–2128.
(48) Anpo, M.; Kondo, M.; Louis, C.; Che, M.; Coluccia, S. *J. Am. Chem. Soc.* **1989**, *111*, 8791–8799.
(49) Anpo, M.; Che, M. *Adv. Catal.* **1999**, *44*, 119–257.
(50) Iwasawa, Y. Academic Press, 1987; Vol. Volume 35, pp. 187–264.
(51) Guan, J.; Yang, G.; Zhou, D.; Zhang, W.; Liu, X.; Han, X.; Bao, X. *Catal. Commun.* **2008**, *9*, 2213–2216.
(52) Guan, J.; Yang, G.; Zhou, D.; Zhang, W.; Liu, X.; Han, X.; Bao, X. *J. Mol. Catal. A: Chem.* **2009**, *300*, 41–47.
(53) Li, X.; Zheng, A.; Guan, J.; Han, X.; Zhang, W.; Bao, X. *Catal. Lett.* **2010**, *138*, 116–123.
(54) Pérez-Ramírez, J.; Mondelli, C.; Schmidt, T.; Schlüter, O. F.-K.; Wolf, A.; Mleczko, L.; Dreier, T. *Energy Environ. Sci.* **2011**, *4*, 4786.
(55) McDaniel, M. P. In *Handbook of Heterogeneous Catalysis*; Wiley-VCH Verlag GmbH & Co. KGaA, 2008.
(56) Busca, G.; Lietti, L.; Ramis, G.; Berti, F. *Appl. Catal., B* **1998**, *18*, 1–36.
(57) Centi, G. *Appl. Catal., A* **1996**, *147*, 267–298.
(58) Gregoriades, L. J.; Dőbler, J.; Sauer, J. *J. Phys. Chem. C* **2010**, *114*, 2967–2979.
(59) Banares, M. A.; Hu, H. C.; Wachs, I. E. *J. Catal.* **1994**, *150*, 407–420.
(60) Oyama, S. T.; Zhang, W. *J. Am. Chem. Soc.* **1996**, *118*, 7173–7177.
(61) Shokhireva, T. K.; Yurieva, T. M.; Chumachenko, N. N. *React. Kinet. Catal. Lett.* **1980**, *14*, 77–80.
(62) Liu, T.-C.; Forissier, M.; Coudurier, G.; Védrine, J. C. *J. Chem. Soc., Faraday Trans. 1* **1989**, *85*, 1607–1618.
(63) Ohler, N.; Bell, A. *J. Catal* **2005**, *231*, 115–130.
(64) Lou, Y.; Wang, H.; Zhang, Q.; Wang, Y. *J. Catal.* **2007**, *247*, 245–255.
(65) Handzlik, J.; Ogonowski, J.; Stoch, J.; Mikolajczyk, M.; Michorczyk, P. *Appl. Catal., A* **2006**, *312*, 213–219.
(66) Amakawa, K.; Wrabetz, S.; Kröhnert, J.; Tzolova-Müller, G.; Schlögl, R.; Trunschke, A. *J. Am. Chem. Soc.* **2012**, *134*, 11462–11473.

(67) Marceau, E.; Carrier, X.; Che, M.; Clause, O.; Marcilly, C. In *Handbook of Heterogeneous Catalysis*; Wiley-VCH Verlag GmbH & Co. KGaA, 2008.

(68) Thielemann, J. P.; Weinberg, G.; Hess, C. *ChemCatChem* **2011**, *3*, 1814–1821.

(69) Roark, R. D.; Kohler, S. D.; Ekerdt, J. G. *Catal. Lett.* **1992**, *16*, 71–76.

(70) Ward, M. B.; Lin, M. J.; Lunsford, J. H. *J. Catal.* **1977**, *50*, 306–318.

(71) Jeziorowski, H.; Knoezinger, H.; Grange, P.; Gajardo, P. *J. Phys. Chem.* **1980**, *84*, 1825–1829.

(72) Ohler, N.; Bell, A. *J. Phys. Chem. B* **2005**, *109*, 23419–23429.

(73) Thielemann, J. P.; Ressler, T.; Walter, A.; Tzolova-Müller, G.; Hess, C. *Appl. Catal., A* **2011**, *399*, 28–34.

(74) Lee, E. L.; Wachs, I. E. *J. Phys. Chem. C* **2007**, *111*, 14410–14425.

(75) Higashimoto, S.; Hu, Y.; Tsumura, R.; Iino, K.; Matsuoka, M.; Yamashita, H.; Shul, Y. G.; Che, M.; Anpo, M. *J. Catal.* **2005**, *235*, 272–278.

(76) Matsuoka, M.; Kamegawa, T.; Takeuchi, R.; Anpo, M. *Catal. Today* **2007**, *122*, 39–45.

(77) Iizuka, Y.; Sanada, M.; Tsunetoshi, J.; Furukawa, J.; Kumao, A.; Arai, S.; Tomishige, K.; Iwasawa, Y. *J. Chem. Soc., Faraday Trans.* **1996**, *92*, 1249–1256.

(78) Radhakrishnan, R.; Reed, C.; Oyama, S. T.; Seman, M.; Kondo, J. N.; Domen, K.; Ohminami, Y.; Asakura, K. *J. Phys. Chem. B* **2001**, *105*, 8519–8530.

(79) Takenaka, S.; Tanaka, T.; Funabiki, T.; Yoshida, S. *J. Phys. Chem. B* **1998**, *102*, 2960–2969.

(80) Iwasawa, Y.; Ogasawara, S. *J. Chem. Soc., Faraday Trans. 1* **1979**, *75*, 1465–1476.

(81) Chempath, S.; Zhang, Y.; Bell, A. T. *J. Phys. Chem. C* **2007**, *111*, 1291–1298.

(82) Lee, E. L.; Wachs, I. E. *J. Phys. Chem. C* **2008**, *112*, 6487–6498.

(83) Guo, C. S.; Hermann, K.; Hävecker, M.; Thielemann, J. P.; Kube, P.; Gregoriades, L. J.; Trunschke, A.; Sauer, J.; Schlögl, R. *J. Phys. Chem. C* **2011**, *115*, 15449–15458.

(84) Cornac, M.; Janin, A.; Lavalley, J. C. *Polyhedron* **1986**, *5*, 183–186.

(85) Thielemann, J. P.; Kröhnert, J.; Hess, C. *J. Phys. Chem. C* **2010**, *114*, 17092–17098.

(86) Ressler, T.; Walter, A.; Huang, Z.-D.; Bensch, W. *J. Catal.* **2008**, *254*, 170–179.

(87) Handzlik, J. *Chem. Phys. Lett.* **2009**, *469*, 140–144.

(88) Handzlik, J.; Ogonowski, J. *J. Phys. Chem. C* **2012**, *116*, 5571–5584.

(89) Fievez, T.; Geerlings, P.; Weckhuysen, B. M.; De Proft, F. *ChemPhysChem* **2011**, *12*, 3281–3290.

(90) Balcar, H.; Mishra, D.; Marceau, E.; Carrier, X.; Zilková, N.; Bastl, Z. *Appl. Catal., A* **2009**, *359*, 129–135.

(91) Amakawa, K.et at., submitted.

(92) Somorjai, G. A.; Li, Y. *Introduction to Surface Chemistry and Catalysis*; 2nd ed.; John Wiley & Sons: Hoboken, New Jersey, 2010.

(93) Libuda, J.; Freund, H.-J. *Surf. Sci. Rep.* **2005**, *57*, 157–298.

(94) Rupprechter, G.; Weilach, C. *J. Phys.: Condens. Matter* **2008**, *20*, 184019.

(95) Zhao, D.; Feng, J.; Huo, Q.; Melosh, N.; Fredrickson, G. H.; Chmelka, B. F.; Stucky, G. D. *Science* **1998**, *279*, 548 –552.

(96) Tian, H.; Roberts, C. A.; Wachs, I. E. *J. Phys. Chem. C* **2010**, *114*, 14110–14120.

(97) Hu, H.; Wachs, I. E.; Bare, S. R. *J. Phys. Chem.* **1995**, *99*, 10897–10910.

(98) Vuurman, M. A.; Wachs, I. E. *J. Mol. Catal.* **1992**, *77*, 29–39.

(99) Dieterle, M.; Weinberg, G.; Mestl, G. *Phys. Chem. Chem. Phys.* **2002**, *4*, 812–821.

(100) Davydov, A. *Molecular spectroscopy of oxide catalyst surface*; John Wiley & Sons Ltd.: Chichester, 2003.

(101) Zhang, B.; Li, Y.; Lin, Q.; Jin, D. *J. Mol. Catal.* **1988**, *46*, 229–241.

(102) Langmuir, I. *J. Am. Chem. Soc.* **1916**, *38*, 2221–2295.

(103) Grabowski, R.; Efremov, A.; Davydov, A.; Haber, E. *Kinet. Catal.* **1981**, *22*, 794–797.

(104) Efremov, A.; Lokhov, Y.; Davydov, A. *Kinet. Catal.* **1981**, *22*, 969–975.

(105) Martín, C.; Rives, V.; Sánchez-Escribano, V.; Busca, G.; Lorenzelli, V.; Ramis, G. *Surf. Sci.* **1991**, *251-252*, 825–830.

(106) Finocchio, E.; Busca, G.; Lorenzelli, V.; Willey, R. J. *J. Chem. Soc., Faraday Trans.* **1994**, *90*, 3347.

(107) Goncharova, O.; Davydov, A. *React. Kinet. Catal. Lett.* **1983**, *23*, 285–289.

(108) Davydov, A.; Efremov, A. *Kinet. Catal.* **1983**, *24*, 1214–1220.

(109) Efremov, A.; Davydov, A. *React. Kinet. Catal. Lett.* **1981**, *18*, 363–366.

(110) Goncharova, O.; Davydov, A.; Yureva, T. *Kinet. Catal.* **1984**, *25*, 124–129.

(111) Sanchez Escribano, V.; Busca, G.; Lorenzelli, V. *J. Chem. Phys.* **1991**, *95*, 5541–5545.

(112) Efremov, A. A.; Davydov, A. A. *React. Kinet. Catal. Lett.* **1981**, *18*, 353–356.

(113) Rendón, N.; Berthoud, R.; Blanc, F.; Gajan, D.; Maishal, T.; Basset, J.-M.; Copéret, C.; Lesage, A.; Emsley, L.; Marinescu, S. C.; Singh, R.; Schrock, R. R. *Chem.—Eur. J.* **2009**, *15*, 5083–5089.

(114) Handzlik, J. *J. Phys. Chem. B* **2005**, *109*, 20794–20804.

(115) Handzlik, J. *J. Catal.* **2003**, *220*, 23–34.

(116) Handzlik, J. *Surf. Sci.* **2007**, *601*, 2054–2065.

(117) Handzlik, J.; Ogonowski, J.; Tokarz-Sobieraj, R. *Catal. Today* **2005**, *101*, 163–173.

(118) Handzlik, J. *Surf. Sci.* **2004**, *562*, 101–112.

(119) Handzlik, J.; Sautet, P. *J. Catal.* **2008**, *256*, 1–14.

(120) Li, X.; Guan, J.; Zheng, A.; Zhou, D.; Han, X.; Zhang, W.; Bao, X. *J. Mol. Catal. A: Chem.* **2010**, *330*, 99–106.

(121) Campbell, K. A.; Janik, M. J.; Davis, R. J.; Neurock, M. *Langmuir* **2005**, *21*, 4738–4745.

(122) Kazansky, V. B. *Catal. Today* **1999**, *51*, 419–434.

(123) Engelhardt, J.; Hall, W. K. *J. Catal.* **1995**, *151*, 1–9.

(124) Moro-oka, Y. *Appl. Catal., A* **1999**, *181*, 323–329.

(125) Elev, I.; Shelimov, B.; Kazansky, V. *Kinet. Catal.* **1989**, *30*, 787–792.

(126) Aritani, H.; Fukuda, O.; Yamamoto, T.; Tanaka, T.; Imamura, S. *Chem. Lett.* **2000**, 66–67.

(127) Debecker, D. P.; Hauwaert, D.; Stoyanova, M.; Barkschat, A.; Rodemerck, U.; Gaigneaux, E. M. *Appl. Catal., A* **2011**, *391*, 78–85.

(128) Thomas, R.; Moulijn, J. A. *J. Mol. Catal.* **1982**, *15*, 157–172.

(129) Dinger, M. B.; Mol, J. C. *Organometallics* **2003**, *22*, 1089–1095.

(130) Crocellà, V.; Cerrato, G.; Magnacca, G.; Morterra, C. *J. Phys. Chem. C* **2009**, *113*, 16517–16529.

(131) Handzlik, J. *J. Phys. Chem. C* **2007**, *111*, 9337–9348.

(132) Taylor, H. S. *Proc. R. Soc. Lond. A* **1925**, *108*, 105–111.

(133) Zambelli, T.; Wintterlin, J.; Trost, J.; Ertl, G. *Science* **1996**, *273*, 1688–1690.

(134) Behrens, M.; Studt, F.; Kasatkin, I.; Kühl, S.; Hävecker, M.; Abild-Pedersen, F.; Zander, S.; Girgsdies, F.; Kurr, P.; Kniep, B.-L.; Tovar, M.; Fischer, R. W.; Nørskov, J. K.; Schlögl, R. *Science* **2012**, *336*, 893–897.

(135) Green, I. X.; Tang, W.; Neurock, M.; Yates, J. T. *Science* **2011**, *333*, 736–739.

(136) Chen, K.; Bell, A. T.; Iglesia, E. *J. Catal.* **2002**, *209*, 35–42.

(137) Wachs, I. E. *Catal. Today* **2005**, *100*, 79–94.

(138) Weber, R. S. *J. Catal.* **1995**, *151*, 470–474.

(139) Lichtenstein, L.; Büchner, C.; Yang, B.; Shaikhutdinov, S.; Heyde, M.; Sierka, M.; Włodarczyk, R.; Sauer, J.; Freund, H.-J. *Angew. Chem. Int. Ed.* **2012**, *51*, 404–407.

(140) Bordiga, S.; Bertarione, S.; Damin, A.; Prestipino, C.; Spoto, G.; Lamberti, C.; Zecchina, A. *J. Mol. Catal. A: Chem.* **2003**, *204–205*, 527–534.

(141) Tielens, F.; Gervais, C.; Lambert, J. F.; Mauri, F.; Costa, D. *Chem. Mater.* **2008**, *20*, 3336–3344.

(142) Braun, S.; Appel, L. G.; Camorim, V. L.; Schmal, M. *J. Phys. Chem. B* **2000**, *104*, 6584–6590.

(143) Bronsted, J. N. *Chem. Rev.* **1928**, *5*, 231–338.

(144) Evans, M. G.; Polanyi, M. *Trans. Faraday Soc.* **1938**, *34*, 11–24.

(145) Vojvodic, A.; Calle-Vallejo, F.; Guo, W.; Wang, S.; Toftelund, A.; Studt, F.; Martínez, J. I.; Shen, J.; Man, I. C.; Rossmeisl, J.; Bligaard, T.; Nørskov, J. K.; Abild-Pedersen, F. *J. Chem. Phys.* **2011**, *134*, 244509–244509–8.

(146) Weckhuysen, B. M.; Wachs, I. E.; Schoonheydt, R. A. *Chem. Rev.* **1996**, *96*, 3327–3350.

(147) McDaniel, M. P.; Welch, M. B. *J. Catal.* **1983**, *82*, 98–109.

(148) Groppo, E.; Lamberti, C.; Bordiga, S.; Spoto, G.; Zecchina, A. *Chem. Rev.* **2005**, *105*, 115–184.

(149) Demmelmaier, C. A.; White, R. E.; Van Bokhoven, J. A.; Scott, S. L. *J. Catal.* **2009**, *262*, 44–56.

(150) Tsilomelekis, G.; Boghosian, S. *Catal. Sci. Technol.* **2013**.

(151) Ek, S.; Root, A.; Peussa, M.; Niinistö, L. *Thermochim. Acta* **2001**, *379*, 201–212.

(152) Ravel, B.; Newville, M. *J. Synchrotron Rad.* **2005**, *12*, 537–541.

(153) Knop-Gericke, A.; Kleimenov, E.; Hävecker, M.; Blume, R.; Teschner, D.; Zafeiratos, S.; Schlögl, R.; Bukhtiyarov, V. I.; Kaichev, V. V.; Prosvirin, I. P.; Nizovskii, A. I.; Bluhm, H.; Barinov, A.; Dudin, P.; Kiskinova, M. *Adv. Catal.* **2009**, *52*, 213–272.
(154) Hävecker, M.; Cavalleri, M.; Herbert, R.; Follath, R.; Knop-Gericke, A.; Hess, C.; Hermann, K.; Schlögl, R. *Phys. Status Solidi B* **2009**, *246*, 1459–1469.
(155) Hermann, K.; Pettersson, L. G. M.; deMon developers group *StoBe software V. 3.6, 2011; see http://www.fhi-berlin.mpg.de/KHsoftware/ StoBe/.*
(156) Geudtner, G.; Calaminici, P.; Carmona-Espíndola, J.; Del Campo, J. M.; Domínguez-Soria, V. D.; Moreno, R. F.; Gamboa, G. U.; Goursot, A.; Köster, A. M.; Reveles, J. U.; Mineva, T.; Vásquez-Pérez, J. M.; Vela, A.; Zúñinga-Gutierrez, B.; Salahub, D. R. *WIREs. Comput. Mol. Sci.* **2012**, *2*, 548–555.
(157) Mestl, G.; Srinivasan, T. K. K. *Catal. Rev. Sci. Technol.* **1998**, *40*, 451.
(158) Baltrus, J. P.; Makovsky, L. E.; Stencel, J. M.; Hercules, D. M. *Anal. Chem.* **1985**, *57*, 2500–2503.
(159) Kakuta, N.; Tohji, K.; Udagawa, Y. *J. Phys. Chem.* **1988**, *92*, 2583–2587.
(160) Yamamoto, T. *X-Ray Spectrom.* **2008**, *37*, 572–584.
(161) Galeener, F. L.; Mikkelsen, J. C. *Phys. Rev. B* **1981**, *23*, 5527–5530.
(162) Jarupatrakorn, J.; Coles, M. P.; Tilley, T. D. *Chem. Mater.* **2005**, *17*, 1818–1828.
(163) Xiong, G.; Li, C.; Feng, Z.; Ying, P.; Xin, Q.; Liu, J. *J. Catal.* **1999**, *186*, 234–237.
(164) Zhu, X.; Li, X.; Xie, S.; Liu, S.; Xu, G.; Xin, W.; Huang, S.; Xu, L. *Catal Surv Asia* **2009**, *13*, 1–8.
(165) Trébosc, J.; Wiench, J. W.; Huh, S.; Lin, V. S.-Y.; Pruski, M. *J. Am. Chem. Soc.* **2005**, *127*, 3057–3068.
(166) Herrera, J. E.; Kwak, J. H.; Hu, J. Z.; Wang, Y.; Peden, C. H. F. *Top. Catal.* **2006**, *39*, 245–255.
(167) Leydier, F.; Chizallet, C.; Chaumonnot, A.; Digne, M.; Soyer, E.; Quoineaud, A.-A.; Costa, D.; Raybaud, P. *J. Catal.* **2011**, *284*, 215–229.
(168) Seman, M.; Kondo, J. N.; Domen, K.; Oyama, S. T. *Chem. Lett.* **2002**, *31*, 1082–1083.
(169) Cao, X.; Cheng, R.; Liu, Z.; Wang, L.; Dong, Q.; He, X.; Liu, B. *J. Mol. Catal. A: Chem.* **2010**, *321*, 50–60.
(170) Matyshak, V. A.; Krylov, O. V. *Kinet. Catal.* **2002**, *43*, 391–407.

Kazuhiko Amakawa

Abstract

This work quantitatively investigates the active sites for propene metathesis over molybdenum oxides supported on the surface of mesoporous silica SBA-15 (MoO_x/SBA-15).

The origin of the active sites for propene metathesis in MoO_x/SBA-15 catalysts was addressed. To monitor catalyst formation, propene adsorption was quantitatively studied by IR and microcalorimetry, while the number of active sites in propene metathesis was measured by a post-reaction titrative metathesis technique using isotope labeling. It was found that at most about 1 % of all Mo atoms represent the metathesis active sites. The active Mo(VI)-alkylidene moieties are generated *in situ* by surface reactions between molybdenum oxide precursor species and the reactant propene itself. It was proposed that the active site formation involves sequential steps requiring multiple functions: protonation of propene to surface Mo(VI)-isopropoxide species driven by surface Brønsted acid sites, subsequent oxidation of isopropoxide to acetone in the adsorbed state owing to the red-ox capability of molybdenum leaving naked Mo(IV) sites after desorption of acetone, and oxidative addition of another propene molecule yielding finally the active Mo(VI)-alkylidene species. The multiple requirements for successful catalyst precursors explain why only minor fraction of Mo atoms can transform into active carbene sites.

The metathesis activity as well as the density of active sites shows a strong dependence to the Mo loading, where an intermediate Mo loading characterized by a co-presence of strained surface molybdena species and a certain density of silanol groups gives a high activity. The structural characterization by IR, Raman, UV—vis, O K-edge NEXAFS, Mo K-edge EXAFS/XANES, H_2-TPR and DFT calculations indicates the formation of two-fold anchored tetrahedral di-oxo $(Si—O—)_2Mo({=}O)_2$ species at the expense of surface silanol groups, where the anchoring Mo—O—Si bonds of the di-oxo $(Si—O—)_2Mo({=}O)_2$ structures become frustrated thus reactive at high Mo density. It is suggested that a reaction at the strained Mo—O—Si bond is involved in the formation of carbene sites, explaining why a certain level of Mo loading is necessary to obtain a high activity in the catalysis. The acidity characterization by ammonia adsorption, IR and ^1H-NMR suggests that the surface silanol groups in the vicinity of surface molybdena serve as Brønsted acid site that provide the protonation function. Taking into account the required trapping function of the by-product acetone by another silanol group, it is proposed that the precursors of the metathesis active sites feature a $(Si—O—)_2Mo({=}O)_2$ structure exhibiting high strain at Mo—O—Si bonds surrounded by at least two adjacent silanol sites that equip the Brønsted acidity and the trapping function for by-product acetone.

Applying the gained insights into the formation mechanism of the carbene sites, we developed simple pretreatment procedures that can assist the carbene site formation and enhance the metathesis activity, which demonstrates the merit of knowledge-based rational approaches and corroborates the proposed mechanism here.

Zusammenfassung

Diese Arbeit untersucht quantitativ die aktiven Zentren in der Metathese von Propen an Molybdänoxiden auf der Oberfläche von mesoporösem Siliciumdioxid-SBA-15 (MoO_x/SBA-15) als Träger.

Es wurde die Entstehung der Aktivzentren für die Propenmetathese an MoO_x/SBA-15 Katalysatoren untersucht. Dazu wurde die Adsorption von Propen mittels IR-Spektroskopie und Mikrokalorimetrie quantitativ studiert. Die Zahl der aktiven Zentren in der Propenmetathese wurde titrimetrisch durch Post-Metathesereaktion unter Verwendung isotopenmarkierter Edukte bestimmt. Es wurde gefunden, dass höchstens etwa 1% aller Molybdänatome katalytisch aktiv sind. Die aktiven Mo(VI)-Alkylidenzentren entstehen in-situ durch die Oberflächenreaktionen zwischen den Molybdänoxid-Vorstufen und dem Edukt Propen selbst. Es wurde ein konsekutiver Bildungsmechanismus vorgeschlagen, der verschiedene Funktionen des Katalysatorvorläufers voraussetzt und der in folgenden Stufen abläuft: Zunächst erfolgt eine Protonierung von Propen durch Brønsted-Säurezentren an der Katalysatoroberfläche unter Bildung von adsorbierem Mo(VI)-Isopropoxid, welches anschließend aufgrund der Redoxeigenschaften der Mo(VI)-Zentren zu Aceton oxidiert wird, was zur Entstehung von vierwertigen Mo-Zentren führt, nach der Desorption von Aceton können sich schließlich durch oxidative Addition eines weiteren Propenmoleküls an den Mo(IV)-Zentren die aktiven Mo (VI)-Alkylidenspezies bilden. Die mit diesem Bildungsmechanismus verbundenen multifunktionalen Anforderungen an erfolgreiche Katalysatorvorläufer erklären, warum nur ein Bruchteil der Mo-Atome in aktive Zentren umgewandelt werden kann.

Die Aktivität der Metathesekatalysatoren und die Dichte der Aktivzentren zeigen eine starke Abhängigkeit von der Mo-Beladung. Eine mittlere Mo-Beladung, die durch das gleichzeitige Vorliegen von Oberflächenmolybdänoxid und Silanolgruppen charakterisiert ist, ergibt die höchste Leistung in der Katalyse. Die strukturelle Charakterisierung durch IR-, Raman-, und UV-vis-Spektroskopie, sowie O K-edge NEXAFS, Mo K-edge EXAFS/XANES, H_2-TPR und DFT Rechnungen zeigt die Bildung von zweifach verankerten, tetraedrischen di-oxo $(Si—O—)_2Mo(═O)_2$ Strukturen, die sich unter Verbrauch der Oberflächen-Silanolgruppen bilden. Mit steigender Mo-Beladung kommt es aufgrund eingeschränkter Verfügbarkeit von Silanolgruppen zur Ausbildung von zunehmend verzerrten Mo—O—Si Bindungen in den di-oxo $(Si—O—)_2Mo(═O)_2$ Strukturen, die bei hohen Mo-Dichten eine erhöhte Reaktivität aufweisen. Es wird vorgeschlagen, dass die Bildung der Carbenzentren an diesen „frustrierten“ Molybdenoxidspecies erfolgt. Diese Hypothese erklärt, warum eine hohe Mo Beladung notwendig ist, um eine hohe Aktivität in der Katalyse zu erreichen. Die Charakterisierung der Säurezentren mit Ammoniakadsorption, IR- und ^{1}H-NMR-Spektroskopie zeigt, dass die Oberflächen-Silanolgruppen in der Nähe der $(Si—O—)_2Mo(═O)_2$ Spezies Brønsted-Azidität besitzen. Unter der Berücksichtigung, dass ein weiteres Adsorptionszentrum in Form einer Silanolgruppe für das Nebenprodukt Aceton zur Verfügung stehen muss, wird vorgeschlagen, dass die Vorläufer der Aktivzentren für die Metathese von Propen aus einer $(Si—O—)_2Mo(═O)_2$ Spezies mit verzerrten Mo-O-Si-Bindungen und mindestens zwei benachbarten Silanolzentren bestehen.

Unter Anwendung der gewonnenen Erkenntnisse in Bezug auf den Bildungsmechanismus der Carbenzentren wurde ein einfaches Vorbehandlungsverfahren entwickelt, das die Bildung von Carbenzentren unterstützt und die Metathese-Aktivität erhöht. Die praktische Realisierbarkeit der vorhergesagten Katalysatoroptimierung bestätigt den vorgeschlagenen Mechanismus und verdeutlicht klar den Wert von wissensbasierten, rationalen Ansätzen in der Katalyseforschung gegenüber einer empirischen Katalysatorentwicklung.

Table of Contents

Abstract i
Zusammenfassung iii
Table of Contents v
List of Figures viii
List of Schemes xi
List of Tables xii
List of Abbreviations xiii

Chapter 1: Introduction 1

1.1 General Introduction 1
1.2 Olefin Metathesis 2
  1.2.1 General Mechanism of Olefin Metathesis 2
  1.2.2 Metathesis Catalysts 2
    1.2.2.1 Homogeneous d^0—Alkylidene Complexes 2
    1.2.2.2 Heterogeneous Supported Metal Oxide Catalysts 4
  1.2.3 Generation of Active Carbene Sites in Supported Molybdena Catalysts 4
    1.2.3.1 Proposed Mechanisms for Carbene Generation 4
    1.2.3.2 Carbene Formation from Reduced Mo Sites 6
    1.2.3.3 Carbene Formation from Fully Oxidized Mo(VI) Catalysts 7
1.3 Structure of Silica-Supported Molybdenum Oxides 8
  1.3.1 Silica 8
  1.3.2 Silica-supported Molybdenum Oxides 9
1.4 Outline of the Work 11
1.5 References 13

Chapter 2: In situ Generation of Active Sites in Olefin Metathesis 17

2.1 Introduction 18
2.2 Experimental Section 19
  2.2.1 Preparation of MoO_x/SBA-15 19
  2.2.2 Physico-chemical characterization of MoO_x/SBA-15 20
  2.2.3 Propene metathesis 20
  2.2.4 Post-reaction ethene-d_4 metathesis for active site counting 20
  2.2.5 Microcalorimetry and in-situ IR spectroscopy of propene adsorption 21
2.3 Results 21
  2.3.1 Physico-chemical characterization of MoO_x/SBA-15 21

2.3.2 Propene metathesis and post-reaction active site counting 23
2.3.3 Microcalorimetry of propene adsorption at the reaction temperature 24
2.3.4 IR study of propene and subsequent ethene-d_4 adsorption 27
2.3.5 Progressive formation of isopropoxide and acetone upon propene adsorption 28
2.3.6 Validation of metathesis activity of the resulting surface 28
2.3.7 Summary of the propene adsorption IR study 30

2.4 Discussion 30

2.4.1 Quantity and quality of active carbene sites 30
2.4.2 Formation route of carbene sites 31
2.4.3 Molecular structure of the carbene sites 34

2.5 Conclusion 35
2.6 Supporting Information 37
2.7 References 43

Chapter 3: Impact of the Strain of Surface Metal Oxide Molecules in Supported Catalysts 47

3.1 Introduction 48
3.2 Results and Discussion 48
3.3 Summary and Conclusions 53
3.4 Experimental Section 54
3.5 Supporting Information 55

3.5.1 Experimental and Theoretical Methods 55

3.5.1.1 Preparation of Supported MoO_x/SBA-15 55
3.5.1.2 General Characterization 55
3.5.1.3 Temperature-Programmed Reduction with Hydrogen (H_2-TPR) 55
3.5.1.4 Spectroscopy 56
3.5.1.5 Theoretical Studies 57
3.5.1.6 Catalytic Test 58

3.5.2 Extended Characterization of MoO_x/SBA-15 59

3.5.2.1 Texture and Dispersion 59
3.5.2.2 Mo K-edge XAS 62
3.5.2.3 O K-edge NEXAFS 64
3.5.2.4 Raman and FTIR 65

3.6 References 68

Chapter 4: Active Sites for Olefin Metathesis in Supported Molybdena Catalysts 71

4.1 Introduction 72
4.2 Results and Discussion 72
4.3 Summary and Conclusion 78
4.4 Experimental Section 78

4.5 Supporting Information 79

4.5.1 Supplemental Figures 79
4.5.2 Experimental Details 82

4.5.2.1 Preparation of supported MoO_x/SBA-15 82
4.5.2.2 Structural Characterization of MoO_x/SBA-15 82
4.5.2.3 Adsorption of Probe Molecules 83
4.5.2.4 Propene Metathesis and Post-reaction Active Site Counting 84

4.6 References 85

Chapter 5: Conclusion 87

Appendix: List of publication 88

List of Figures

Figure 2-1. IR spectra of MoO_x/SBA-15 and SBA-15; (A): DRIFT spectra measured at room temperature after pretreatment in 20% O_2 at 823 K for 0.5 h. (B): Transmission IR spectra recorded after adsorption of ammonia at p=10 hPa and subsequent evacuation at 353 K. The catalyst was pretreated in 20 kPa of O_2 at 823 K for 0.5 h. The spectrum before ammonia dosing was used as background.

Figure 2-2. Propene metathesis activity of MoO_x/SBA-15 at T=323 K and a contact time of 0.75 s g ml^{-1}. The catalyst was activated in a 20% O_2 flow at 823 K for 0.5 h. Regeneration was performed applying the same procedure as the initial activation (823 K in 20% O_2 for 0.5 h).

Figure 2-3. Propene adsorption studied by microcalorimetry at 323 K on MoO_x/SBA-15 and SBA-15 pretreated in O_2 at 823 K and at 20 kPa for 0.5 h; differential heat as a function of the amount of adsorbed propene on MoO_x/SBA-15 (A) and SBA-15 (B); re-adsorption profiles were measured after evacuation at ~10^{-3} Pa for 2 h; the regeneration was performed applying the same procedure as the initial pretreatment (in O_2 at 823 K and at 20 kPa for 0.5 h); the adsorption isotherm of propene over MoO_x/SBA-15 and SBA-15 measured at 323 K is shown in (C); measured data points up to an amount of adsorbed propene of 16 μmol g^{-1} were used to fit the data of MoO_x/SBA-15 based on the Langmuir equation.

Figure 2-4. Evolution of the heat signals upon propene adsorption at 323 K on MoO_x/SBA-15 (pretreated in 20% O_2 at 823 K for 0.5 h) at the cumulative adsorption amount of 6 (A) and 26 μmol g^{-1} (B)

Figure 2-5. IR spectra recorded after propene adsorption on MoO_x/SBA-15 for 0.5(magenta) and 18 h (blue) and subsequent evacuation (A). The difference spectrum shown in (B) was obtained by subsequent ethene-d_4 dosing at p=3 hPa and T=323 K for 18 h and evacuation using the blue spectrum in (A) as subtrahend. Propene was dosed at 323 K and 3.0 hPa after the pretreatment in 20 kPa of O_2 at 823 K for 0.5 h. The inset in (B) shows the frequency range of the C-D stretching.

Figure 2-6. Propene metathesis activity of MoO_x/SBA-15 (323 K, contact time=0.35 s g ml^{-1}) after different regeneration procedures. (1): standard oxidative regeneration (20% O_2 flow at 823 K for 0.5 h) was performed. (2): in addition to the standard oxidative regeneration, the catalyst was treated in neat propene flow at 300 K for 1 h followed by heat treatment in argon flow at 823 K (heating rate 10 K min^{-1}) for 0.5 h.

Figure 3-1. Temperature-programmed reduction (H_2-TPR) of supported MoO_x/SBA-15 measured at a heating rate of 10 K min^{-1} in 2% H_2 in Ar after pretreatment in 20% O_2 in Ar at 823 K for 0.5 h.

Figure 3-2. (a) UV-vis, (b) Mo K-edge XANES, (c) Fourier-transformed phase-uncorrected Mo K-edge EXAFS, and (d) O K-edge NEXAFS spectra of dehydrated MoO_x/SBA-15.

Figure 3-3. Schematic illustration of the suggested anchoring patterns of di-oxo $(—Si—O—)_2Mo(=O)_2$ structures on a 2D silica surface at different surface molybdenum densities. Two 2D models (a, b) are shown to illustrate the real 3D space. The differently colored dots-terminated lines in “a) top view” represent the di-oxo species having different anchoring geometries.

Figure 3-4. Catalytic performance of MoO_x/SBA-15. Propene metathesis at 323 K and at 15 h of time on stream. The catalysts were pretreated in 20% O_2 in Ar at 823 K for 0.5 h.

Figure 4-1. Propene metathesis performance of MoO_x/SBA-15 at 323 K and at 15~21 h of time on stream: (a) metathesis rate and active carbene site (Mo=CHR) density, (b) turn

over frequency (TOF). The catalysts were pretreated in 20%O_2 at 823 K for 0.5 h. Error bars are estimated by two repeated measurements

Figure 4-2. Propene adsorption onto MoO_x/SBA-15 at 323 K. **(a):** IR spectra collected after propene dosing at 3 hPa for 18 h and subsequent evacuation. The C—H vibrations (stretching : 2983, 2939, 2880 cm^{-1}; deformation: 1465, 1455, 1389, 1375 cm^{-1}) and ν(C═O) at 1668 cm^{-1} are assigned to isopropoxide and acetone, respectively.[7] **(b):** Differential heat of propene adsorption as a function of coverage determined by microcalorimetry. Surface Mo density (Mo_atoms nm^{-2}) is indicated close to the data.

Figure 4-3. Study on acidity and hydroxyl groups in MoO_x/SBA-15. **(a):** ^{1}H-MAS-NMR spectra of SBA-15 and MoO_x/SBA-15 (1.27 Mo_atoms nm^{-2}). The spectrum of MoO_x/SBA-15 is magnified by factor of 5. **(b):** Density of isolated silanol and ammonia adsorption sites estimated by IR. **(c):** Schematic illustration of the suggested model for Brønsted acid sites. The IR spectra and the quantification procedure are presented in the Supporting Information (Figures S4-2 and S4-3). The catalysts were pretreated in O_2 at 823 for 0.5 h

Figure 4-4. Propene metathesis activity of of MoO_x/SBA-15 (0.85 Mo_atoms nm^{-2}) after different pretreatment procedures. (1) Standard pretreatment (20% O_2, 823 K, 0.5 h). (2) Methanol pretreatment (4% CH_3OH-Ar, 523 K, 0.5h) and subsequent desorption (Ar, 823 K, 0.5h) after the standard pretreatment. The inset shows signal of mass spectrometer for m/e=69 (pentene) and m/e=56 (butenes) at initial period of the reaction with the methanol pretreatment.

Figure S 2-1. Adsorption/desorption isotherms (at 77 K) of nitrogen on MoO_x/SBA-15 and SBA-15.

Figure S 2-2. Raman spectra of MoO_x/SBA-15 and SBA-15 (pretreated in 20% O_2 at 823 K for 0.5 h) as well as MoO_3 (no pretreatment) upon excitation with a 632 nm laser measured at room temperature. The spectra were offset for clarity.

Figure S 2-3. UV-vis diffused reflectance spectrum of MoO_x/SBA-15 (pretreated in 20% O_2 at 823 K for 0.5 h) measured at room temperature. The mother SBA-15 was used as white standard.

Figure S 2-4. IR spectra for isopropanol and acetone adsorbed at 1 hPa and 323 K on MoO_x/SBA-15 pretreated in 20 kPa of O_2 at 823 K for 0.5 h.

Figure S 3-1. Geometric structure of the molybdena—silica model clusters having tetrahedral di-oxo units in a stick-ball representation: (a) MO_4—$Si_7O_{10}H_8$, (b) $(MoO_4)_2$—$Si_6O_7H_6$, (c) MO_4—$Si_8O_{12}H_6$

Figure S 3-2. Selected adsorption/desorption isotherms of nitrogen on supported MoO_x/SBA-15 (13.3wt%_Mo) and SBA-15 measured at 77 K. Note that all the supported MoO_x/SBA-15 samples show similar Type-IV isotherms with H1 type hysteresis patterns at P/P_0 = ~0.65.

Figure S 3-3. High resolution SEM images of SBA-15 (a) and 13.3Mo (b). Plate-like crystalline MoO_3 particles are highlighted by the yellow circles in (b).

Figure S 3-4. Magnitudes of Fourier-transformed k^2-weighted Mo K-edge EXAFS spectra in non-phase-corrected *R* space for the dehydrated MoO_x/SBA-15 (dot) with curve fits to the single-scattering models for the tetrahedral-dioxo structure (red line) and the pentahedral mono-oxo structure (blue line, only for 2.1Mo): (A) 2.1Mo, (B) 8.2Mo, and (C) 13.3Mo. The fits were performed for the *R* range of 1~2.09 Å.

Figure S 3-5. Theoretical and experimental O K-edge NEXAFS spectra. (A) Theoretical spectra for clusters **a**—**c** and experimental spectra of 2.1Mo and 6.6Mo. (B) Experimental spectra of 8.2Mo and 13.3Mo and theoretical spectra of modified cluster **a** and **c**

where the O═Mo═O angle is changed to 53 and 47.9°, respectively. The spectra are arbitrary offset and scaled for clarity. Note that the absorption due to silica above 533 eV makes a large contribution in 2.1Mo due to the high Si/Mo ratio.

Figure S 3-6. In situ Raman and FTIR spectra of supported MoO_x/SBA-15 at the dehydrated state (pretreated in 20% O_2 at 823 K for 0.5 h) measured at room temperature: overview Raman spectra upon 1.96 eV (633 nm) excitation (A), a magnification of panel A (B), IR spectra in the OH stretching region (C), and IR spectra in the Mo=O and Mo—O—Si stretching region (D). The IR spectra were normalized by the SBA-15 intensity at 1865 cm^{-1}. The Raman spectra were vertically offset for clarity.

Figure S 3-7. Calculated IR spectra for clusters **a** ($(Si—O—)_2Mo(=O)_2$ with a Si—O—H in the vicinity) and **b** (two adjacent $(Si—O—)_2Mo(=O)_2$ units).

Figure S 3-8. In situ Raman spectra of the dehydrated 8.2Mo measured at room temperature using excitation energies of 3.82 and 1.96 eV. The intensity was normalized at the Mo=O band at 994—996 cm^{-1}. The spectra were vertically offset for clarity.

Figure S 4-1. Time trend of the propene metathesis activity of MoO_x/SBA-15 normalized by BET surface area: (a) Fresh catalysts, and (b) regenerated catalysts. Reaction conditions: T = 323 K, contact time = 0.75 s g ml^{-1}, p = 0.1 MPa, neat propene. Pretreatment or regeneration: T = 823 K, 0.5 h in 20% O_2-Ar, subsequent purge with pure Ar at 323 K.

Figure S 4-2. Relationship between the propene adsorption microcalorimetry data and the density of active carbene (Mo=CHR) sites found after propene metathesis. a) Density of the Mo=CHR sites as a function of the initial heat of propene adsorption, and b) density of the Mo=CHR sites as a function of the density of propene adsorption sites exhibiting heat of adsorption higher than 30 kJ mol^{-1}. See also Figures 1 2b in the main text.

Figure S 4-3. IR spectra of MoO_x/SBA-15 measured at RT after pretreatement in 20% oxygen at 823 K for 0.5 h. The sharp band at 3745 cm^{-1} due to isolated silanol groups decrease with increasing the Mo density. The broad band due to hydrogen-bonded silanol groups occurs at 3745 cm^{-1} upon introduction of surface molybdena.

Figure S 4-4. IR spectra of MoO_x/SBA-15 recorded after ammonia dosing (7 hPa, 353 K) and subsequent evacuation for 1h. The catalysts were pretreated in O_2 at 823 K and at 20 kPa for 0.5 h. Spectra before ammonia dosing were used as reference. The catalysts were pretreated in O_2 at 823 K and at 20 kPa for 0.5 h.

Figure S 4-5. Profiles of temperature programmed desorption of ammonia (NH_3-TPD) from MoO_x/SBA-15 at a ramp rate of 10 K min^{-1}. The similar profiles suggest no significant variation in average acid strength. The catalysts were pretreated in 20% O_2 in Ar at 823 K for 0.5 h, which was followed by ammonia adsorption at 353 K by feeding 1% NH_3 in Ar and subsequent purge in a He stream at 353 K for 0.5h.

Figure S 4-6. Temperature programmed desorption (TPD) profile after propene metathesis over MoO_x/SBA-15 (1.1 Mo atoms nm^{-2}). The concurrent occurrence of m/e = 58 and 43 with an intensity ratio of approximately 1:4 indicates the desorption of acetone. Besides, the desorption of propene (m/e 41) and butenes (m/e 55) was observed. Metathesis reaction conditions: T = 323 K, contact time = 0.75 s g ml^{-1}, p = 0.1 MPa, neat propene, 16 h of reaction time. Pretreatment: T = 823 K, 0.5 h in 20% O_2-Ar, subsequent purge with pure Ar at 323 K. Post-reaction TPD: ramp rate of 10 K min^{-1} in Ar.

List of Schemes

Scheme 1-1. General scheme of olefin metathesis.

Scheme 1-2. Mechanism of propene metathesis catalyzed by Mo—alkylidene species.

Scheme 1-3. Structure of Mo(VI)—alkylidene metathesis catalysts: (a) Mo(VI)—imido alkylidene complex developed by Schrock,[8] (b) Schrock-type complexes anchored on silica surface,[11] and (c) suggested structure of active sites derived from MoO_x species supported on silica.[12–15]

Scheme 1-4. Proposed mechanisms for initial carbene formation upon contact of the catalyst with an olefin. M = active metal center for metathesis reaction, S = support element.

Scheme 1-5. Suggested mechanism of the photoreduction of a surface molybdate by CO and subsequent creation of a carbene site by cyclopropane dosing followed by thermal treatment.[5]

Scheme 1-6. Suggested mechanism of the photoreduction of a surface molybdate by CO and subsequent creation of a carbene site by cyclopropane dosing followed by thermal treatment.[47,49]

Scheme 1-7. Reactions of a silanol group with a proton in water media.

Scheme 1-8. Proposed structures of molybdena species

Scheme 1-9. Illustration of the overview of the present thesis.

Scheme 2-1. Proposed mechanisms for initial carbene formation upon contact of the catalyst with an olefin. M = active metal center for metathesis reaction, S = support element.

Scheme 2-2. Reaction mechanism of propene metathesis according to Chauvin.[1] The titration reaction of Mo-ethylidene with ethene-d_4 is described in red color.

Scheme 2-3. Proposed route for the carbene formation starting from a Mo(VI) site upon interaction with two propene molecules: general scheme (A), a scheme assuming a tetrahedral dioxo structure as the pre-catalyst (B) compared to the structure of reference Schrock-type homogeneous catalysts (C).[66]

Scheme 4-1. Suggested mechanisms for the generation of a Mo(IV)—carbene site in propene metathesis: in the cases without **(a)** and with **(b)** methanol pretreatment.

List of Tables

Table 2-1. Summary of propene metathesis activity and post-reaction active site counting over MoO_x/SBA-15.

Table S 3-1. Bond distances and angles in the Mo—Si—O clusters having tetrahedral di-oxo MoO_4 structures (Figure S3-1).
Table S 3-2. Properties of MoO_x/SBA-15
Table S 3-3. Curve fit parameters for the single-scattering refinements[a] of the EXAFS spectra of the dehydrated MoO_x/SBA-15 for the tetrahedral di-oxo $(O{=})_2Mo(—O—Si)_2$ model (Figure S3-5). Uncertainties in the last significant digits are given in parentheses.
Table S 4-1. Properties of MoO_x/SBA-15

List of Abbreviations

BET	Adsorption isotherm model of Brunauer, Emmet and Teller
DFT	Density functional theory
DR	Diffuse reflectance
DRIFT	Diffuse reflectance infrared Fourier transform
EDX	Energy dispersive X-ray spectroscopy
EXAFS	Extended x-ray absorption fine structure
FT	Fourier transformation
IR	Infrared spectroscopy
MS	Mass spectrometry
NEXAFS	Near edge x-ray absorption fine structure
NLDFT	Non localized density functional theory
NMR	Nuclear magnetic resonance
SEM	Scanning electron microscopy
TG	Thermo gravimetry
TPR	Temperature programmed reduction
UV-Vis	Ultraviolet-visible spectroscopy
XANES	X-ray absorption near edge structure
XAS	X-ray absorption spectroscopy
XRD	X-ray diffraction
XRF	X-ray fluorescence

Chapter 1: Introduction

1.1 General Introduction

Heterogeneous catalysts have been playing an indispensable role in our life. Continuous evolution of heterogeneous catalysts is essential for a sustainable future of human beings.

Since catalysis is a *macroscopic* phenomenon observed by detecting the transformation of reactants, assessment of catalytic performance does not provide information on the underlying mechanisms at a *microscopic* (e.g. molecular) level. This fact puts an intrinsic and huge knowledge gap in heterogeneous catalysis research. A description of the property of successful catalysts does not consist of a molecular structure of active site (as in the case of homogeneous catalysis), but consists of empirical parameters (e.g. composition, preparation methods, spectroscopic and physicochemical properties) like a secret recipe of a three-stared restaurant. The structure and number of active sites, the most fundamental information, are highly challenging to determine and mostly unknown.[1] The actual use of numerous heterogeneous catalysts, whose mechanistic details are unclear, eloquently demonstrates that the catalysis as a practical technology does not require in-depth understanding into the structure of the catalysts and the set of reactions that comprise a catalytic turn over. Nevertheless, as the history of the catalysis has proven, phenomenological optimization of heterogeneous catalysts works efficiently when directed by an adequate mechanistic understanding. It is believed that in-depth understanding in to heterogeneous catalysis not only contributes to fundamental science but also benefits our life through improvements of catalysts by rational approaches.

To correctly tackle the quest for the understanding into a heterogeneous catalysis, identification of the structure and quantity the active site as well as the mechanism of a catalytic turnover is a prerequisite. However, in reality, this information is known in no heterogeneous catalytic system.

Heterogeneous olefin metathesis is a rare system where the general structural motif of active sites is established in analogy to homogeneous catalysis[2] and thus quantification of active sites is accessible.[3] Hence, it is an exceptionally advantageous catalytic system to disclose the details of active sites at a molecular level. The metathesis of lower olefins over heterogeneous catalysts is of practical significance. Especially, propene production by heterogeneous metathesis has been gaining the importance.[4]

This work intends to establish a quantitative description of the active sites of heterogeneous metathesis catalysts with an understanding into the site structure at a molecular level. Propene metathesis was chosen as the catalytic reaction considering the advantages for the mechanistic study and the practical importance.

In this chapter, knowledge on heterogeneous olefin metathesis over molybdenum catalysts and on the structure of silica-supported molybdenum oxides is first summarized, which is followed by an outline of the work.

1.2 Olefin Metathesis

1.2.1 General Mechanism of Olefin Metathesis

In catalytic olefin metathesis reactions, the carbon—carbon double bonds of two olefin molecules are rearranged to form new olefin molecules, as shown in the scheme 1-1.

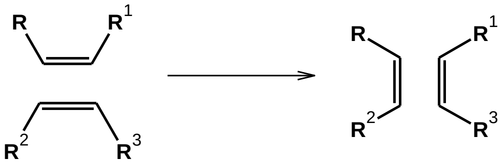
R
R1
R2
R3
R
R1
R2
R3

Scheme 1-1. General scheme of olefin metathesis.

Metal carbene species are the active sites for the reaction.[2,5] The catalytic cycle involves the formation of a metallacyclobutane intermediate by a [2+2] cycloaddition reaction between an olefin and a metal alkylidene (i.e. carbene) complex and subsequent decomposition of the metallacyclobutane intermediate into a product olefin and a metal alkylidene. Scheme 1.2 shows the reaction mechanism of propene self-metathesis catalyzed by Mo—carbene species. A metallacyclobutane intermediate decomposes either to yield a new olefin molecule (i.e. productive pathway) or to regenerate the starting olefin molecule (i.e. unproductive pathway). Two types of Mo—alkylidene, namely Mo—methylidene and Mo—ethylidene, are present under the steady state of propene metathesis.

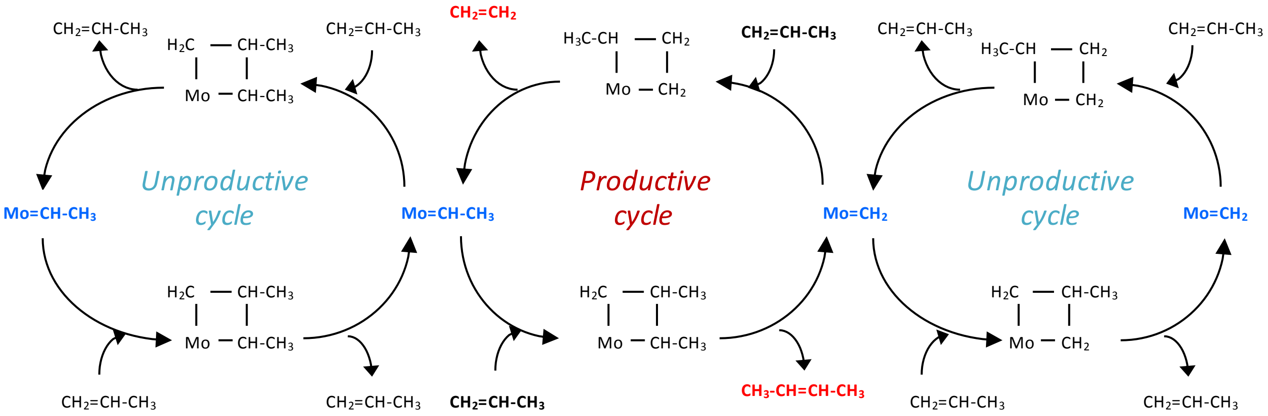
CH2=CH-CH3
H2C — CH-CH3
Mo — CH-CH3
CH2=CH-CH3
CH2=CH2
H3C-CH — CH2
Mo — CH2
CH2=CH-CH3
CH2=CH-CH3
H3C-CH — CH2
Mo — CH2
CH2=CH-CH3
Mo=CH-CH3
Unproductive cycle
Mo=CH-CH3
Productive cycle
Mo=CH2
Unproductive cycle
Mo=CH2
H2C — CH-CH3
Mo — CH-CH3
H2C — CH-CH3
Mo — CH-CH3
H2C — CH-CH3
Mo — CH2
CH2=CH-CH3
CH2=CH-CH3
CH2=CH-CH3
CH3-CH=CH-CH3
CH2=CH-CH3
CH2=CH-CH3

Scheme 1-2. Mechanism of propene metathesis catalyzed by Mo—alkylidene species.

1.2.2 Metathesis Catalysts

The metathesis reaction can be catalyzed by both homogeneous and heterogeneous catalysts that can form the metal—carbene active sites.

1.2.2.1 Homogeneous d^0—Alkylidene Complexes

It has been found that transition metal—carbene complexes exhibiting a d^0 configuration are active for olefin metathesis where Ta, Mo and W are typical active metals.[6,7] Mo(VI) imido alkylidene complexes with alkoxide ligands (Scheme 1-3 a) developed by Schrock and co-workers represent most efficient metathesis catalysts. The well-defined structure of the homogeneous Mo(VI)—alkylidene complex catalysts has allowed detailed investigations into structure—reactivity relationships.

The tetrahedral coordination is considered to be essential in order to allow a facile access of reactant olefin.[8]

Role of Alkoxide Ligands. The alkoxide ligands exhibit a great impact on the metathesis activity, where electron-withdrawing ligands (e.g. $OCMe(CF_3)_2$) give high activity.[7] Feher and co-workers showed that Schrock-type Mo(VI)—alkylidene complexes anchored to molecular silsesquioxane frameworks via a Mo—O—Si linkage exhibited an excellent metathesis activity, which was correlated to the highly electron-withdrawing character of siloxide (Si—O) ligands.[9] In agreement with this observation, anchoring Schrock-type catalysts onto a dehydrated silica surface by substituting an *tert*-butoxide ligand to a siloxide linkage (Mo—O—Si) results in a dramatic enhancement of the catalytic activity in propene metathesis,[10] yielding an excellent "heterogenized homogeneous catalyst" (Scheme 1-3 b).

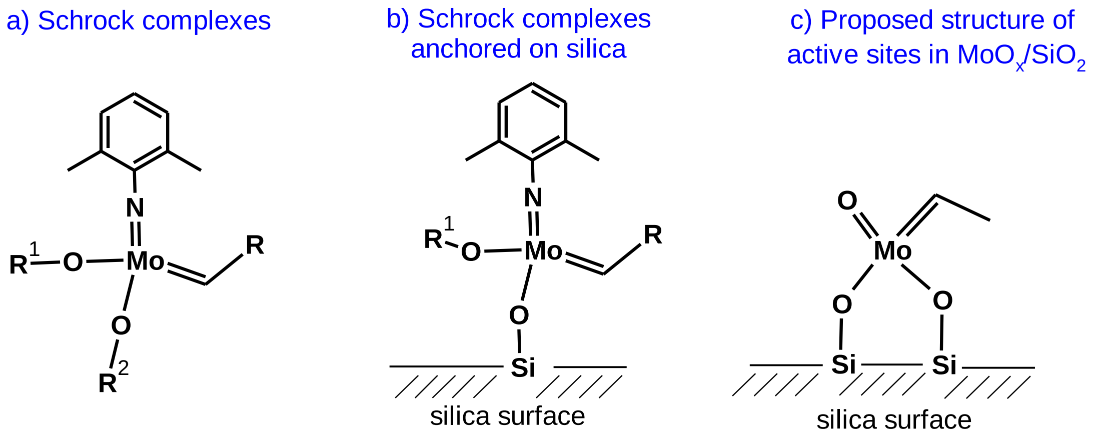
a) Schrock complexes
b) Schrock complexes anchored on silica
c) Proposed structure of active sites in MoOx/SiO2
N
Mo
O
R1
R2
R
Si
O
silica surface
silica surface

Scheme 1-3. Structure of Mo(VI)—alkylidene metathesis catalysts: (a) Mo(VI)—imido alkylidene complex developed by Schrock,[8] (b) Schrock-type complexes anchored on silica surface,[11] and (c) suggested structure of active sites derived from MoO_x species supported on silica.[12–15]

Imido- and Oxo- Ligands. Historically, the imido ligand with a bulky group in the Schrock-type Mo(VI)—alkylidene complexes has been developed to mimic the electronic structure of the oxo ligand while providing a protection from the self-condensation by equipping the bulky alkyl phenyl group, as the oxo—carbene Tungsten complexes show considerable metathesis activity but rapidly deactivate due to the self-condensation.[16,17] The self-condensation leading to the collapse of the oxo-carbene complexes can be avoided by anchoring oxo-carbene complexes on a solid to keep spacious isolation. Recently, tungsten oxo alkyl species are successfully anchored on dehydrated silica surface, yielding active and stable metathesis catalysts exhibiting an improved stability than the imido analogue.[18] This result is consistent with the recent theoretical comparison of the oxo and imido ligands which predicts a slightly lower activity and improved stability of the oxo ligand.[19]

1.2.2.2 Heterogeneous Supported Metal Oxide Catalysts

Monolayer-type metal (e.g., Mo, W and Re) oxides deposited on porous supports (e.g. silica alumina and silica-alumina) are important metathesis catalysts.[20–25] WO_x/SiO_2 catalysts are currently employed for propene production from ethene and butenes at elevated temperature (>573 K), while MoO_x/Al_2O_3 catalysts are used at ca. 373 K for the production of olefins with longer carbon chains.[20]

These supported metal oxide catalysts need an activation at elevated temperature (typically at 823 K) in an inert atmosphere before use,[5] which dehydrate the surface and change the structure of surface metal oxide species.[26] These catalysts allow regeneration by oxidative calcination,[27] which is an essential property for industrial long-term use.

Despite the vital use in industry, the nature of the metathesis active sites in supported metal oxide catalysts remains unclear. It is generally assumed that metal-carbene species generated on the surface during the reaction are responsible for the catalytic activity. The number of active carbene species in these catalysts is at most 2 % of the total metal content.[3,28,29] The low abundance of active sites makes characterization of the active sites extremely challenging. As surface metal oxide species exhibit metal—oxygen double bonds, metal—carbene species with a oxo ligand (e.g. c in Scheme 1-3) have been often considered to occur in heterogeneous metathesis catalysts derived from supported metal oxides.[12–15]

1.2.3 Generation of Active Carbene Sites in Supported Molybdena Catalysts

The occurrence of metathesis activity in supported metal oxide catalysts is due to the generation of carbene sites that happens on a minor (~2%) fraction of metal oxide species present. The mechanism of the active site formation in supported metal oxide catalysts remains elusive.

1.2.3.1 Proposed Mechanisms for Carbene Generation

The surface reaction between catalyst precursor and olefin is a demanding process, since the metal oxides need to accomplish carbene synthesis in one-pot and in-situ. Several surface reactions via different intermediates have been proposed (Scheme 2-1): (A) formation of a π-complex between the reacting alkene and a coordinatively unsaturated metal ion followed by a 1,2-hydrogen shift (1,2-hydrogen shift mechanism),[30,31] (B) formation of a π -complex followed the transformation of the π-allyl hydride intermediate into a metallacyclobutane (allyl mechanism),[32–34] (C) formation of a metal-oxo intermediate mediated by a surface Brønsted acid site and subsequent hydrogen shift (H-assisted mechanism),[35] and (D) formation of an oxametallacyclobutane and subsequent elimination of a carbonyl compound (pseudo-Wittig mechanism).[15,28,36–38]

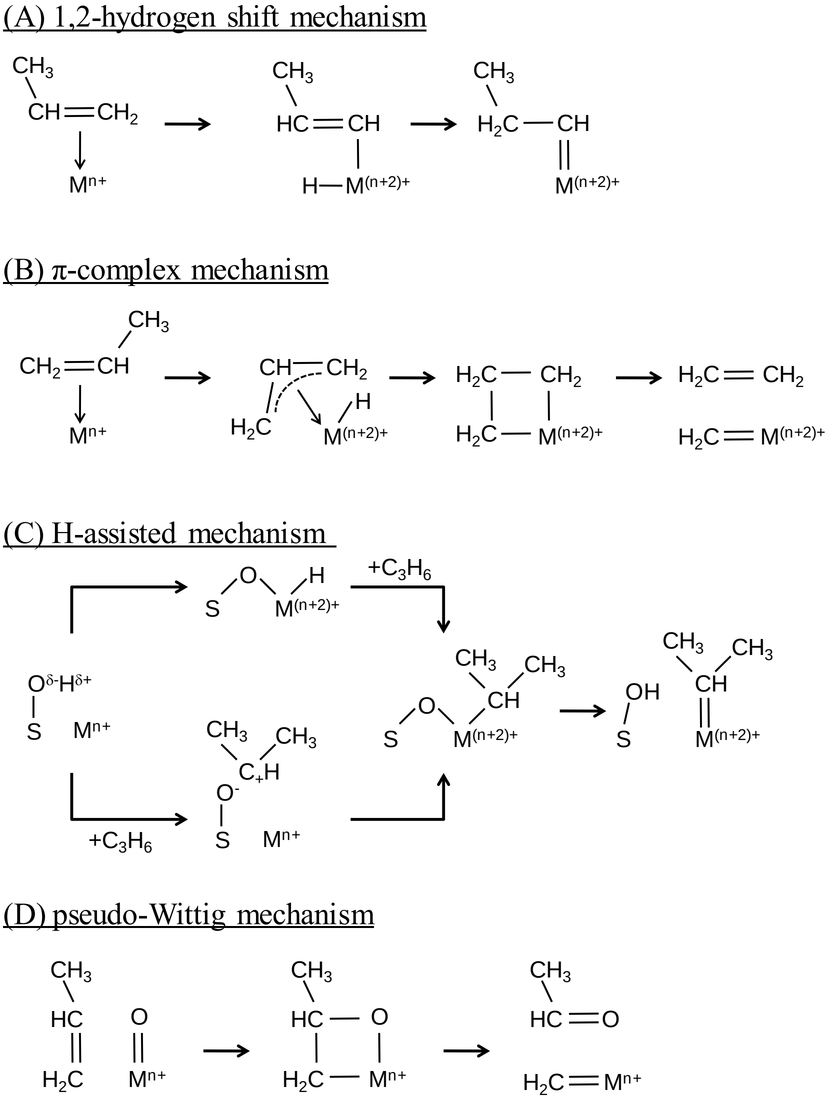

(A) 1,2-hydrogen shift mechanism

(B) π-complex mechanism

(C) H-assisted mechanism

(D) pseudo-Wittig mechanism

Scheme 1-4. Proposed mechanisms for initial carbene formation upon contact of the catalyst with an olefin. M = active metal center for metathesis reaction, S = support element.

All reaction pathways, except the pseudo-Wittig mechanism, involve an oxidative addition reaction, in which metal centers are required that can be oxidized by losing two electrons. Since catalyst pretreatment and regeneration of supported metal oxides are typically performed by oxidative treatment at elevated temperature,[20,27] the pseudo-Wittig mechanism would be the only applicable carbene formation route.

1.2.3.2 Carbene Formation from Reduced Mo Sites

It is agreed that reduced Mo(IV) sites act as a good precursor for the active carbene sites,[5] although several different mechanisms are proposed with respect to the detailed pathways (Scheme 1-4 A—C).

From Coordinatively Unsaturated Mo(IV) Sites. Fabrication of active carbene sites through a controlled creation of coordinatively unsaturated Mo(IV) sites and subsequent implantation of carbon species has allowed valuable insights. Early studies found that reductive treatments with hydrogen or CO enhanced metathesis activity.[39,40]

Selective reduction of supported MoO_x/SiO_2 catalysts exhibiting tetrahedral di-oxo ((Si—O—)$_2$Mo(═O)$_2$ structures by CO assisted by UV irradiation allows formation of mono-oxo Mo(IV) sites in a high efficiency.[41,42] Subsequent dosing cyclopropane to the resulting reduced surface at room temperature yields highly active metathesis catalysts (Scheme 1-5).[41,42] The metathesis catalysts derived by the photoreduction allowed fundamental insights into the nature of active carbene sties with respect to spectroscopic property, bonding energy, and number of active sites as well as intrinsic activity of them.[12,43–46]

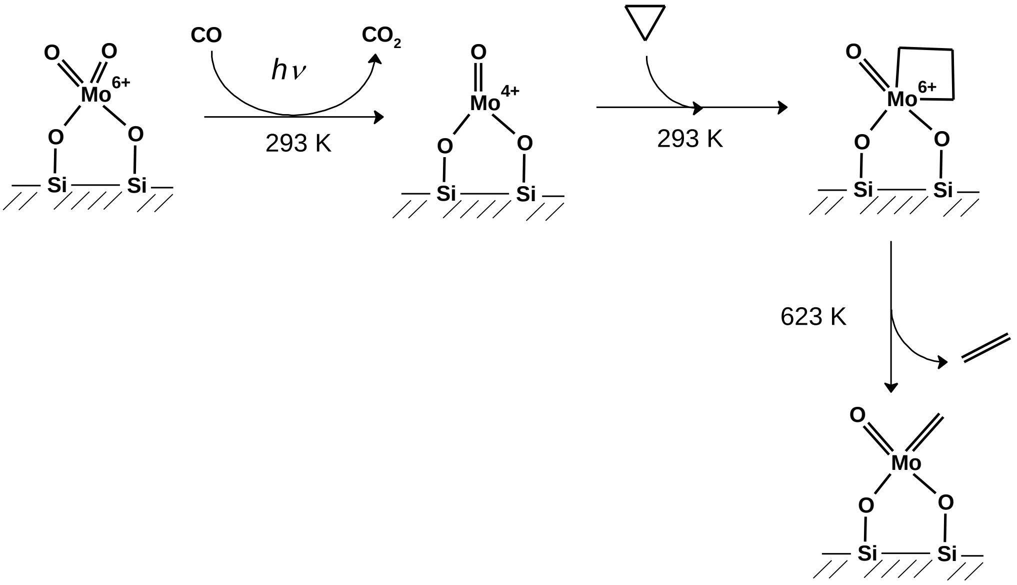

Scheme 1-5. Suggested mechanism of the photoreduction of a surface molybdate by CO and subsequent creation of a carbene site by cyclopropane dosing followed by thermal treatment.[5]

Related to the UV-assisted CO reduction of surface molybdena, propene metathesis over similar supported MoO_x/SiO_2 under irradiation of UV light at room temperature was studied by Anpo and co-workers.[14,47–49] It is proposed that Mo(V) species generated by the excitation by UV absorption in a long-living triplet state reacts with a propene molecule in a pseudo-Wittig-like manner to give a carbene site (Scheme 1-6). This conclusion was drawn by the detection of ethanal (Scheme 1-6) in the reaction atmosphere and photoluminescence studies that probe the excited triplet states. Somewhat puzzling in this study is that the reaction stops upon light-off. This observation suggests that the carbene species formed are extremely short living, or the metathesis reaction is directly photo-catalyzed in an unknown mechanism.

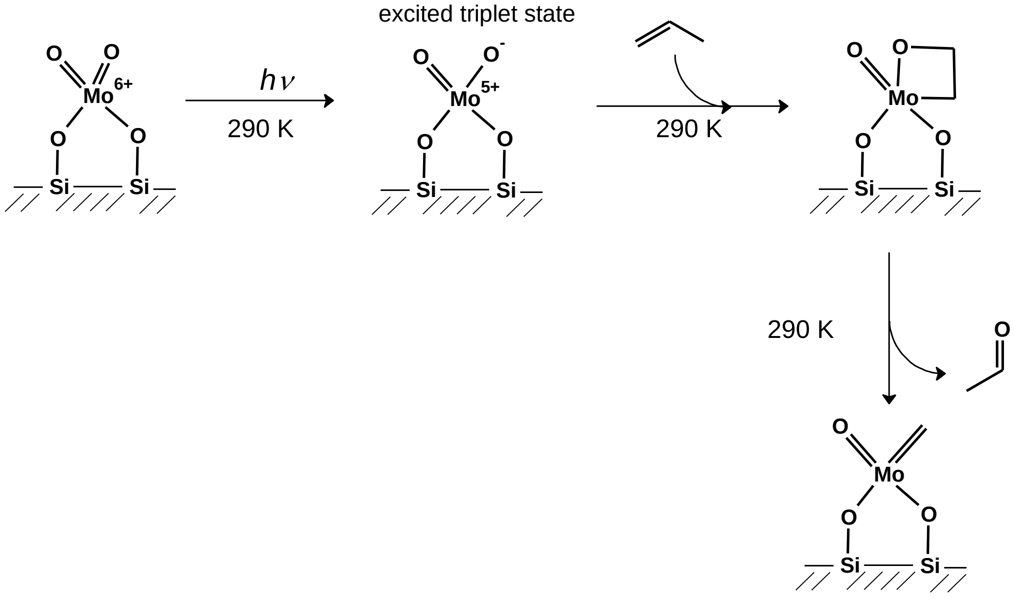

Scheme 1-6. Suggested mechanism of the photoreduction of a surface molybdate by CO and subsequent creation of a carbene site by cyclopropane dosing followed by thermal treatment.[47,49]

Iwasawa and co-workers anchored highly dispersed (presumably monomeric) molybdenum species using the reaction between Mo(π-C_3H_5)$_4$ and surface hydroxyl groups of silica and alumina supports, and concluded that isolated and coordinatively unsaturated Mo(IV) species (actually the same as the Mo(IV) species obtained by the CO-photoreduction in Scheme 1-5) are the precursor of the active sites.[13,30,31,50] Whereas, Mo(VI) and Mo(II) species obtained by the oxidation or reduction of the same materials showed no appreciable activity.[13]

1.2.3.3 Carbene Formation from Fully Oxidized Mo(VI) Catalysts

Pseudo-Wittig Mechanism. Pseudo-Wittig mechanism has been often assumed in the case of supported metal oxide catalysts.[28,36] This might be due to the absence of alternative hypothesis explaining the carbene formation from Mo(VI). Pseudo-Wittig mechanism was first proposed by Rappe and Goddard[15] based on a purely theoretical basis, which has been followed by a few theoretical investigations.[51–53] Taking into account that only a minor fraction of metal species is active sites, theoretical investigations assuming models representing abundant species may not represent the case well.

Little experimental evidence for pseudo-Wittig mechanism has been reported so far. Salameh and co-workers[28] studied olefin metathesis over a Re_2O_7/Al_2O_3 catalyst varying the reactant olefin. The authors supported the pseudo-Wittig mechanism based on the observation that Z-stylbene (1,2-diphenylethene) exhibiting no allylic C—H bond could propagate the metathesis reaction.

Despite the high relevance to the industrial metathesis catalysis, the origin of active carbene species from fully oxidized supported metal oxide species remains largely elusive, which is in contrast to the active site generation from Mo(IV) sites.

1.3 Structure of Silica-Supported Molybdenum Oxides

Monolayer-type transition metal oxides deposited on high surface area supports are of importance in a number of industrial catalytic processes that are indispensable for our everyday living.[20,54–57] Among such catalysts, the supported molybdena—silica system represents a model catalyst for important catalytic reactions including selective oxidation of alcohols,[58–60] alkenes[61,62] and alkanes[63,64] as well as olefin metathesis.[65,66]

1.3.1 Silica

Silica is often applied as support material of heterogeneous catalysts. The surface of silica possesses silanol groups, which play important roles in supporting active metal elements. The density of the surface silanol groups decreases upon a heat treatment at elevated temperature as a consequence of dehydration due to the self-condensation reaction of surface silanol groups.

The acid-base interaction between surface silanol groups and metal precursor species is crucial to determine the dispersion of resulting supported metal oxide catalysts. The silanol groups are acidic in aqueous solution, showing an isoelectronic point at pH 1.5~3.[67] In an aqueous media, the surface of silica is negatively charged when pH is above the value of isoelectronic point, whereas the surface becomes positively charged only under strongly acidic conditions (Scheme 1-4). Accordingly, it is generally difficult to establish an intact interaction between anionic metal species and silica surface if the anionic metal species are unstable at strongly acidic conditions.

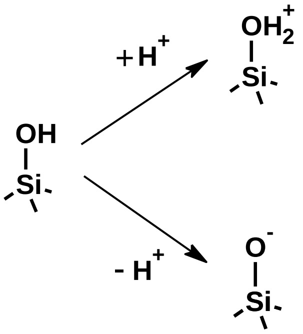

Scheme 1-7. Reactions of a silanol group with a proton in water media.

To obtain a good dispersion of metal species on silica by an aqueous impregnation approach, it is desirable to establish a cation-anion interaction between the silica surface and precursor metal species. In the case of molybdenum, however, molybdenum forms anionic species in a wide range of pH, leading to a repulsing interaction with the deprotonated silica surface, resulting in an aggregation of molybdenum species after drying and calcination thus poor dispersion. Substituting the surface silanol groups by alkylamino groups offers cationic counter-partners for molybdate anions, allowing a preparation of highly dispersed supported molybdena catalysts.[68]

While the acid—base interaction play a major role in aqueous impregnation processes, the surface silanol groups serve as chemical anchoring points to form dispersed molybdena species upon thermal treatments (e.g. calcination), wherein covalent Mo—O—Si bonds are established.[69]

1.3.2 Silica-supported Molybdenum Oxides

The loading of molybdenum oxides onto silica surface can yield dispersed surface molybdena species. The molecular structure of the surface molybdena species on silica has been extensively studied over the past three decades.[70,71] A variety of supported molybdena species, including surface monomeric, surface polymeric and crystalline MoO_3 nanoparticles may be present on the silica support.

Hydrated and Dehydrated States. It has been established that the structure of surface molybdenum oxide species changes reversibly in response to hydration/dehydration.[26] The surface molybdena species are in polymeric forms similar to the heptamolybdate anion under ambient conditions (i.e. hydrated state), while dehydration at elevated temperature in a dry atmosphere leads to a de-polymerization of polymolybdate species yielding highly dispersed surface molybdena anchored on silica.[26,68] The discovery of this reversible structural change has clarified some of the contradicting observations with respect to the condensation degree of surface molybdate species.

Molecular Structures. The molecular structural details of the catalytically often relevant[66,72] oxidized and dehydrated state, however, is still being debated.[58,73,74] A number of spectroscopic techniques (in particular, Raman, IR, X-ray absorption, UV—vis and photoluminescence), have been employed to investigate the molecular structure of the dehydrated surface molybdena species on silica. The two distinct surface monomeric Mo(VI) species, namely tetrahedral di-oxo MoO_4[48,62,74–83] and pentahedral mono-oxo MoO_5,[59,72,74,82,84] are often proposed as the major surface species on silica (Scheme 1-4), the presence of polymeric species has also been suggested.[73,85,86]

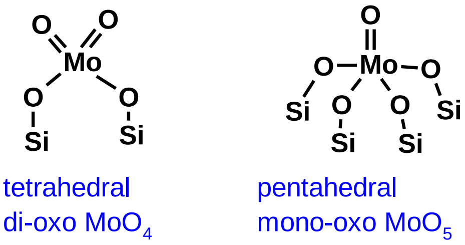

Scheme 1-8. Proposed structures of molybdena species

Based on Raman and UV-vis spectroscopy, Lee and Wachs[74,82] proposed the predominance of tetrahedral di-oxo species with a minor fraction of the pentahedral mono-oxo species. This view is in general in agreement with a number of theoretical investigations[58,81,83,87–89] that analyzed the stability of the various proposed surface molybdena species on silica[81,87,88] and their spectroscopic features (vibrational frequencies of Mo═O stretching,[58,81,87–89] Mo K-edge XAS[81] and O K-edge NEXAFS[83]). The theoretical studies also found that the calculated frequencies for ν(Mo═O) of the di-oxo and mono-oxo species fall in a narrow range at around 970-1030 cm^{-1}.[58,81,87–89] and that the relative vibrational positions of the di-oxo and the mono-oxo surface species vary depending on the model and theoretical method applied, which makes the differentiation between di-oxo and mono-oxo surface species somewhat ambiguous.[58,81,87–89] The quality of the theoretical studies has been improved[58,78,81,83,87–89] because of the continuously growing computational power and the use of periodic slab models rather than cluster models. In the most recent report by Handzlik and Ogonowski, a large set of silica models (planes of β-cristobalite as well as various amorphous silica structures) was considered as anchoring sites of monomeric molybdena surface species.[88] It was again concluded that the di-oxo ((Si—O—

$)_2Mo(=O)_2$ surface species should be favorable over the mono-oxo $(Si—O—)_4Mo=O$ surface species considering geometric restrictions for the anchoring Si—O—Mo bonds.[88]

The presence of polymeric species besides crystalline MoO_3 has also been suggested.[73,85,86] Thielemann et al. suggested the presence of polymeric molybdena species in MoO_x/SBA-15 based on in situ IR measurements using NO adsorption onto the material reduced by hydrogen.[85] The same authors analyzed the structure of MoO_x/SBA-15 using Raman, UV-vis, and Mo K-edge XANES/EXAFS, and concluded that the materials contain both monomeric and polymeric surface molybdena species.[73] In this report, a model based on the structure of hexagonal MoO_3 was used to fit the EXAFS data to conclude the presence of connected molybdena species while neglecting possible contribution of monomeric species and Mo—O—Si anchoring bonds that likely coexist. In a somewhat contradiction, the characterization of the same materials by O K-edge NEXAFS combined with DFT calculations indicates the predominance of monomeric di-oxo $((Si—O—)_2Mo(=O)_2$ surface species.[83]

The molybdenum oxide loading below the onset of crystalline MoO_3 formation greatly affects the catalytic performance in selective oxidation[7,12,35] and olefin metathesis[65,90]. Consequently, the structural evolution of surface molybdena species at sub-monolayer loadings is of significant relevance to the catalytic performance of supported MoO_3/SiO_2 catalysts. Only a few studies, however, addressed the structural evolution of the dehydrated surface molybdena species on silica as a function of molybdena loading within sub-monolayer coverage (i.e. below the onset of the formation of crystalline MoO_3) in depth.[73,74]

Thus, the important influence of molybdenum oxide loading for supported MoO_3/SiO_2 on catalyst performance still requires further fundamental insights about the surface molybdena molecular structure on silica.

1.4 Outline of the Work

The work investigates propene metathesis over monolayer-type silica-supported molybdenum oxide catalysts. Supported catalysts in a fully oxidized form are chosen due to its high relevance to industrial metathesis catalysts that are repeatedly regenerated by oxidative calcination processes. A series of surface molybdena deposited on mesoporous silica SBA-15 (MoO_x/SBA-15) were used as model catalysts. Silica was chosen as support material due to its inert nature to minimize the complications due to the support material.

Particular interest is devoted to mechanistic understanding into the origin of active carbene sites in supported molybdena catalysts. Understanding on the reason for the minority active sites may pave the way to improve the catalytic performance by rational approaches.

Scheme 1-9 illustrates the overview of the work will be presented. The work addresses quantitative characterization of active sites of olefin metathesis.

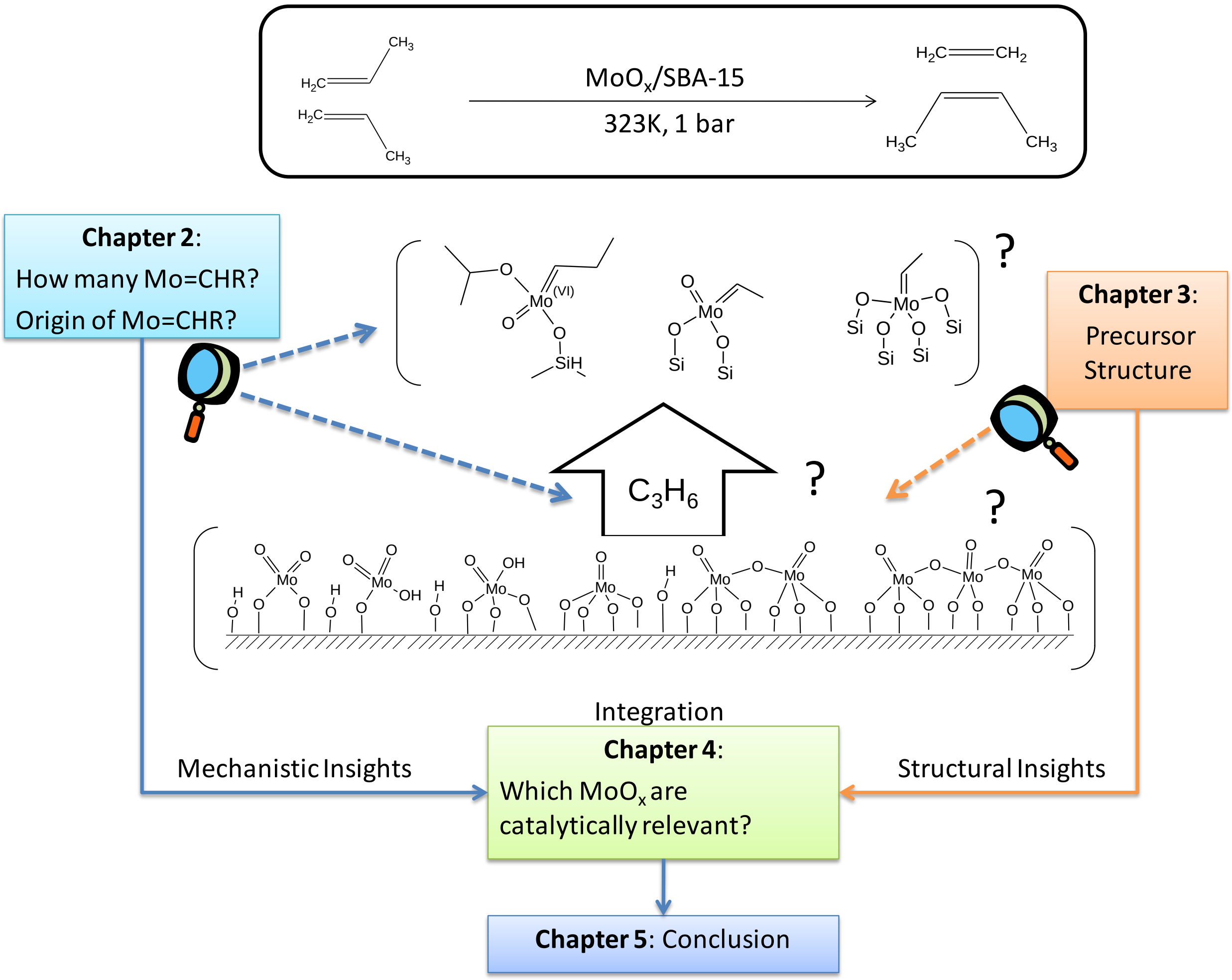
MoOx/SBA-15
323K, 1 bar
Chapter 2:
How many Mo=CHR?
Origin of Mo=CHR?
Chapter 3:
Precursor Structure
C3H6
?
Integration
Mechanistic Insights
Structural Insights
Chapter 4:
Which MoOx are catalytically relevant?
Chapter 5: Conclusion

Scheme 1-9. Illustration of the overview of the present thesis.

In Chapter 2, the origin of the active sites for propene metathesis is quantitatively described.[66] To this end, the catalytic test with an active site counting technique is combined with the propene adsorption study traced by microcalorimety and in situ IR. This work highlights that only a minor fraction of Mo atoms takes part in the catalysis. Based on the data of the propene adsorption studies, functional criteria for the relevant pre-catalyst species are proposed.

In Chapter 3, a comprehensive structural characterization of MoO_x/SBA-15 using multiple spectroscopic techniques is presented.[91] The influence of the density of surface MoO_x species and the consequence to the reactivity is highlighted. The structural information on the surface MoO_x species, that representing an integral picture of all the species present, serves as a basis to discuss structure—reactivity relationships

In Chapter 4, the structure of relevant catalyst precursor species in molybdenum oxides supported on mesoporous silica SBA-15 (MoO_x/SBA-15) is disclosed by investigating the influence of the surface Mo density. The insights gained Chapters 2 and 3 are integrated to discriminate the minor MoO_x species relevant for the catalysis from the major spectator MoO_x species.

Finally, Chapter 5 concludes the significance of the work.

1.5 References

(1) Dumesic, J. A.; Huber, G. W.; Boudart, M. In *Handbook of Heterogeneous Catalysis 2nd ed.*; Wiley-VCH: Weinheim, 2008; pp. 1–15.

(2) Chauvin, Y. *Angew. Chem. Int. Ed.* **2006**, *45*, 3740–3747.

(3) Handzlik, J.; Ogonowski, J. *Catal. Lett.* **2003**, *88*, 119–122.

(4) Ding, J.; Hua, W. *Chem. Eng. Technol.* **2013**, *36*, 83–90.

(5) Mol, J. C.; Leeuwen, P. W. N. M. *Metathesis of Alkens in "Handbook of Heterogeneous Catalysis"*; 2nd ed.; Wiley-VCH,: Weinheim, 2008.

(6) Schrock, R. R. *Acc. Chem. Res.* **1986**, *19*, 342–348.

(7) Schrock, R. R. *Angew. Chem. Int. Ed.* **2006**, *45*, 3748–3759.

(8) Schrock, R. R.; Hoveyda, A. H. *Angew. Chem. Int. Ed.* **2003**, *42*, 4592–4633.

(9) Feher, F. J.; Tajima, T. L. *J. Am. Chem. Soc.* **1994**, *116*, 2145–2146.

(10) Blanc, F.; Rendon, N.; Berthoud, R.; Basset, J.-M.; Coperet, C.; Tonzetich, Z. J.; Schrock, R. R. *Dalton Trans.* **2008**, 3156–3158.

(11) Blanc, F.; Thivolle-Cazat, J.; Basset, J.-M.; Copéret, C.; Hock, A. S.; Tonzetich, Z. J.; Schrock, R. R. *J. Am. Chem. Soc.* **2007**, *129*, 1044–1045.

(12) Vikulov, K. A.; Shelimov, B. N.; Kazansky, V. B. *J. Mol. Catal.* **1991**, *65*, 393–402.

(13) Iwasawa, Y.; Ichinose, H.; Ogasawara, S.; Soma, M. *J. Chem. Soc., Faraday Trans. 1* **1981**, *77*, 1763–1777.

(14) Anpo, M.; Kondo, M.; Kubokawa, Y.; Louis, C.; Che, M. *J. Chem. Soc., Faraday Trans. 1:* **1988**, *84*, 2771–2782.

(15) Rappe, A. K.; Goddard, W. A. *J. Am. Chem. Soc.* **1982**, *104*, 448–456.

(16) Wengrovius, J. H.; Schrock, R. R.; Churchill, M. R.; Missert, J. R.; Youngs, W. J. *J. Am. Chem. Soc.* **1980**, *102*, 4515–4516.

(17) Kress, J. R. M.; Russell, M. J. M.; Wesolek, M. G.; Osborn, J. A. *J. Chem. Soc., Chem. Commun.* **1980**, 431–432.

(18) Mazoyer, E.; Merle, N.; Mallmann, A. de; Basset, J.-M.; Berrier, E.; Delevoye, L.; Paul, J.-F.; Nicholas, C. P.; Gauvin, R. M.; Taoufik, M. *Chem. Commun.* **2010**, *46*, 8944–8946.

(19) Solans-Monfort, X.; Copéret, C.; Eisenstein, O. *Organometallics* **2012**, *31*, 6812–6822.

(20) Mol, J. *J. Mol. Catal. A: Chem.* **2004**, *213*, 39–45.

(21) Debecker, D. P.; Stoyanova, M.; Colbeau-Justin, F.; Rodemerck, U.; Boissière, C.; Gaigneaux, E. M.; Sanchez, C. *Angew. Chem. Int. Ed.* **2012**, *51*, 2129–2131.

(22) Debecker, D. P.; Bouchmella, K.; Stoyanova, M.; Rodemerck, U.; Gaigneaux, E. M.; Mutin, P. H. *Catal. Sci. Technol.* **2011**.

(23) Debecker, D. P.; Schimmoeller, B.; Stoyanova, M.; Poleunis, C.; Bertrand, P.; Rodemerck, U.; Gaigneaux, E. M. *J. Catal.* **2011**, *277*, 154–163.

(24) Debecker, D. P.; Stoyanova, M.; Rodemerck, U.; Gaigneaux, E. M. *J. Mol. Catal. A: Chem.* **2011**, *340*, 65–76.

(25) Debecker, D.; Bouchmella, K.; Poleunis, C.; Eloy, P.; Bertrand, P.; Gaigneaux, E.; Mutin, P. *Chem. Mater.* **2009**, *21*, 2817–2824.

(26) Boer, M.; Dillen, A. J.; Koningsberger, D. C.; Geus, J. W.; Vuurman, M. A.; Wachs, I. E. *Catal. Lett.* **1991**, *11*, 227–239.

(27) Howman, E. J.; Mgcrath, B. P.; Williams, K. V. Catalyst regeneration process. British Patent 1,144,085, March 5, **1969**.

(28) Salameh, A.; Copéret, C.; Basset, J.-M.; Böhm, V. P. W.; Röper, M. *Adv. Synth. Catal.* **2007**, *349*, 238–242.

(29) Chauvin, Y.; Commereuc, D. *J. Chem. Soc., Chem. Commun.* **1992**, 462–464.

(30) Iwasawa, Y.; Hamamura, H. *J. Chem. Soc., Chem. Commun.* **1983**, 130–132.

(31) Iwasawa, Y.; Kubo, H.; Hamamura, H. *J. Mol. Catal.* **1985**, *28*, 191–208.

(32) McCoy, J. R.; Farona, M. F. *J. Mol. Catal.* **1991**, *66*, 51–58.
(33) Farona, M. F.; Tucker, R. L. *J. Mol. Catal.* **1980**, *8*, 85–90.
(34) Grubbs, R. H.; Swetnick, S. J. *J. Mol. Catal.* **1980**, *8*, 25–36.
(35) Laverty, D. T.; Rooney, J. J.; Stewart, A. *J. Catal.* **1976**, *45*, 110–113.
(36) Grünert, W.; Stakheev, A. Y.; Feldhaus, R.; Anders, K.; Shpiro, E. S.; Minachev, K. M. *J. Catal.* **1992**, *135*, 287–299.
(37) Chen, X.; Zhang, X.; Chen, P. *Angew. Chem. Int. Ed.* **2003**, *42*, 3798–3801.
(38) Basrur, A. G.; Patwardhan, S. R.; Was, S. N. *J. Catal.* **1991**, *127*, 86–95.
(39) ECHIGOYA, E.; NAKAMURA, R. *NIPPON KAGAKU KAISHI* **1972**, 500–&.
(40) Engelhardt, J. *J. Mol. Catal.* **1980**, *8*, 119–125.
(41) Shelimov, B. N.; Elev, L. V.; Kazansky, V. B. *J. Catal.* **1986**, *98*, 70–81.
(42) Mol, J. *Catal. Lett.* **1994**, *23*, 113–118.
(43) Vikulov, K. A.; Shelimov, B. N.; Kazansky, V. B. *J. Mol. Catal.* **1992**, *72*, 1–11.
(44) Vikulov, K. A.; Elev, I. V.; Shelimov, B. N.; Kazansky, V. B. *J. Mol. Catal.* **1989**, *55*, 126–145.
(45) Shelimov, B. N.; Elev, I. V.; Kazansky, V. B. *J. Mol. Catal.* **1988**, *46*, 187–200.
(46) Vikulov, K. A.; Shelimov, B. N.; Kazansky, V. B.; Mol, J. C. *J. Mol. Catal.* **1994**, *90*, 61–67.
(47) Anpo, M.; Tanahashi, I.; Kubokawa, Y. *J. Chem. Soc., Faraday Trans. 1:* **1982**, *78*, 2121–2128.
(48) Anpo, M.; Kondo, M.; Louis, C.; Che, M.; Coluccia, S. *J. Am. Chem. Soc.* **1989**, *111*, 8791–8799.
(49) Anpo, M.; Che, M. *Adv. Catal.* **1999**, *44*, 119–257.
(50) Iwasawa, Y. Academic Press, 1987; Vol. Volume 35, pp. 187–264.
(51) Guan, J.; Yang, G.; Zhou, D.; Zhang, W.; Liu, X.; Han, X.; Bao, X. *Catal. Commun.* **2008**, *9*, 2213–2216.
(52) Guan, J.; Yang, G.; Zhou, D.; Zhang, W.; Liu, X.; Han, X.; Bao, X. *J. Mol. Catal. A: Chem.* **2009**, *300*, 41–47.
(53) Li, X.; Zheng, A.; Guan, J.; Han, X.; Zhang, W.; Bao, X. *Catal. Lett.* **2010**, *138*, 116–123.
(54) Pérez-Ramírez, J.; Mondelli, C.; Schmidt, T.; Schlüter, O. F.-K.; Wolf, A.; Mleczko, L.; Dreier, T. *Energy Environ. Sci.* **2011**, *4*, 4786.
(55) McDaniel, M. P. In *Handbook of Heterogeneous Catalysis*; Wiley-VCH Verlag GmbH & Co. KGaA, 2008.
(56) Busca, G.; Lietti, L.; Ramis, G.; Berti, F. *Appl. Catal., B* **1998**, *18*, 1–36.
(57) Centi, G. *Appl. Catal., A* **1996**, *147*, 267–298.
(58) Gregoriades, L. J.; Döbler, J.; Sauer, J. *J. Phys. Chem. C* **2010**, *114*, 2967–2979.
(59) Banares, M. A.; Hu, H. C.; Wachs, I. E. *J. Catal.* **1994**, *150*, 407–420.
(60) Oyama, S. T.; Zhang, W. *J. Am. Chem. Soc.* **1996**, *118*, 7173–7177.
(61) Shokhireva, T. K.; Yurieva, T. M.; Chumachenko, N. N. *React. Kinet. Catal. Lett.* **1980**, *14*, 77–80.
(62) Liu, T.-C.; Forissier, M.; Coudurier, G.; Védrine, J. C. *J. Chem. Soc., Faraday Trans. 1* **1989**, *85*, 1607–1618.
(63) Ohler, N.; Bell, A. *J. Catal* **2005**, *231*, 115–130.
(64) Lou, Y.; Wang, H.; Zhang, Q.; Wang, Y. *J. Catal.* **2007**, *247*, 245–255.
(65) Handzlik, J.; Ogonowski, J.; Stoch, J.; Mikolajczyk, M.; Michorczyk, P. *Appl. Catal., A* **2006**, *312*, 213–219.
(66) Amakawa, K.; Wrabetz, S.; Kröhnert, J.; Tzolova-Müller, G.; Schlögl, R.; Trunschke, A. *J. Am. Chem. Soc.* **2012**, *134*, 11462–11473.
(67) Marceau, E.; Carrier, X.; Che, M.; Clause, O.; Marcilly, C. In *Handbook of Heterogeneous Catalysis*; Wiley-VCH Verlag GmbH & Co. KGaA, 2008.
(68) Thielemann, J. P.; Weinberg, G.; Hess, C. *ChemCatChem* **2011**, *3*, 1814–1821.
(69) Roark, R. D.; Kohler, S. D.; Ekerdt, J. G. *Catal. Lett.* **1992**, *16*, 71–76.
(70) Ward, M. B.; Lin, M. J.; Lunsford, J. H. *J. Catal.* **1977**, *50*, 306–318.
(71) Jeziorowski, H.; Knoezinger, H.; Grange, P.; Gajardo, P. *J. Phys. Chem.* **1980**, *84*, 1825–1829.
(72) Ohler, N.; Bell, A. *J. Phys. Chem. B* **2005**, *109*, 23419–23429.

(73) Thielemann, J. P.; Ressler, T.; Walter, A.; Tzolova-Müller, G.; Hess, C. *Appl. Catal., A* **2011**, *399*, 28–34.

(74) Lee, E. L.; Wachs, I. E. *J. Phys. Chem. C* **2007**, *111*, 14410–14425.

(75) Higashimoto, S.; Hu, Y.; Tsumura, R.; Iino, K.; Matsuoka, M.; Yamashita, H.; Shul, Y. G.; Che, M.; Anpo, M. *J. Catal.* **2005**, *235*, 272–278.

(76) Matsuoka, M.; Kamegawa, T.; Takeuchi, R.; Anpo, M. *Catal. Today* **2007**, *122*, 39–45.

(77) Iizuka, Y.; Sanada, M.; Tsunetoshi, J.; Furukawa, J.; Kumao, A.; Arai, S.; Tomishige, K.; Iwasawa, Y. *J. Chem. Soc., Faraday Trans.* **1996**, *92*, 1249–1256.

(78) Radhakrishnan, R.; Reed, C.; Oyama, S. T.; Seman, M.; Kondo, J. N.; Domen, K.; Ohminami, Y.; Asakura, K. *J. Phys. Chem. B* **2001**, *105*, 8519–8530.

(79) Takenaka, S.; Tanaka, T.; Funabiki, T.; Yoshida, S. *J. Phys. Chem. B* **1998**, *102*, 2960–2969.

(80) Iwasawa, Y.; Ogasawara, S. *J. Chem. Soc., Faraday Trans. 1* **1979**, *75*, 1465–1476.

(81) Chempath, S.; Zhang, Y.; Bell, A. T. *J. Phys. Chem. C* **2007**, *111*, 1291–1298.

(82) Lee, E. L.; Wachs, I. E. *J. Phys. Chem. C* **2008**, *112*, 6487–6498.

(83) Guo, C. S.; Hermann, K.; Hävecker, M.; Thielemann, J. P.; Kube, P.; Gregoriades, L. J.; Trunschke, A.; Sauer, J.; Schlögl, R. *J. Phys. Chem. C* **2011**, *115*, 15449–15458.

(84) Cornac, M.; Janin, A.; Lavalley, J. C. *Polyhedron* **1986**, *5*, 183–186.

(85) Thielemann, J. P.; Kröhnert, J.; Hess, C. *J. Phys. Chem. C* **2010**, *114*, 17092–17098.

(86) Ressler, T.; Walter, A.; Huang, Z.-D.; Bensch, W. *J. Catal.* **2008**, *254*, 170–179.

(87) Handzlik, J. *Chem. Phys. Lett.* **2009**, *469*, 140–144.

(88) Handzlik, J.; Ogonowski, J. *J. Phys. Chem. C* **2012**, *116*, 5571–5584.

(89) Fievez, T.; Geerlings, P.; Weckhuysen, B. M.; De Proft, F. *ChemPhysChem* **2011**, *12*, 3281–3290.

(90) Balcar, H.; Mishra, D.; Marceau, E.; Carrier, X.; Zilková, N.; Bastl, Z. *Appl. Catal., A* **2009**, *359*, 129–135.

(91) Amakawa et al., *submitted*.

Chapter 2: In situ Generation of Active Sites in Olefin Metathesis

Kazuhiko Amakawa, Sabine Wrabetz, Jutta Kröhnert, Genka Tzolova-Müller, Robert Schlögl and Annette Trunschke

Abstract

The depth of our understanding in catalysis is governed by the information we have about the number of active sites and their molecular structure. The nature of an active center on the surface of a working heterogeneous catalyst is, however, extremely difficult to identify and precise quantification of active species is generally missing. In metathesis of propene over dispersed molybdenum oxide supported on silica, only 1.5 % of all Mo atoms in the catalyst are captured to form the active centers. Here we combine infrared spectroscopy *in operando* with microcalorimetry and reactivity studies using isotopic labeling to monitor catalyst formation. We show that the active Mo(VI)-alkylidene moieties are generated *in-situ* by surface reaction of grafted molybdenum oxide precursor species with the substrate molecule itself gaining insight into the pathways limiting the number of active centers on the surface of a heterogeneous catalyst. The active site formation involves sequential steps requiring multiple catalyst functions: protonation of propene to surface Mo(VI)-isopropoxide species driven by surface Brønsted acid sites, subsequent oxidation of isopropoxide to acetone in the adsorbed state owing to the red-ox capability of molybdenum leaving naked Mo(IV) sites after desorption of acetone, and oxidative addition of another propene molecule yielding finally the active Mo(VI)-alkylidene species. This view is quite different from the one-step mechanism, which has been accepted in the community for three decades, however, fully consistent with the empirically recognized importance of acidity, reducibility and strict dehydration of the catalyst. The knowledge acquired in the present work has been successfully implemented for catalyst improvement. Simple heat treatment after the initial propene adsorption doubled the catalytic activity by accelerating the oxidation and desorption-capturing steps, demonstrating the merit of knowledge-based strategies in heterogeneous catalysis. Molecular structure of active Mo(VI)-alkylidene sites derived from surface molybdena is discussed in the context of similarity to the highly active Schrock-type homogeneous catalysts.

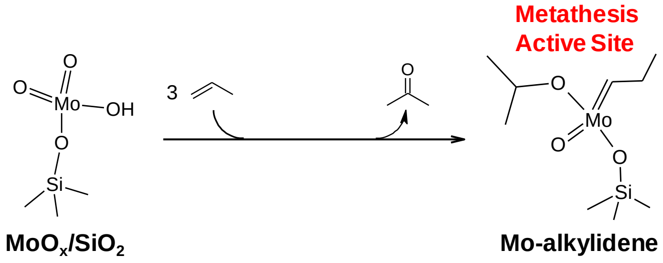

Acknowledgement

The authors thank M. Hashagen for her help with the IR experiments, G. Lorenz for measuring N_2 physisorption, Dr. F. Girgsdies, and E. Kitzelmann for performing XRD analysis, Dr. T. Cotter for Raman experiments, and A. Klein-Hoffmann for XRF measurements. Dr. B. Frank is acknowledged for valuable discussion. This work was conducted in the framework of the COE “UniCat” (www.unicat.tu-berlin.de) of the German Science Foundation. K.A. is grateful to Mitsubishi Gas Chemical Co. Inc. for a fellowship.

2.1 Introduction

Despite the vital branch of industrial production that involves heterogeneous catalysis, underlying research in the entire range of complexity from model studies over single-crystals to the investigation of applied catalyst formulations generally lacks in the most essential information: structure and number of active sites.[1] The termination of the solid surface that represents the catalytic interface is, even for model catalysts, enormously diverse[2] and changes dynamically under reaction conditions.[3,4] Hence, despite significant progress in the field of molecular surface science,[2–4] identification of catalytically relevant surface structures (i.e., active sites) among the existing variety of structures and counting of active sites remains extremely challenging and the catalyst is still a “Holy Grail”.[1] Heterogeneous olefin metathesis is an exceptional case where the general structural motif of active sites is established and thus quantification is accessible.[5] It is generally accepted that metal carbene species (M=CHR) catalyze the reaction according to the metallacyclobutane intermediate mechanism in analogy to homogeneous catalysis.[6] Irrespective of the specific metal carbene structure, quantification of active sites is possible applying post-reaction metathesis using a probe olefin.[5,7,8]

Monolayer-type metal (e.g., Mo, W and Re) oxides deposited on porous supports (e.g. silica alumina and silica-alumina) are important metathesis catalysts.[9–14] The number of active carbene species in these catalysts is at most 2 % of the total metal content.[5,7,8] The low abundance is attributed to multiple geometric configurations allowing only a minor fraction of surface metal oxide species to be transformed into the metal carbene upon contact with the olefin. Understanding the formation mechanism of the active centers and their in-depth structural description will provide the criteria for the relevant precursor structures disclosing access to more sustainability and improved economics via rational catalyst design.

The surface reaction between catalyst precursor and olefin is a demanding process, since the metal oxides need to accomplish carbene synthesis in one-pot and in-situ. Several surface reactions via different intermediates have been proposed (Scheme 2-1): (A) formation of a π-complex between the reacting alkene and a coordinatively unsaturated metal ion followed by a 1,2-hydrogen shift (1,2-hydrogen shift mechanism),[15,16] (B) formation of a π -complex followed the transformation of the π-allyl hydride intermediate into a metallacyclobutane (allyl mechanism),[17–19] (C) formation of a metal-oxo intermediate mediated by a surface Brønsted acid site and subsequent hydrogen shift (H-assisted mechanism),[20] and (D) formation of an oxametallacyclobutane and subsequent elimination of a carbonyl compound (pseudo-Wittig mechanism).[7,21–24]

All reaction pathways, except the pseudo-Wittig mechanism, involve an oxidative addition reaction, in which metal centers are required that can be oxidized by losing two electrons. Since catalyst pretreatment and regeneration of supported metal oxides are typically performed by oxidative treatment at elevated temperature,[9,25] the pseudo-Wittig mechanism would be the only applicable carbene formation route.

In this paper, we describe the origin of active carbene species in propene metathesis over a well-defined model catalyst that contains dispersed molybdenum oxide species supported on meso-structured silica. We investigated propene adsorption using microcalorimetry and *in-situ* IR spectroscopy to trace the genesis of active carbene sites. Our experimental findings deny the pseudo-Wittig mechanism, and provide a new picture, which is fully consistent with the empirical criteria for high-performing catalysts. The established mechanism allows sorting out possible molecular structures of surface oxide precursor species and resulting metal carbene configurations and resulted in the successful implementation of a new catalyst pretreatment procedure. The molecular structure of metal carbene species derived from surface molybdena is discussed in the context of similarities to highly active Schrock-type homogeneous catalysts.

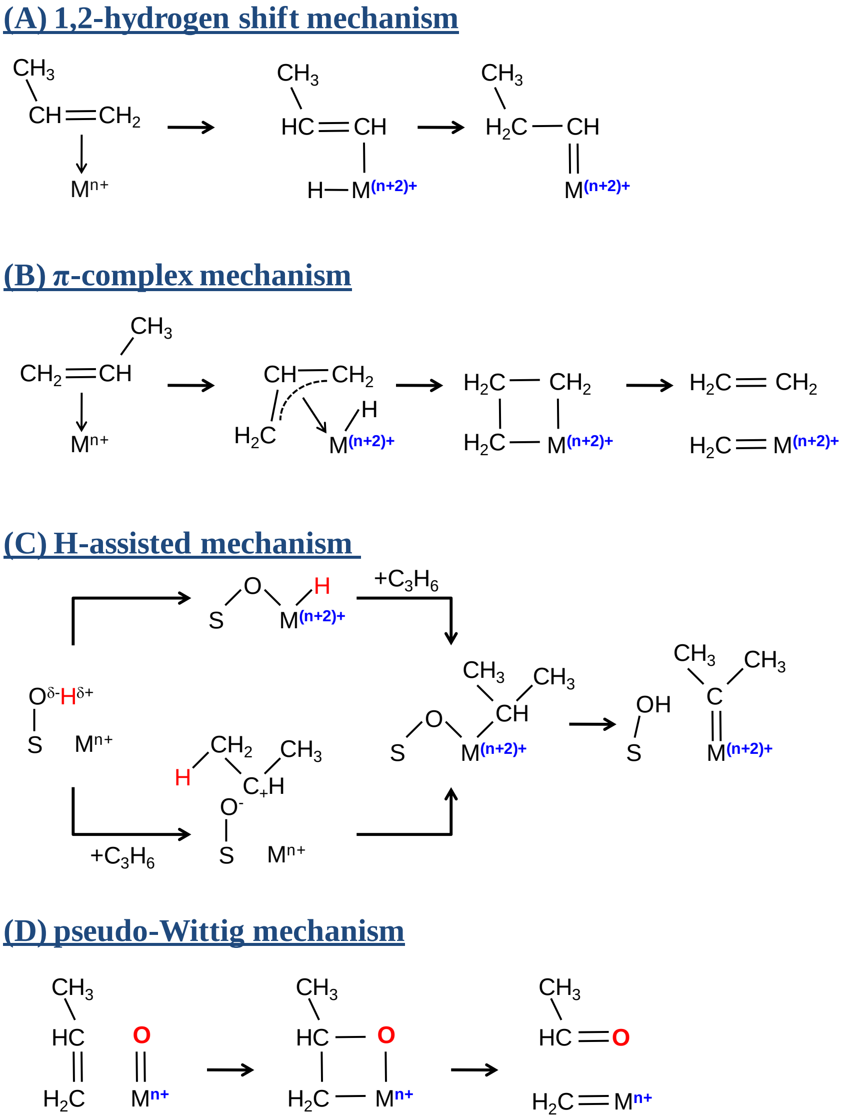

Scheme 2-1. Proposed mechanisms for initial carbene formation upon contact of the catalyst with an olefin. M = active metal center for metathesis reaction, S = support element.

2.2 Experimental Section

The experimental details are presented in the Supporting Information. Below, the most important information is briefly summarized.

2.2.1 Preparation of MoO_x/SBA-15

Molybdenum oxide was dispersed on the surface of mesoporous silica SBA-15[26] applying an anion exchange procedure.[27] According to this, freshly prepared SBA-15 (specific surface area (S_{BET}) = 859 m^2 g^{-1}, internal sample ID 8233) was at first functionalized with propylammonium chloride using (3-aminopropyl)trimethoxysila-ne followed by treatment with hydrochloric acid. Then, anion exchange employing an aqueous solution of ammonium heptamolybdate was performed. After washing and filtration, the material was dried and calcined at 823 K in air to remove organic moieties as well as chlorine and to anchor molybdena species on silica, yielding MoO_x/SBA-15 with actual molybdenum loading of 9.7 % which corresponds to the surface molybdenum density of 1.1 Mo/nm^2 (S_{BET} = 556 m^2 g^{-1}, internal sample ID 8438). The nitrogen adsorption study (Table S2-1, Figure S2-1) confirmed that the cylindrical mesopore structure of the SBA-15 was preserved after the molybdenum loading. Due to the decrease in the S_μ/ S_{BET} ratio (Table S2-1), preferential filling of the micropores with molybdenum oxides is suggested.

2.2.2 Physico-chemical characterization of MoO_x/SBA-15

Nitrogen adsorption was carried out at 77 K to determine specific surface area S_{BET} , micropore surface area $S_{\square}$, pore volume and pore size distribution. X-ray fluorescence (XRF), powder X-ray diffraction (XRD), ultraviolet-visible (UV-vis) diffuse reflectance spectroscopy using SBA-15 as reference, Raman spectroscopy applying an excitation wavelength at 632.8 nm, and laser power of 1.5 mW at the sample position, and diffuse reflectance infrared Fourier transform (DRIFT) spectroscopy using KBr as reference were employed to characterize the catalyst and the support. Prior to Raman, DRIFT, and UV-vis spectroscopy, the samples were pretreated at 823 K (heating rate 10 K·min^{-1}) for 0.5 h in a dry 20 % O_2 in Ar flow. To probe acidity, ammonia adsorption FTIR was performed in transmission mode using self-supporting wafers. Ammonia was adsorbed at 353 K after pretreatment of the samples at 823 K in dry oxygen.

2.2.3 Propene metathesis

Catalytic activity in metathesis of propene to ethene and 2-butenes was measured using a fixed-bed tubular flow reactor at atmospheric pressure. The catalyst bed was pretreated at 823 K for 0.5 h in a flow of a thoroughly dried gas mixture of 20 % O_2 in Ar, cooled to 323 K in the same gas flow, and then flushed with a flow of Ar before reaction. Dried and deoxygenated neat propene was fed to the catalyst bed at 323 K at atmospheric pressure. Inlet and outlet gases were analyzed by on-line gas chromatography. The selectivity to the metathesis products (ethene, *cis*- and *trans*-butene) was higher than 99.5 %, while trace amounts of 1-butene and higher hydrocarbons were detected. The activity is presented as formation rate of the metathesis products (*i.e.*, sum of ethene, *cis*- and *trans*-butene) normalized to the mass of the catalyst. Regeneration of the catalyst was performed using the same procedure as the initial activation.

2.2.4 Post-reaction ethene-d_4 metathesis for active site counting

A modified version of the dynamic active site counting technique originally developed by Handzlik[5] was employed, wherein ethene-d_4 (CD_2=CD_2) was used instead of non-labeled ethene as the probe olefin to titrate metal carbene centers after the catalysis. According to the Chauvin mechanism[6] (Scheme 2-2), equal amounts of molybdenum methylidene (Mo=CH_2) and molybdenum ethylidene (Mo=CH–CH_3) species are present under steady state conditions of propene metathesis on the catalyst surface. The active site counting consists of the quantification of molybdenum-ethylidene (Mo=CH–CH_3) species by titration with ethene-d_4 (CD_2=CD_2), which results in liberation of propene-1,1-d_2 (CD_2=CH–CH_3) via metathesis reaction according to equation (1) and Scheme 2-2.

$$CD_2{=}CD_2 + Mo{=}CH{-}CH_3 \rightarrow CD_2{=}CH{-}CH_3 + Mo{=}CD_2 \qquad (1)$$

Subsequent to the metathesis reaction, the reactor was flushed with flowing Ar, then the feed gas was switched to 1% C_2D_4 in Ar at 323 K. The formation of propene-1,1-d_2 was monitored and quantified with a quadrupole mass spectrometer (QMS200, Balzer) using the signal of m/z = 43. The active site density corresponds to the two-fold amount of liberated propene-1,1-d_2 normalized to the weight of the catalyst.

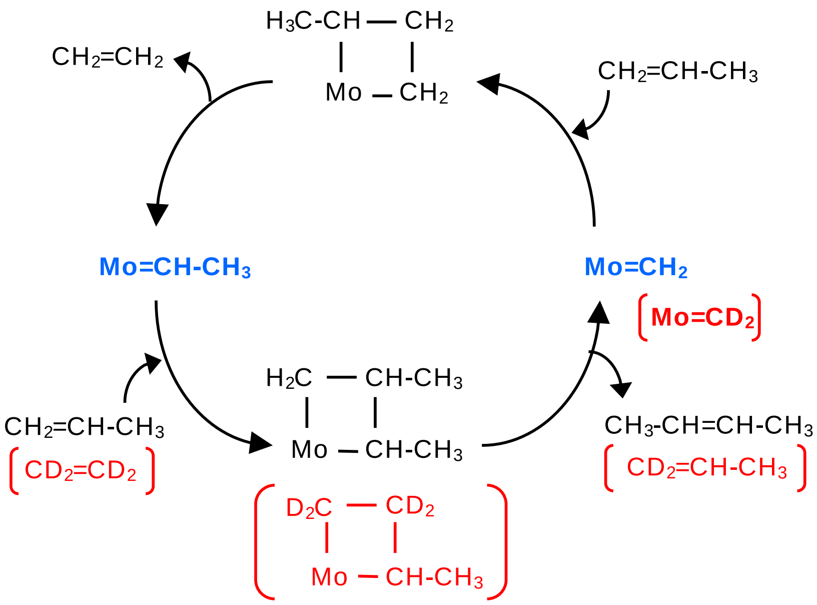

Scheme 2-2. Reaction mechanism of propene metathesis according to Chauvin.[1] The titration reaction of Mo-ethylidene with ethene-*d*$_4$ is described in red color.

2.2.5 Microcalorimetry and in-situ IR spectroscopy of propene adsorption

Microcalorimetry was performed using a MS70 Calvet Calorimeter (SETRAM). The calorimeter was combined with a custom-designed high vacuum and gas dosing apparatus equipped with a volumetric system, which allows measurements of adsorption isotherms. The IR experiments were carried out in transmission mode using a Perkin Elmer 100 FTIR spectrometer equipped with an *in-situ* cell. In both methods, propene was admitted at 323 K after pretreatment of the catalyst in 20 kPa of oxygen at 823 K for 0.5 h and subsequent evacuation at 323 K. Adsorption of C_2D_4 after propene adsorption as well as adsorption of isopropanol and acetone were also conducted in the IR study.

2.3 Results

2.3.1 Physico-chemical characterization of MoO_x/SBA-15

After the oxidative pretreatment, highly dispersed molybdenum oxide species with molybdenum in the highest oxidation state exist on the catalyst surface. The presence of bulk-like MoO_3 and $H_4SiMo_{12}O_{40}$ impurities is excluded not only by the absence of any related reflection peak in the XRD patterns (not shown), but, in particular, by lacking in bands at 816 cm^{-1} for MoO_3, and 909 cm^{-1} for $H_4SiMo_{12}O_4$ [28] in the Raman spectrum (Figure S2-2). The Raman bands near 990 and 970 cm^{-1} due to molybdenum-oxygen stretching vibrations (νMo=O) (Figure S2-2) as well as the absorption bands in the UV-vis spectrum near 225 and 270 nm (ligand to metal charge transfer from O^{2-} to Mo^{6+}) (Figure S2-3) are typical fingerprints indicating highly dispersed molybdenum oxide surface species in the dehydrated state.[28–31] The absence of absorption due to d-d transitions of molybdenum ions (> 500 nm)[32] evidences that molybdenum is exclusively present as Mo(VI).

The DRIFT spectrum (Figure 2-1A) of MoO_x/SBA-15 shows significantly weaker intensity of the band due to isolated Si-OH (silanol) groups[33] at 3745 cm^{-1} than bare SBA-15, indicating that loading of molybdenum involves consumption of surface silanol groups to yield anchored surface molybdate species. Moreover, the DRIFT spectrum of MoO_x/SBA-15 features a broad

OH stretching mode at 3620 cm^{-1}, which clearly indicates the occurrence of hydrogen-bonded OH groups when molybdenum is loaded onto the silica SBA-15 surface. The latter band is attributed to a superposition of O-H stretching vibrations in molybdenol (Mo-OH) groups involved in hydrogen bonding to neighboring oxygen atoms, *e.g.*, in O=Mo–OH moieties and silanol groups that undergo hydrogen interaction with oxygen atoms of molybdena species in the vicinity.

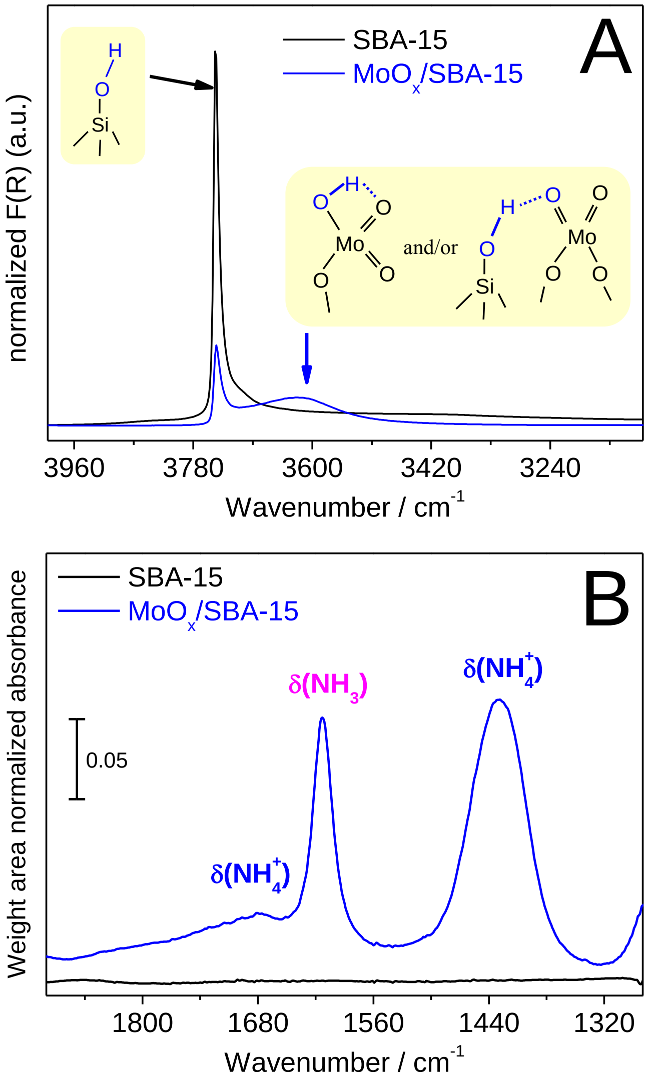

Figure 2-1. IR spectra of MoO$_x$/SBA-15 and SBA-15; (A): DRIFT spectra measured at room temperature after pretreatment in 20% O$_2$ at 823 K for 0.5 h. (B): Transmission IR spectra recorded after adsorption of ammonia at p=10 hPa and subsequent evacuation at 353 K. The catalyst was pretreated in 20 kPa of O$_2$ at 823 K for 0.5 h. The spectrum before ammonia dosing was used as background.

The adsorption of ammonia revealed the presence of both Brønsted and Lewis acid sites. Whereas almost no ammonia adsorbs on SBA-15 (black line in Figure 2-1B), the IR spectrum of MoO_x/SBA-15 after ammonia adsorption (blue line in Figure 2-1B) shows the presence of ammonium ions formed by reaction of NH_3 with Brønsted acid sites (1678 cm^{-1} (δ_{sym} NH) and 1431 cm^{-1} ($\delta_{as}NH_4^+$)) and molecular ammonia coordinated at Lewis acid sites (1613 cm^{-1} (δ_{as} NH_3)).[33] The detection of Brønsted acid sites indicates either the presence of molybdenol (Mo–OH) groups or the formation of acid Si-OH groups by interaction of terminal silanol groups with surface molybdenum oxide species. The broad OH stretching mode at 3620 cm^{-1} detected in MoO_x/SBA-15 (Figure 2-1A) may contain contributions from either of them. Lewis acid sites are considered as coordinatively unsaturated Mo(VI) centers. Irrespective of the specific assignment, ammonia adsorption clearly indicates the generation of acid sites by introduction of molybdenum oxide species into the pores of SBA-15.

In summary, the MoO_x/SBA-15 model catalyst is characterized by extensive coverage of the silica surface with highly dispersed MoO_x species containing Mo in its highest oxidation state, and comprising Mo oxo (Mo=O) moieties. The presence of Brønsted acid sites and coordinatively unsaturated Mo(VI) species (Lewis acid sites) is evidenced by ammonia adsorption IR.

2.3.2 Propene metathesis and post-reaction active site counting

Figure 2-2 shows the propene metathesis activity of MoO_x/SBA-15 at 323 K as a function of time on stream. The metathesis activity gradually develops with time on stream, reaching 7.5 mmol g^{-1} h^{-1} (corresponds to apparent TOF of 2.06 $mmol_{propene}$ mol_{Mo}^{-1} s^{-1}) after 15 h. The metathesis activity and apparent TOF are rather low comparing to the recent most successful silica-alumina supported molybdena catalysts reported by Debecker et al.[11,12] The gradual evolution of the activity suggests slow generation and continuous accumulation of active molybdenum carbene centers.[34] The catalyst is regenerable with an excellent reproducibility in the reactivity (Fig. 2).

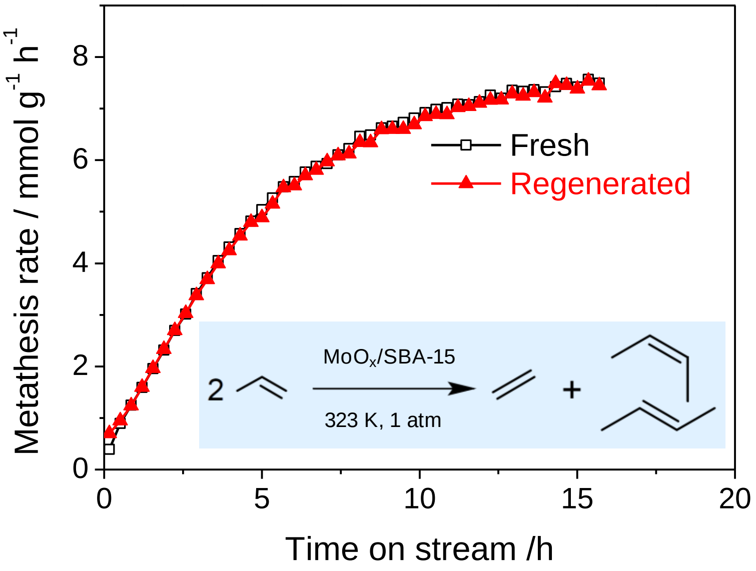

Figure 2-2. Propene metathesis activity of MoO_x/SBA-15 at T=323 K and a contact time of 0.75 s g ml^{-1}. The catalyst was activated in a 20% O_2 flow at 823 K for 0.5 h. Regeneration was performed applying the same procedure as the initial activation (823 K in 20% O_2 for 0.5 h).

Table 2-1. Summary of propene metathesis activity and post-reaction active site counting over MoO_x/SBA-15.

Catalyst	Activity[a] (mmol g^{-1} h^{-1})	Active sites[b] (μmol g^{-1})	Active site fraction [c] (atom%)	TOF[d] (s^{-1})
Fresh	7.50	15.0	1.5	0.14
Regenerated	7.44	14.0	1.4	0.15

[a] propene metathesis activity measured immediately before the post-reaction active site counting procedure (TOS=15 h) for MoO_x/SBA-15 (see also Figure 2-2); Metathesis reaction condition: T=323 K, p= 0.1 MPa, contact time=0.75 s ml g^{-1}, pretreatment or regeneration at T=823 K for 0.5 h under 20% O_2-Ar flow. [b] the two fold amount of evolved propene-d_2 upon ethene-d_4 dosing after the propene metathesis. [c] active site density divided by Mo loading. [d] metathesis activity divided by active site density.

Table 2-1 summarizes the data on the metathesis activity and the post-reaction active site counting as well as the derived active site fraction and turn over frequencies. The active site density corresponds to about 1.5 % of total molybdenum atoms in the catalyst. The value is similar to reported data on MoO_x/Al_2O_3[5] and ReO_x/Al_2O_3.[7,8]

2.3.3 Microcalorimetry of propene adsorption at the reaction temperature

To gain insight into the process of carbene site formation, we studied propene adsorption by microcalorimetry at the reaction temperature. The metathesis reaction does not disturb the calorimetric measurement, because (1) the heat of reaction is very small (ΔH_{323K} = 1.2 kJ $mol_{propene}^{-1}$) and, consequently, thermal contributions from the catalytic reaction can practically be neglected in the measurement of the heat of adsorption, and (2) the total number of molecules remains constant through the reaction, which allows volumetric determination of the amount of adsorbed propene molecules because the total pressure is not falsified due to the reaction. This situation opens up the opportunity to trace thermal events, which are presumably relevant to the genesis of activity.

Figure 2-3 A and B report the differential heat of propene adsorption on MoO_x/SBA-15 (A) and SBA-15 (B) as a function of propene coverage. While the differential heat measured on SBA-15 is slightly higher than the heat of propene condensation and remains constant at 23±1 kJ mol^{-1} with increasing coverage (Figure 2-3B), the MoO_x/SBA-15 catalyst shows significantly higher heats of adsorption up to certain levels of coverage (Figures 2-3A). The catalyst MoO_x/SBA-15 (Figure 2-3A) is characterized by a plateau up to 16 μmol g^{-1}, which corresponds to 1.6 % of total molybdenum atoms in the catalyst. The differential heat of propene adsorption in this range (78±2 kJ mol^{-1}) is quite high, which indicates strong adsorption of propene on energetically homogeneous adsorption sites. Further increase in surface coverage leads to a gradual decrease in the heat of adsorption up to a coverage of 29 μmol g^{-1} that corresponds to 2.9 % of total molybdenum atoms in the catalyst where another plateau is approached. The heat of adsorption (22 kJ mol^{-1}) is close to the value measured on SBA-15 (Figure 2-3B). Notably, the concentration of strong adsorption sites (16 μmol g^{-1} within the first plateau) coincides with the active site density estimated by active site counting after the catalysis (15 μmol g^{-1}, Table 2-1). The consistency strongly suggests the relevance of sites titrated by propene adsorption in the microcalorimetric experiment to the genesis of active carbene species.

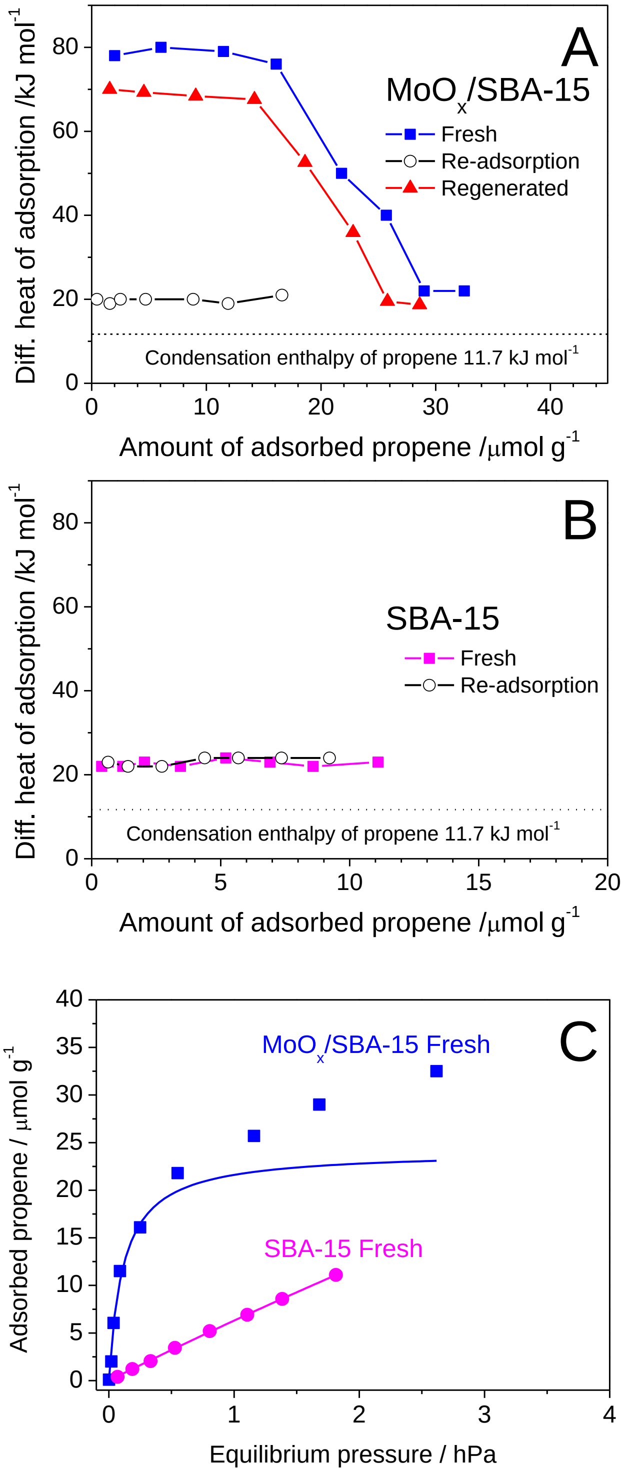

Figure 2-3. Propene adsorption studied by microcalorimetry at 323 K on MoO$_x$/SBA-15 and SBA-15 pretreated in O_2 at 823 K and at 20 kPa for 0.5 h; differential heat as a function of the amount of adsorbed propene on MoO$_x$/SBA-15 (A) and SBA-15 (B); re-adsorption profiles were measured after evacuation at ~10^{-3} Pa for 2 h; the regeneration was performed applying the same procedure as the initial pretreatment (in O_2 at 823 K and at 20 kPa for 0.5 h); the adsorption isotherm of propene over MoO$_x$/SBA-15 and SBA-15 measured at 323 K is shown in (C); measured data points up to an amount of adsorbed propene of 16 μmol g^{-1} were used to fit the data of MoO$_x$/SBA-15 based on the Langmuir equation.

Strong interaction of propene with MoO_x/SBA-15 is also reflected in the Langmuir constant. The Langmuir adsorption equation has been formally applied to model the measured adsorption isotherms (lines in Figure 2-3C) neglecting that chemical transformations are probably involved in adsorption of propene on MoO_x/SBA-15 using equation (2),[35]

$$N_{ads} = N_{mono}\frac{Kp}{1+Kp} \qquad (2)$$

where N_{ads} is the amount of propene adsorbed at equilibrium pressure p, N_{mono} is the monolayer adsorption capacity, and K is the Langmuir constant, which is the ratio of the rate constant of adsorption and desorption describing the strength of adsorption. The fit curve for the MoO_x/SBA-15 depicted in Figure 2-3C deviates from the data points above ~20 µmol g^{-1}, which indicates that the propene uptake in this high coverage region is predominantly due to a different type of adsorption mechanism. The part of the adsorption isotherm curve above 20 µmol g^{-1} is roughly parallel to the SBA-15 (Figure 2-3C), suggesting that a same type of physisorption onto silica species and/or inert molybdenum oxide species become predominant at the higher coverage. This view is also supported by the faster decay of the heat evolution upon adsorption (*vide infra*). A Langmuir fit taking into account data of propene adsorption on MoO_x/SBA-15 up to a coverage of ~ 16 µmol g^{-1}, where a quasi-constant and high heat of adsorption was found, yielded K = 8.6±2.8 hPa^{-1}, whereas the fit for propene adsorption on SBA-15 including the entire data points resulted in a much lower value of K = 0.039±0.001 hPa^{-1}. These results clearly indicate strong adsorption of propene on a small fraction of molybdenum oxide surface sites on MoO_x/SBA-15.

Propene adsorption on SBA-15 is fully reversible. In contrast, the re-adsorption profile measured on MoO_x/SBA-15 after evacuation (Figure 2-3A) was almost identical to the adsorption profile measured on bare SBA-15 (Figure 2-3B), which evidences again strong and irreversible adsorption of propene on MoO_x sites during the first adsorption cycle. In accordance with this observation, the integral heat of desorption measured during the evacuation after the first adsorption steps was much lower than the integral heat of adsorption. Apparently, irreversible surface reactions happen, which contribute substantially to the heat signal measured during the first propene adsorption experiment. These reactions are most likely related to the formation of the active sites.

Evaluation of the kinetics of the heat evolution allows further insight into the adsorption process. The response of the exothermic signals in the range of the first plateau of propane adsorption on MoO_x/SBA-15 (at coverage of 6 µmol g^{-1}) shows an extremely slow decay continuing for ~7 h (Figure 2-4A). In contrast, the evolution of heat at higher coverage (Figure 2-4B), where the differential heat of adsorption is slightly higher than the heat of propene adsorption measured on SBA-15 (at a coverage of 26 µmol g^{-1}), is relatively fast completed. The initial decay of the heat signals was evaluated applying an exponential decay model as described in equation (3),

$$I(t) = I_0 \exp(-t/\tau) \qquad (3)$$

wherein $I(t)$ is the net thermosignal intensity at time t, I_0 is the maximum of the net thermosignal intensity after an increment of dosing pressure, t is the elapsed time after reaching the I_0, and τ is the time constant. The calculated time constants are about 3000 and 255 s for 6 and 26 µmol g^{-1}, respectively (Figure 2-4). The latter value approximately matches the time constant of the calorimeter used, indicating weak and reversible adsorption. The significantly increased time constant at low coverage indicates that the adsorption is superimposed by slow surface reactions. The deviation of the fit curve at prolonged times (Figure 2-4A) is due to the occurrence of secondary exothermic processes that are supposed to be consecutive reactions of adsorbed species. The deviation is less pronounced for the adsorption at 26 µmol g^{-1} reflecting the predominance of reversible adsorption in accordance with the moderate differential heat of adsorption (40 kJ mol^{-1}). These observations indicate that the strong and irreversible adsorption involves slow and probably consecutive reactions on the surface, which might be related to the genesis of the molybdenum carbene sites. The sustaining generation of heat for ~7 h bears resemblance to the slow evolution of metathesis activity over 10-15 hours, which are required to reach steady state activity (Figure 2-2).

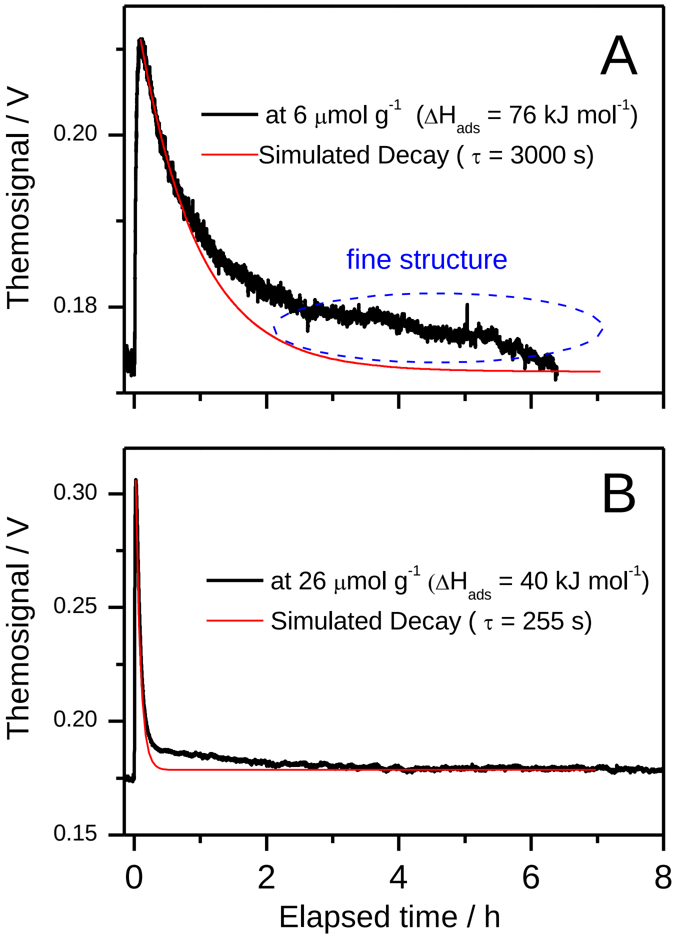

Figure 2-4. Evolution of the heat signals upon propene adsorption at 323 K on MoO_x/SBA-15 (pretreated in 20% O_2 at 823 K for 0.5 h) at the cumulative adsorption amount of 6 (A) and 26 µmol g^{-1} (B)

2.3.4 IR study of propene and subsequent ethene-d_4 adsorption

Microcalorimetry revealed irreversible and possibly reactive adsorption of propene on MoO_x/SBA-15 up to a certain level of coverage. The chemical reactions are presumably associated with the genesis of the active carbene sites. We employed *in-situ* IR spectroscopy at the same temperature (323 K) to obtain information about the nature of the surface species involved in the processes occurring upon propene adsorption on the MoO_x/SBA-15 surface. The equilibrium pressure of propene was adjusted initially to p = 3 hPa, which corresponds to complete coverage of strong adsorption sites according to the results of microcalorimetry. A reference experiment using SBA-15 showed no adsorbed species that persist after evacuation, which is consistent with the reversible adsorption found by the microcalorimetry experiment.

2.3.5 Progressive formation of isopropoxide and acetone upon propene adsorption

After propene dosing for 0.5 h and subsequent evacuation, the spectrum (magenta line in Figure 2-5A) features bands due to the stretching modes of C-H bonds in methyl groups at 2983, 2939, and 2880 cm^{-1}, and the corresponding deformation modes at 1465, 1455, 1390, and 1377 cm^{-1}. Notably, characteristic C-H stretching bands of olefinic methylene species[36,37] at ~3010 and at ~3090 cm^{-1} as well as C=C stretching mode at 1610~1650 cm^{-1} are not detected, indicating the absence of C=C bonds in strongly adsorbed species that persist evacuation at 323 K. Thus, strong adsorption involves a reaction, which leads to conversion of the olefinic C=C bond in propene. The detected peak patterns agree well with the bands of isopropoxy species adsorbed on the surface of metal oxides.[38–41] In fact, adsorption of isopropanol on MoO_x/SBA-15 results in a quite similar spectrum (Figure 2-S4 (1)), confirming that isopropoxide is the major species formed by adsorption of propene at 323 K on MoO_x/SBA-15. The transformation of propene into isopropoxide happens via protonation of the olefin by acidic surface OH groups. Accordingly, the detection of surface isopropoxy species confirms the presence of Brønsted acid sites on the surface of MoO_x/SBA-15 in agreement with ammonia adsorption (Figure 2-1B) and clearly indicates involvement of Brønsted acidity in the surface reactions of adsorbed propene.

After the 18 h of propene dosing and subsequent evacuation, (blue line in Figure 2-5A), all the bands became considerably more intense, which evidences progressive slow adsorption as found by microcalorimetry. Moreover, new band at 1668 and 1417 cm^{-1} are clearly visible, which can be assigned to the C=O stretching mode of the carbonyl group and the deformation mode of methyl groups, respectively, of coordinated acetone.[38,40,42,43] Occurrence of these bands upon acetone adsorption (Figure S2-4 (3)) as well as the development of a similar carbonyl stretching band at 1673 cm^{-1} upon prolonged (18 h) isopropanol adsorption (Figure S2-4 (2)) corroborate the formation of acetone by oxidation of isopropoxide surface species. The modest intensity of the carbonyl band at 1668 cm^{-1} (blue line in Figure 2-5A) compared to the spectrum of acetone adsorption (Figure S2-4 (3)) suggests that only a fraction of the isopropoxide species undergoes oxidation into acetone. Formation of acetone implies the involvement of surface molybdenum oxide species acting as oxidizing agent and resulting in partial reduction of molybdenum on the silica surface. Essentially the same observation has been reported for alumina-supported molybdena catalysts. The formation of isopropoxide and the consecutive oxidation to acetone upon propene adsorption takes place on MoO_x/Al_2O_3 even at room temperature.[40,41] Besides the formation of acetone, the broad peaks arising in the range 1550-1650 cm^{-1} and below 1490 cm^{-1} (Figure 2-5A) imply the gradual accumulation of various other surface deposits, such as carboxylates[44] or enolates.[45]

2.3.6 Validation of metathesis activity of the resulting surface

The metathesis activity of the resulting surface was confirmed by testing the reactivity with ethene-d_4. After propene adsorption for 18 h and subsequent evacuation, an equilibrium pressure of p = 3 hPa ethene-d_4 was adjusted at 323 K in the IR cell. Under these conditions, surface Mo-alkylidene species, if present, should be transformed into deuterium-labeled Mo-methylidene species (eq (1)). The spectrum presented in Figure 2-5B was obtained after dosing ethene- d_4 followed by evacuation using the spectrum before the ethene-d_4 dosing (blue line in Figure 2-5A) as background. The negative peaks due to C-H stretching modes at 2984, 2939, 2898 and 2877 cm^{-1} and C-H deformation modes at 1468, 1389 and 1375 cm^{-1}, and the appearance of C-D stretching modes at 2100-2300 cm^{-1} (Figure 2-5B inset) evidence the exchange of stable (not removable by evacuation) surface organic species into ethene-d_4 originated surface species most likely due to a metathesis reaction catalyzed by surface Mo-carbene sites. The negative peaks due to C-H stretching modes agree well with the bands of Mo-ethylidene species at 2985, 2910, 2890 and 2850 cm^{-1},[46] indicating the presence of this species before dosing of ethene-d_4. The positions of the observed C-D stretching modes at 2230 and 2160-2200 cm^{-1} are close to those reported for deuterated methylidene ($Mo=CD_2$) species detected on MoO_x/SiO_2 (2245 and 2160 cm^{-1}),[47] which further corroborates the presence of Mo-carbene sites on the surface of MoO_x/SBA-15 and the metathesis activity of the catalyst surface, which has been generated during the IR experiment of propene adsorption. The intensities of the negative peaks due to C-H stretching modes (Figure 2-5B) are low compared to the original spectrum (blue line in Figure 2-5A), indicating that the concentration of carbene species is low in contrast to the concentration of other surface species, *e.g.*, the remaining isopropoxide species.

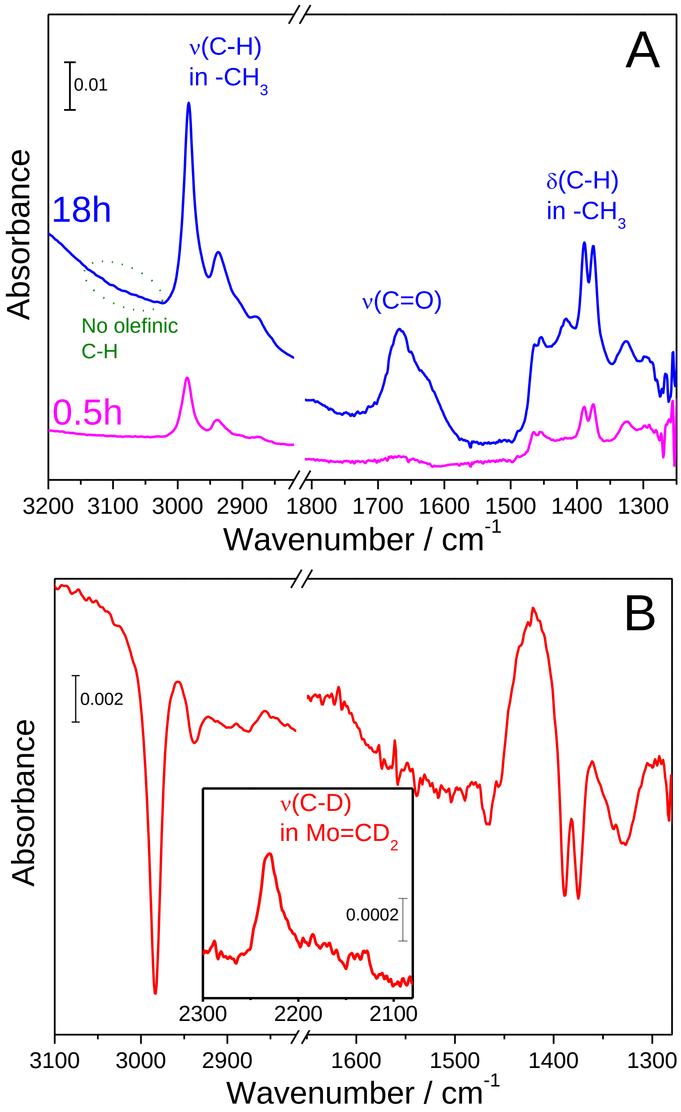

r

Figure 2-5. IR spectra recorded after propene adsorption on MoO_x/SBA-15 for 0.5(magenta) and 18 h (blue) and subsequent evacuation (A). The difference spectrum shown in (B) was obtained by subsequent ethene-d_4 dosing at p=3 hPa and T=323 K for 18 h and evacuation using the blue spectrum in (A) as subtrahend. Propene was dosed at 323 K and 3.0 hPa after the pretreatment in 20 kPa of O_2 at 823 K for 0.5 h. The inset in (B) shows the frequency range of the C-D stretching.

2.3.7 Summary of the propene adsorption IR study

The IR study revealed that adsorbed propene is slowly protonated on the catalyst surface to yield isopropoxide, which undergoes oxidation to give acetone. These reactions require bi-functionality of the catalyst in terms of concurrent abundance of Brønsted acid sites and redox active molybdena centers. The evolution of Mo-carbene species evidenced by ethene-d_4 adsorption indicates that these processes are related to the genesis of the active Mo-carbene sites. We relate the very slow generation of isopropoxide and acetone as observed by IR spectroscopy to the prolonged heat generation registered in the microcalorimetric experiment (Figure 2-3A) and to the retarded evolution of the metathesis activity (Figure 2-2).

2.4 Discussion

2.4.1 Quantity and quality of active carbene sites

Investigation of MoO_x/SBA-15 by post-reaction active site titration detected the expected metathesis product (*i.e.*, CD_2=CH-CH_3) formed by reaction of surface Mo-ethylidene species with the probe ethene-d_4 (CD_2=CD_2) (Table 2-1), providing evidence that the Chauvin mechanism (Scheme 2-2) is operative over supported molybdena catalysts.

The titration experiment reveals that only 1.5 % of the molybdenum atoms in the catalyst belong to the pool of active carbene centers. Accordingly, it is extremely challenging to establish structure-activity relationships, because structural characterization generally displays an average picture of the variety of species usually present on the catalyst surface. A strategy, which allows selective detection of the essential information is certainly necessary to distinguish catalytically relevant surface sites from spectator species. The present approach takes these considerations into account and tackles the task by applying a combination of microcalorimetry and IR spectroscopy for investigation of propene adsorption on the catalyst surface at the reaction temperature.

Quantification of active sites by titrative metathesis allows the determination of an average intrinsic metathesis activity per active site, *i.e.*, the measurement of turnover frequencies in the strict sense of molecular catalysis. This is a rare case in heterogeneous catalysis due to frequently encountered difficulties in quantification of active sites, which often lead to the wrong assumption that all atoms of a specific catalyst component contribute to the activity. Accordingly, the data in the literature, which allow a reliable comparison of turnover frequencies for MoO_x/SBA-15 catalysts, are rather limited. Instead, homogeneous catalysts anchored on silica may represent suitable reference systems. The optimized Schrock-type Mo-alkylidene complexes, which are among the most active propene metathesis catalysts, show, when anchored on silica, much higher turnover frequencies (*e.g.*, TOF of 1.9 s^{-1} at 303 K) than MoO_x/SBA-15 (~0.15 s^{-1}, Table 2-1).[48] The difference probably arises from a different geometric and electronic structure of the carbene centers. Substantial influence of the structure on the activity has been demonstrated for structurally well-defined catalysts prepared by grafting of organometallic complexes on silica.[49] The structure sensitivity has been confirmed by theoretical studies, in which various anchoring configurations of oxo-molybdenum carbene sites on silica[50] and alumina were considered.[51–55]

MoO_x/SBA-15 contains molybdenum atoms in a multitude of different geometric arrangements, which are hardly distinguishable by spectroscopic techniques. Therefore, we follow a bottom-up approach starting with the elucidation of the building mechanism of the active carbene sites, which comprise only the minor fraction of Mo atoms that are characterized by a specific and catalytically favorable local geometric environment.

2.4.2 Formation route of carbene sites

The genesis of Mo-carbene sites is a consequence of the reaction between surface molybdena species and the reactant propene.

The pseudo-Wittig mechanism (Scheme 2-1D) has persisted to be the only mechanism for three decades since Rappe and Goddard proposed it based on purely theoretical considerations. However, the detected high heat of propene adsorption (78±2 kJ mol^{-1}, Figure 2-3A) is not in accord with this route. The pseudo-Wittig mechanism has estimated significantly positive Gibbs energies for the carbene formation, especially in the case of supported molybdena catalysts[56–58] (*e.g.*, ΔG_{300} = +16 kJ mol^{-1} for the reaction of Cl_2MoO_2 and ethene; estimated by an *ab initio* calculation[21]; ΔEnergy = ca. +60 kJ mol^{-1} for the reaction of a supported molybdena (Mo(VI)-oxo centers in a Beta zeolite cluster with propene; estimated by a DFT calculation[57]). Accordingly, the pseudo-Wittig mechanism is a thermodynamically unfavorable route. In previous experimental reports concerning fully oxidized supported W[24] and Re[7] catalysts, the detection of carbonyl compounds during the genesis of metathesis activity and the dependency of the reactivity from the type of reacting olefin have been considered as experimental proofs for the pseudo-Wittig mechanism.[7,24] Based on our calorimetric and spectroscopic findings during the genesis of metathesis activity, we propose an alternative mechanism (Scheme 2-3), which is not in contradiction to the reported experimental results mentioned above.

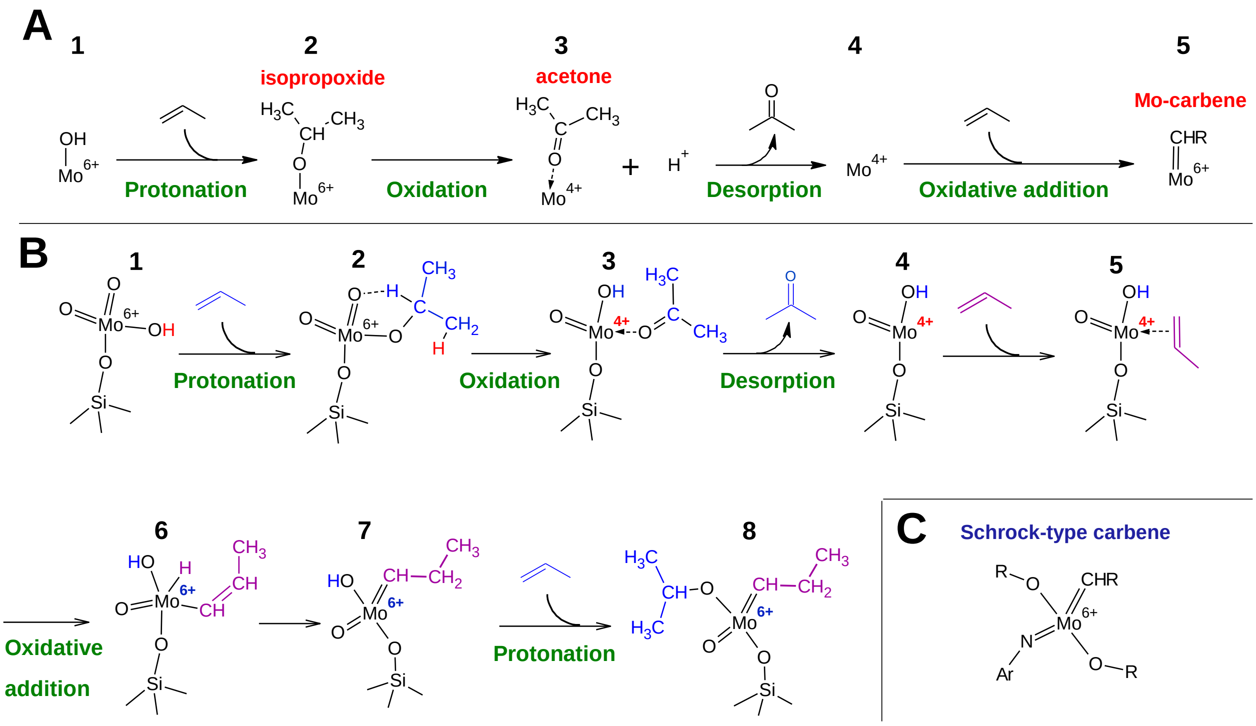

Scheme 2-3. Proposed route for the carbene formation starting from a Mo(VI) site upon interaction with two propene molecules: general scheme (A), a scheme assuming a tetrahedral dioxo structure as the pre-catalyst (B) compared to the structure of reference Schrock-type homogeneous catalysts (C).[66]

On the surface of MoO_x/SBA-15, molybdenum occurs in its highest oxidation state in form of highly dispersed surface molybdenum oxide species that comprise terminating oxo (Mo=O) groups. Brønsted acidity, probably originated by Mo-OH groups, and Lewis acidity due to coordinatively unsaturated Mo(VI) centers are found to be present as well (Section 3.1).

The quantitative agreement between the concentrations of strong adsorption sites found by microcalorimetry (2-3A) and the post-reaction active site titration (Table 2-1) suggests that the strong exothermic adsorption of propene on the catalyst is in relationship with the genesis of the carbene sites.

IR spectroscopy provides the explanation for the exothermic events during the propene adsorption. The IR spectra for propene and subsequent ethene-d_4 adsorption revealed the slow formation of isopropoxy species followed by oxidation to coordinated acetone (Figure 2-5A) during the genesis of metathesis activity (Figure 2-5B). Experimental[59] and theoretical[59–61] studies have shown that formation of surface isopropoxide readily occurs by protonation upon adsorption of an olefin on Brønsted acidic catalysts with the heat of olefin adsorption of about 80-100 kJ mol^{-1}. These values agree well with the differential heats of propene adsorption measured by microcalorimetry (Figure 2-3). Having evidence for the presence of Brønsted acid sites in the catalyst (Figure 2-1B, Figure 2-5A), we consider that the major event upon propene adsorption is the formation of isopropoxide species through protonation of the olefin by Brønsted acid sites.

The subsequent event detected by IR spectroscopy during the genesis of the metathesis activity is the formation of coordinated acetone (Figure 2-5A). Although the formation of carbonyl compounds is in line with the pseudo-Wittig mechanism (Scheme 2-1D), it is rather reasonable to consider that carbonyl compounds are formed through oxidation of the isopropoxy intermediate on the redox-active MoO_x/SBA-15 catalyst. It is well known that the oxidation of propene to acetone via the isopropoxy intermediate takes place with acidic molybdena based mixed oxide catalysts at relatively low (393-473 K) temperature.[62] We consider that the same type of reaction occurs in the present case. The formation of a carbonyl compound should involve the reduction of molybdenum centers, *i.e.*, Mo(VI) to Mo(IV), if the reduction takes place at a single molybdenum atom.

Importantly, coordinatively unsaturated monomeric Mo(IV) centers are known to be good precursors of Mo-carbene sites that are formed via an oxidative addition of the propene molecule to Mo(IV) surface species.[15,16,63–65] Actually, most of highly active molybdenum oxide-based metathesis catalysts are prepared via efficient creation of coordinatively unsaturated monomeric Mo(IV) centers by a reductive pretreatment of the catalyst.[46,63] This inspires us to propose a new route for the carbene formation presented in Scheme 2-3A.

The first step involves the reduction of Mo(VI) to Mo(IV) via formation of an isopropoxy species by an acid-base reaction and the subsequent oxidative dehydrogenation of the isopropoxide intermediate to acetone (Scheme 2-3A, 1 to 3). The second step includes desorption of acetone followed by an oxidative addition of another propene molecule to the Mo(VI) center to form the active Mo(VI)-carbene species (Scheme 2-3A, 3 to 5). Consequently, bi-functionality of the catalyst comprehending Brønsted acidity and the ability to accomplish oxidative dehydrogenation is considered as an essential requirement for the first step. The carbene formation via an oxidative addition of a propene molecule to Mo(VI) is a well established event,[15,16,63–65] which likely takes place via 1,2-hydrogen shift mechanism (as shown in the Scheme 2-1A). The positive effect of acidity in olefin metathesis is well recognized by the observation that the use of acidic silica-alumina supports yields relatively active catalysts.[67–69] It is also known that reducibility is relevant to the metathesis activity.[70] The present proposal is quite consistent with these facts and provides mechanistic explanation for the role of acidity and reducibility. The slow development of the metathesis activity (Figure 2-2) compared to silica-alumina supported molybdena catalysts[10–12] might be related to the limited acidity of

MoO_x/SBA-15. Considering progressive slow formation of isopropoxide and acetone in the *in-situ* IR experiment, these surface reactions (Scheme 2-3A 1 to 3) most likely represent the kinetic bottleneck of the evolution of active carbene sites. It is noted that the color of the catalyst bed remained white during the metathesis reaction, suggesting the absence of reduced molybdenum centers. Probably, the desorption of acetone and subsequent oxidative addition of propene (Scheme 2-3A 3 to 5) are much faster than the foregoing steps in the case of MoO_x/SBA-15, which gives rise to a very small concentration of the Mo(IV) intermediate.

Besides Brønsted acidity and reducibility, the formation of Mo-carbene species requires desorption of the coordinated acetone (Scheme 2-3A, 3 to 4) and subsequent oxidative addition of another propene molecule (Scheme 2-3A, 4 to 5). We consider that strict dehydration of the catalyst and abundant presence of propene molecules are indispensable requirements to achieve these steps. The oxidation of the olefin to a carbonyl compound via the alkoxy intermediate (Scheme 2-3A, 1 to 4) is accelerated by the presence of water;[62] whereas, water as well as carbonyl compounds are known to inhibit the metathesis reaction.[66,71,72] Although the presence of water might be favorable for the oxidation of propene via an alkoxy intermediate (Scheme 2-3A, 1 to 4), it is expected that the presence of water or carbonyl compounds lead to the decomposition of carbene sites, or more likely, disturb the carbene formation (Scheme 2-3A, 4 to 5) by blocking Mo(IV) sites. In fact, we observed lower catalytic activity accompanied by the color change of the catalyst from white to bluish when we use a less purified propene feed (i.e. the reaction was done using the same propene feed but without placing the water-trapping silica guard beds above and below the catalyst bed (see Supporting Information for experimental details), while the catalyst color remained white after 15 h of time on stream in standard reaction condition. The blue coloration observed in the experiment using less purified feed indicates the formation of reduced molybdenum species that are stabilized and blocked by the adsorption of water ligands, which suggests that the oxidative addition of propene was disturbed by likely water contamination. It is well known that pretreatment of the catalyst at elevated temperature (typically 773-873 K) in dry atmosphere is certainly necessary to obtain the catalytic activity. We consider that the dehydrated surface acts as an efficient trap for acetone and any byproduct of the reaction between surface molybdena with propene allowing the access of the second propene molecule to Mo(IV) sites, which leads to the generation of carbene species. It has been established that surface molybdena[73] and silanol groups[33] undergo structural reconstruction during the dehydration at elevated temperature, leaving surface sites which readily absorb water[33] and acetone.[74] Probably, the presence of this kind of dehydrated sites on the catalyst in a dry propene feed facilitates efficient trapping of acetone and access of the second propene molecule, allowing the formation of carbene sites (Scheme 2-3A, 3 to 5). In fact, we detected no carbonyl compounds (*e.g.* acetone) in the reactor effluent during the propene metathesis by mass spectrometry, indicating that generated carbonyl compounds are trapped on the catalyst surface.

To prove these assumptions, we have performed an additional experiment, which validated the hypothesis established here and succeeded in improving the catalytic performance. Before starting the metathesis reaction, we inserted a propene adsorption-desorption pretreatment. After the standard oxidative regeneration, the MoO_x/SBA-15 catalyst was exposed to neat propene at 300 K followed by thermal treatment in flowing argon at 823 K applying a temperature program with a heating rate of 10 K min^{-1}. As a consequence, we succeeded to double the activity and to eliminate the induction period (Figure 2-6). The heating after propene adsorption at 300 K accelerates the oxidation of surface isopropoxide species, forming Mo(IV) sites. During further temperature rise, desorption of oxidation products (oxygenates and possibly water) is accelerated, which leaves bare Mo(IV) sites that are the precursors of the active carbene sites in metathesis. Thus, the heating has two effects: promotion of oxidation and desorption of the oxidation products. We demonstrate here, how a knowledge-based approach efficiently improves catalytic performance. Systematic optimization of the activation protocol as well as the control of catalyst structure according to the present knowledge is required to improve the catalytic performance further.

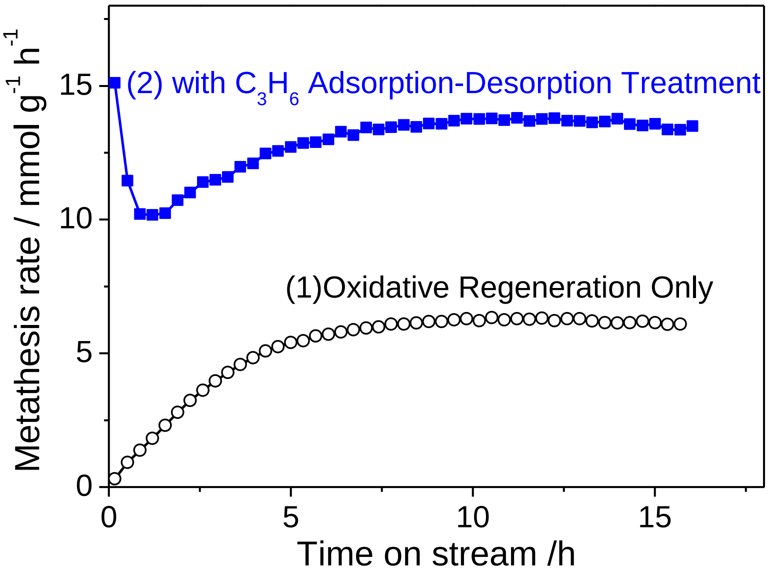

Figure 2-6. Propene metathesis activity of MoO_x/SBA-15 (323 K, contact time=0.35 s g ml^{-1}) after different regeneration procedures. (1): standard oxidative regeneration (20% O_2 flow at 823 K for 0.5 h) was performed. (2): in addition to the standard oxidative regeneration, the catalyst was treated in neat propene flow at 300 K for 1 h followed by heat treatment in argon flow at 823 K (heating rate 10 K min^{-1}) for 0.5 h.

We further consider the suggested route and criteria of carbene formation is applicable to other important heterogeneous metathesis catalysts, *i.e.* supported tungsten(VI) oxide and rhenium(VII) oxide. These oxides are also acidic, reducible and deposited on “desiccant-like” high surface area supports. The reducibility decreases in the order Re(VII) > Mo(VI) > W(VI) in general; this ranking is in agreement with the activity in olefin metathesis. These facts are quite consistent with the present conclusion.

2.4.3 Molecular structure of the carbene sites

According to the proposed mechanism, successful pre-catalyst sites should fulfill multiple functions, namely, Brønsted acidity, capability to perform isopropoxide oxidation and trapping capacity with respect to acetone and water. Apparently, only few grafted molybdenum oxide species meet all of these criteria simultaneously. It is, therefore, understandable why only 1.5 % of the existing molybdenum atoms take place in catalysis.

Raman (Figure S2-1) and UV-Vis (Figure S2-2) spectroscopy suggest that monomeric dioxo molybdena species in tetrahedral geometry are the predominant species,[28,31,75–77] although certain amount of non-nomomeric molybdena species probably coexist.[12,78,79] Monomeric molybdena has been suggested to be the relevant catalyst precursors.[12] In homogeneous metathesis, four-coordinated monomeric Mo(VI) alkylidene species represent the common general structure of active Mo-based metathesis catalysts.[66] In accordance with this fact, recent DFT calculations[52,55,80] as well as experimental studies[16,47] using well-defined catalysts with low Mo loadings have confirmed the metathesis activity of four-coordinated monomeric Mo(VI)-

alkylidene species in the class of supported Mo catalysts. Furthermore, if the oxidation of isopropoxide occurs at non-monomeric molybdena having Mo–O–Mo bonding, the two-electrons reduction of molybdenum (*i.e.* oxidation of isopropoxide to acetone) may possibly result in the formation of two Mo(V) centers instead of the formation of a Mo(IV) site that is the precursor of a carbene site. Monomeric molybdena species are likely surrounded by reactive silanol groups and Si-O-Si bonds created during the high-temperature pretreatment step, which provide the trapping function. Hence, monomeric molybdena species and resulting monomeric Mo(VI) alkylidene species are most likely candidates for pre-catalysts and active sites. Taking into account the presence of Mo–OH groups (*i.e.,* Brønsted acid sites) and their involvement in the formation of carbene species, we propose geometrically accessible tetrahedral monomeric dioxo species with a molybdenol group (Scheme 2-3B 1) as a candidate for the relevant pre-catalyst.

Scheme 2-3B describes the detailed scheme assuming the 1,2-hydrogen shift mechanism (Scheme 1A) in the oxidative addition step (Scheme 2-3B 5 to 7). Upon the formation of acetone (Scheme 2-3B 2 to 3), the released proton is likely hosted by the oxo oxygen on the same molybdenum atom in cooperation with concurrent reduction of the molybdenum atom, leaving a new molybdenol group (Scheme 2-3B, 3). It is speculated that this molybdenol further undergoes addition of another propene molecule to yield an isopropoxide group owing to its acidic character (Scheme 2-3B, 7 to 8). Accordingly, the final molecular structure of Mo carbene species (Scheme 2-3B, 8) features an isopropoxide group, an anchoring Mo–O–Si bond, an oxo group and an alkylidene group. Actually, this structure is an analogue of Schrock-type Mo-alkylidene complexes (Scheme 2-3C).[66] While Schrock-type complexes comprise two alkoxy ligands and an imido ligand besides the alkylidene ligand, the suggested surface Mo-alkylidene has an oxo ligand and an anchoring bond instead of an imido ligand and an alkoxy ligand, respectively. Insight obtained in the present study allows us to clearly envisage the molecular structure of active sites in supported transition metal oxide-derived heterogeneous catalysts, opening a possibility to address the material gap between homogeneous and heterogeneous catalysts. Further information concerning the molecular structure of the precursor surface molybdenum oxide species that can readily undergo transformation to Mo-carbene sites will bring deeper understanding and will allow the rational design of the catalyst. The specifically low turnover frequency of the present system indicates that the actual carbene structure is not optimal and improvements might be possible. Modification of the electronic structure of the active centers by appropriate support modification is the design target mimicking the N-containing ligands of the molecular analogues.

2.5 Conclusion

We contribute to understanding in catalysis through structural identification of active sites on the surface of a heterogeneous, meso-structured molybdenum oxide model catalyst for propene metatheses applying *operando* techniques on a strictly quantitative level. The genesis of active sites in such a system is a demanding *in-situ* and *one-pot* synthesis of metal carbene species from surface metal oxides, which involves Brønsted acid-base chemistry, oxidation-reduction processes, by-product capture and oxidative addition. In the present propene metathesis over MoO_x/SBA-15, only 1.5 % of total Mo atoms accomplish this process. The mechanistic insight into the genesis of active carbene sites obtained by microcalorimetry and *in-situ* IR delivers the explanation for the low abundance of active species, and provides the criteria for successful molecular structures of the pre-catalyst, which allows us to envisage resulting configurations of metal carbenes by applying established general mechanisms of acid-base and red-ox chemistry. To our surprise, we find structural similarity between the anticipated surface Mo(VI)-alkylidene and highly active Schrock-type catalysts. This encourages us to implement inputs from homogeneous catalysis in prospective catalyst synthesis approaches.

We embark two strategies towards catalyst improvement based on the gained insight: (1) controlling the surface carbene synthesis, and (2) knowledge-based design of the pre-catalyst.

Concerning strategy (1), the simple temperature pre-treatment (Figure 2-6) demonstrates that favorable activation conditions can assist the carbene formation disclosing a great and, in particular, easy option. Moreover, further control and optimization of the alkyl ligand in the carbene species should be possible by extending the choice of activating reagents instead of using merely the reactant itself. For example, use of isobutene instead of propene would facilitate the formation of the alkoxide intermediate due to increased stability of the *tert*-butoxide. In addition, the presence of the bulky *tert*-butoxide group at the final carbene site would contribute to improve the stability of the carbene species. Another option would be the use of alcohols (*e.g.* methanol, *tert*-butanol) for efficient creation of reduced metal centers (*i.e.* precursor for the carbene sites). By using alcohols, Brønsted acid sites are not necessarily required. The knowledge in homogeneous catalysis and organometallic synthesis will strongly contribute to the selection of prospective activating agents.

Strategy (2) benefits from the spatial separation of metal species that can be accomplished on the surface of a heterogeneous catalyst. Irreversible anchoring prevents self-condensation of complexes, which is a major difficulty in homogeneous catalysis. The presence of highly reactive molybdenol groups accounting for Brønsted acidity can be implemented within transition metal oxide species anchored on solid surfaces. Synthesis of isolated surface molybdenum oxide moieties having molybdenol ligands is a specific target, since our microcalorimetry results indicate that the amount of Brønsted acid sites is a limiting factor with respect to the number of active centers in the final catalyst.

Building bridges in catalysis research on the basis of our case study propene metathesis, we demonstrate here that the highly interdisciplinary field of heterogeneous catalysis will find more solid link to related fields in chemistry through in-depth understanding.

2.6 Supporting Information

Contents:

- Nitrogen adsorption isotherms of MoO_x/SBA-15 and SBA-15
- Raman spectra of MoO_x/SBA-15 and SBA-15
- UV-vis diffused reflectance spectrum of MoO_x/SBA-15
- IR spectra of isopropanol and acetone adsorption on MoO_x/SBA-15
- Experimental details

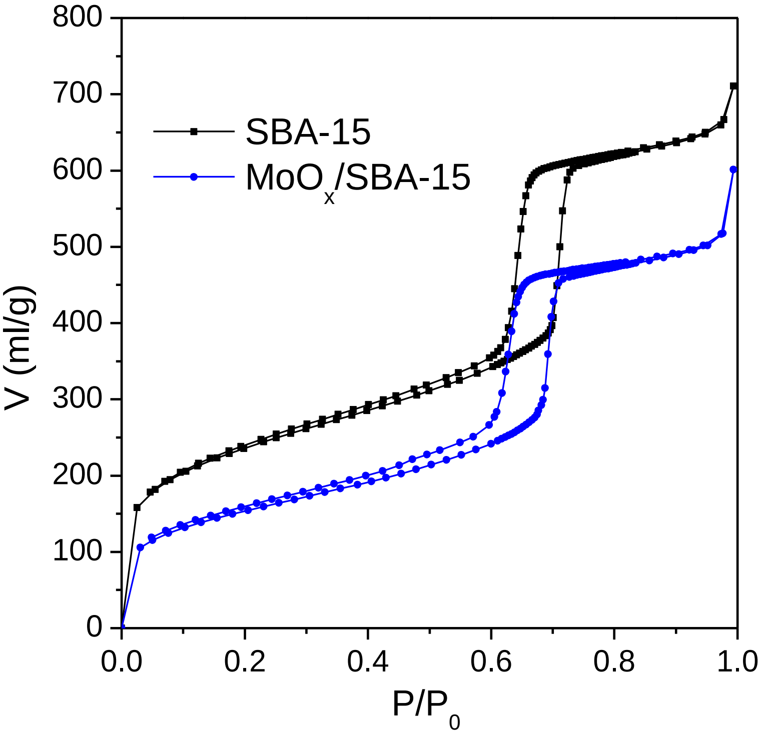

Figure S 2-1. Adsorption/desorption isotherms (at 77 K) of nitrogen on MoO_x/SBA-15 and SBA-15.

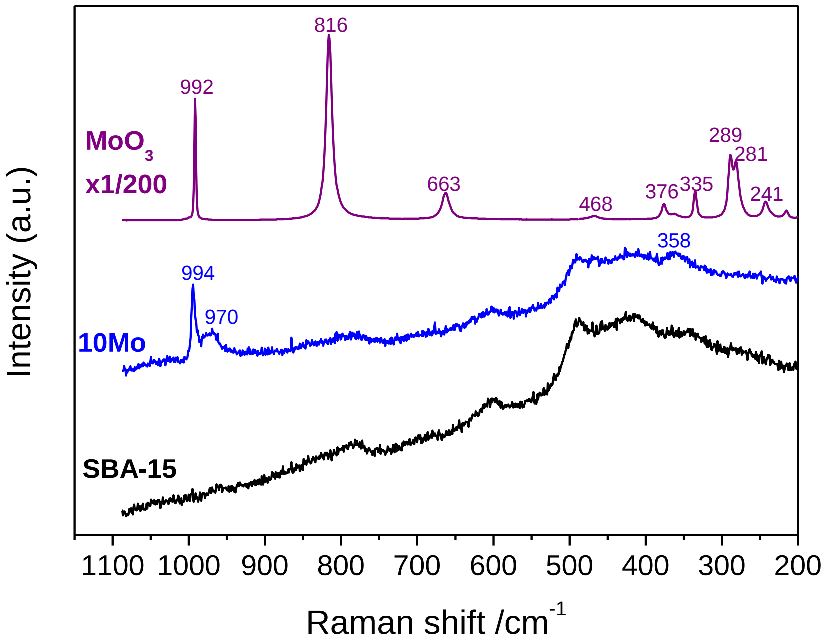

Figure S 2-2. Raman spectra of MoO_x/SBA-15 and SBA-15 (pretreated in 20% O_2 at 823 K for 0.5 h) as well as MoO_3 (no pretreatment) upon excitation with a 632 nm laser measured at room temperature. The spectra were offset for clarity.

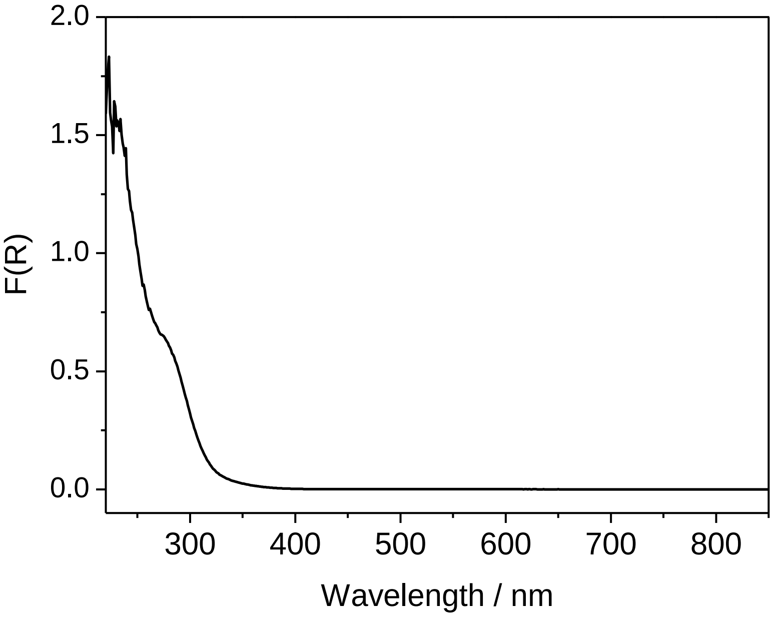

Figure S2-3. UV-vis diffused reflectance spectrum of MoO_x/SBA-15 (pretreated in 20% O_2 at 823 K for 0.5 h) measured at room temperature. The mother SBA-15 was used as white standard.

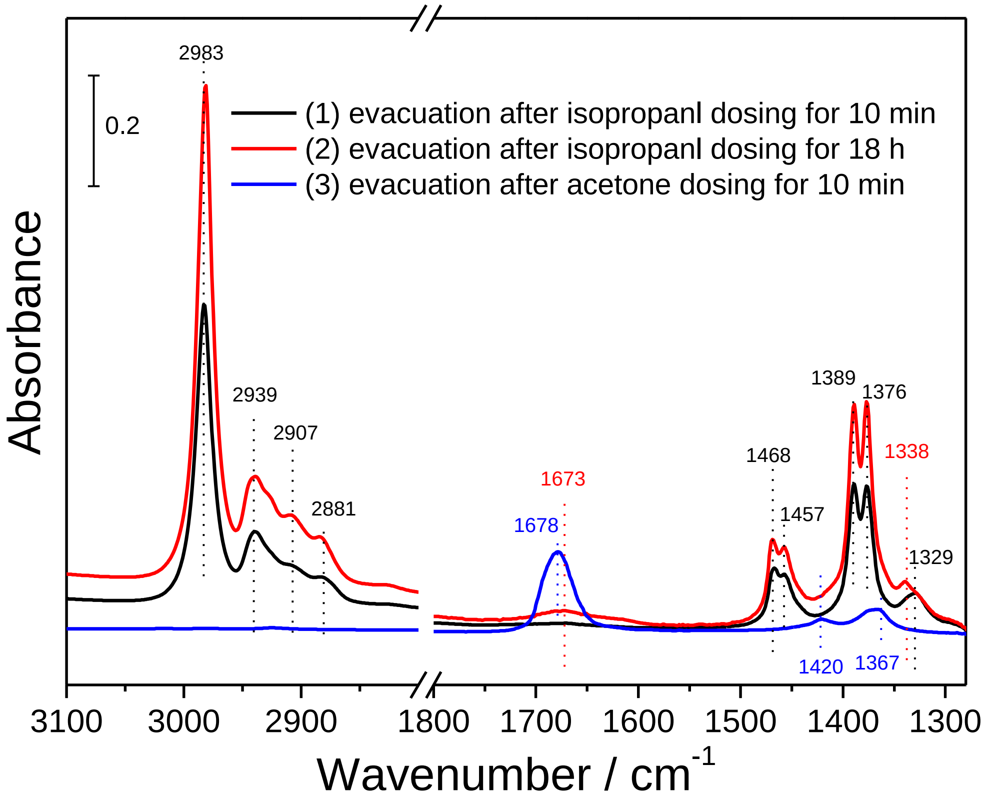

Figure S2-4. IR spectra for isopropanol and acetone adsorbed at 1 hPa and 323 K on MoO_x/SBA-15 pretreated in 20 kPa of O_2 at 823 K for 0.5 h.

Experimental Details:

Materials and reagents Triblock co-polymer $EO_{20}PO_{70}EO_{20}$ (EO = ethylene glycol, PO = propylene glycol, BASF Pluronic P123), tetraethoxysilane (> 99 %, Alfa Aesar), hydrochloric acid (ACS reagent grade, 37%, Aldrich), 3-aminopropyltrimethoxysilane (97 %, Aldrich), ammonium heptamolybdate (> 99 %, Acros) and silica gel (Silicagel 60, Fluka; BET surface area = 428 m^2 g^{-1}) were used as received. Ultrapure water for preparation of the aqueous solutions and washing procedures was produced using Milli-Q Synthesis System.

Argon (> 99.999 %, Westfalen) was dehydrated and deoxygenated with trapping filters (AirLiquide). Oxygen (> 99.999%, Westfalen) was dehydrated with a trapping filter (AirLiquide). Propene (> 99.95 %; contains 0.04 % of propane, Westfalen) was purified over molecular sieve (Agilent) and a reduced manganese oxide supported on molecular sieve (Agilent) filters. 1 % ethene-d_4 in argon prepared from neat ethene-d_4 (99 atom% D, Aldrich) and argon (> 99.9999%, Westfalen) was purified over a home-made oxygen and moisture trap (a bed of alumina supported copper, reduced with hydrogen and then flushed with Ar at 673 K). Ethene-d_4 (99 atom% D, Aldrich) was used for the IR study as received. Isopropanol (> 99.8%, Aldrich) and acetone (> 99.5 %, Aldrich) used for the IR study were purified by freeze-pump-thaw cycles.

Preparation of MoO_x/SBA-15 SBA-15 was synthesized using an automated laboratory reactor (LabMax, Mettler-Toledo). In brief, 40 g of the triblock co-polymer $EO_{20}PO_{70}EO_{20}$ were dissolved at 308 K in 1470 ml 1.6 M HCl, yielding a clear solution after several hours under stirring. Subsequently, 77.4 g of tetraethoxysilane were added dropwise. The solution was stirred for 12 h at 308 K, then heated up to 358 K with a rate of 5 K min^{-1}. After aging under stirring for 24 h at 358 K, the suspension was filtered and washed two times with water. The resulting white cake was dried at 353 K overnight, crushed into a fine powder and calcined in static air at 823 K (heating rate 1 K min^{-1}) for 4 h. After cooling down to room temperature, ca. 21.5 g of SBA-15 were obtained.

The subsequent loading of SBA-15 with molybdenum was achieved by a grafting/anion exchange procedure. The first step consists of a surface functionalization using 3-aminopropyltrimethoxysilane followed by the protonation of the resulting amine with HCl. Twenty gram of SBA-15 were suspended in 800 ml of toluene and heated to 338 K under stirring. To this suspension, 52 g of 3-aminopropyltrimethoxysilane were added dropwise and stirred at 338 K for 12 h. Afterwards the solid was filtered and washed with toluene. The recovered white powder was dried overnight and again suspended and stirred in 1200 ml 0.3 M HCl for 12 h. After filtering and washing with water, the SBA-15 was dried at 363 K overnight in static air. The second step consists of an ion exchange of the chloride ions in the surface ammonium chloride groups with molybdate anions. Under stirring, 0.436 g of ammonium heptamolybdate was added to a batch of 2.5 g functionalized SBA-15 in 60 ml water at room temperature and allowed stirring for 12 h. The resulting cake was filtered, washed with distilled water, dried at 383 K overnight, and calcined for 8 h at 823 K (heating rate 1 K min^{-1}) in static air to yield a white powder.

N_2 physisorption Nitrogen adsorption was carried out at 77 K on a Quantachrome Autosorb-6B analyzer. Prior to the measurement, the samples were outgassed in vacuum at 393 K for 16 h. All data treatments were performed using the Quantachrome Autosorb software package. The specific surface area S_{BET} was calculated according to the multipoint Brunauer-Emmett-Teller method (BET) in the p/p_0 = 0.05-0.15 pressure range assuming the N_2 cross sectional area of 16.2 Å^2. The micropore surface area S_{micro} was estimated using the *t*-plot method in the statistical thickness t = 4.5-6.5 Å range. The total pore volumes were estimated by using the amount of physisorbed nitrogen at a relative pressure p/p_0 = 0.95. The pore size distribution was determined by NLDFT method using a model based on equilibrated adsorption of N_2 on silica assuming cylindrical pores at 77 K.

X ray fluorescence The content of molybdenum was determined by X-ray fluorescence (XRF), using a Bruker S4 Pioneer X-ray spectrometer. For sample preparation, the mixture of 0.1 g of the sample and 8,9 g of lithium tetraborate (> 99.995 %, Aldrich) was fused into a disk using a automated fusion machine (Vulcan 2 MA, Fluxana).

X-ray diffraction Powder X-ray Diffraction (XRD) analysis was performed using a STOE STADI-P transmission diffractometer equipped with $CuK_{\alpha1}$ radiation.

UV-visible spectroscopy UV-visible (UV-vis) diffuse reflectance spectra were taken in the 200-850 nm range with a PerkinElmer Lambda 650 instrument equipped with an *in-situ* cell (Harrick Praying Mantis™ diffuse reflectance attachment DRP-P72 in combination with a HVC-VUV reaction chamber). Spectra were presented in the Kubelka-Munk function (F(R)) calculated from reflectance of the UV-vis diffuse reflectance spectra. Spectra of the pretreated samples were taken at 323 K after the pretreatment at 823 K (heating rate 10 $K{\cdot}min^{-1}$) for 0.5 h in a dehydrated 20 % O_2 in Ar flow (total flow 40 ml min^{-1}). The molybdenum-free bare SBA-15 used for the preparation of MoO_x/SBA-15 was used as white standard.

Raman spectroscopy Confocal Raman spectroscopy was performed using a Horiba Jobin LABRAM instrument equipped with a microscope. A He-Ne laser (wavelength 632.8 nm, 1.5 mW at the sample position) was used for the excitation. A pressed wafer of the sample (ca. 30 mg) was mounted in a home made *in-situ* cell, which allows treatments at desired temperature and gas flow. Spectra of the pretreated samples were taken at room temperature after the pretreatment at 823 K (heating rate 10 $K{\cdot}min^{-1}$) for 0.5 h in a dehydrated 20 % O_2 in Ar flow (total flow 40 ml min^{-1}). Typical acquisition time was 0.5 h.

Diffuse reflectance FT infrared spectroscopy Diffuse reflectance FT infrared (DRIFT) spectra were collected on a Bruker IFS66 spectrometer equipped with a liquid nitrogen-cooled MCT detector at a spectral resolution of 4 cm^{-1} and accumulation of 1024 scans. An *in-situ* cell (Harrick Praying Mantis™ diffuse reflectance attachment DRP-P72 in combination with a HVC-VUV reaction chamber) was used. Spectra of the pretreated samples were taken at room temperature after the pretreatment at 823 K (heating rate 10 $K{\cdot}min^{-1}$) for 0.5 h in a dehydrated 20 % O_2 in Ar flow (total flow 40 ml min^{-1}). KBr was used as reference material.

Propane metathesis The catalytic activity for the self metathesis of propene to ethene and 2-butenes was measured using a fixed-bed tube flow reactor at atmospheric pressure. The catalysts were pressed under ~135 MPa, crushed and sieved to a particle size of 250-355 μm. Then, 100 mg of the catalyst was loaded into a U-shaped quartz reactor with an inner diameter of 4 mm. Guard beds consisting of silica gel (BET surface area = 428 m^2 g^{-1}) were placed both immediately above (100 mg) and below (50 mg) the catalyst bed in order to protect the catalyst bed from possible contamination by water. A blank test using bare SBA-15 with silica beds confirmed inertness of the apparatus and the guard beds. The catalyst was activated at 823 K (heating rate 10 $K{\cdot}min^{-1}$) for 0.5 h, cooled to 323K in a 20 % O_2 in Ar (20 ml min^{-1}), and then flushed with a flow of Ar (20 ml min^{-1}) before reaction. A neat propene flow of 8 ml min^{-1} was fed to start the reaction. Inlet and outlet gases were analyzed by on-line gas chromatography using an Agilent Technologies 6890A GC system equipped with a flame ionization detector. The conversion of propene was kept below 5 % to stay in a differential regime. The selectivity to the metathesis products (ethane, *cis*- and *trans*-butene) was above 99.5 %, while trace amounts of 1-butene and higher hydrocarbons were detected. The activity is presented as formation rate of the metathesis products (i.e. sum of ethane, *cis*- and *trans*-butene) normalized by the mass of catalyst.

Regeneration of the catalysts was performed using the same procedure as the initial activation. Namely, spent catalyst was treated at 823 K (heating rate 10 $K \cdot min^{-1}$) for 0.5 h and cooled to 323 K in a dehydrated 20 % O_2 in Ar, then flushed with Ar before starting the reaction.

Post-reaction ethene-d4 metathesis for active site counting After the metathesis reaction, the reactor was flushed with flowing Ar (purified in the abovementioned way, 20 ml min^{-1} for 10 min, then 5 ml min^{-1} for 20 min), then the feed gas was switched to 5 ml min^{-1} of 1%C_2D_4 in Ar. The formation of propene-1,1-d_2 was monitored and quantified with a quadrupole mass spectrometer (QMS200, Balzer) using the signal of m/z = 43. The formation of propene-1,1-d_2 was also confirmed by the simultaneous detection of the molecular ion (m/z = 44). The two-fold amount of the liberated amount of propene-1,1-d_2 normalized by the weight of the catalyst was assumed as the active site density.

Microcalorimetry of propene adsorption Differential heats of adsorption were determined using a MS70 Calvet Calorimeter (SETRAM). The calorimeter was combined with a custom-designed high vacuum and gas dosing apparatus. Catalysts were pretreated in the calorimeter cell under oxygen at 20 kPa and at 823 K (heating rate 10 $K \cdot min^{-1}$) for 0.5 h. The gas was repeatedly replaced by fresh oxygen every 5 minutes. Then the cell was cooled to room temperature under oxygen and finally evacuated for 1h ($p < 3 \cdot 10^{-6}$ Pa). The cell was then transferred into the calorimeter and heated to the adsorption temperature of 323 K. Propene was stepwise introduced into the initially evacuated cell, and the pressure evolution and the heat signal were recorded for each dosing step. After the last step, the cell was evacuated at the same temperature for 1 h ($p < 3 \cdot 10^{-6}$ Pa) to desorb reversibly adsorbed species, then followed by repetition of the adsorption steps (i.e. re-adsorption measurement). The regeneration of catalysts comprises of the same procedure as the pretreatment (i.e. under a flow of oxygen at 20 kPa and at 823 K (heating rate 10 $K \cdot min^{-1}$) for 0.5 h, then cooled to room temperature and finally evacuated for 1h ($p < 3 \cdot 10^{-6}$ Pa)). The adsorption isotherm was derived from the dosed amount and the equilibrium pressure. The differential heats of adsorption were calculated by converting the signal area into a heat by using the calorimeter’s calibration factor and then dividing the heat by the number of molecules adsorbed in this step.

In-situ FTIR spectroscopy The IR experiments were carried out using a Perkin Elmer 100 FTIR spectrometer equipped with a DTGS detector at a spectral resolution of 4 cm^{-1} and accumulation of 64 scans. The samples were pressed (125 MPa) into self-supporting wafers, which were placed in an *in-situ* infrared transmission cell. The IR cell was directly connected to a vacuum system (residual pressure of 3 10^{-6} Pa) equipped with a gas dosing line. Before adsorption of probe molecules, the catalysts were pretreated in oxygen at 200 hPa and at 823 K for 0.5 h followed by evacuation at room temperature.

Propene, ethene-d_4, isopropanol and acetone were dosed at 323 K at the pressure up to 3 hPa. Ammonia was dosed at 353 K at the pressure up to 10 hPa. In each experiment, the spectrum taken before probe dosing was used as background. Contribution of gas phase species was not significant due to short path length of the *in-situ* cell.

2.7 References

(1) Dumesic, J. A.; Huber, G. W.; Boudart, M. In *Handbook of Heterogeneous Catalysis 2nd ed.*; Wiley-VCH: Weinheim, 2008; pp. 1–15.

(2) Somorjai, G. A.; Li, Y. *Introduction to Surface Chemistry and Catalysis*; 2nd ed.; John Wiley & Sons: Hoboken, New Jersey, 2010.

(3) Libuda, J.; Freund, H.-J. *Surf. Sci. Rep.* **2005**, *57*, 157–298.

(4) Rupprechter, G.; Weilach, C. *J. Phys.: Condens. Matter* **2008**, *20*, 184019.

(5) Handzlik, J.; Ogonowski, J. *Catal. Lett.* **2003**, *88*, 119–122.

(6) Chauvin, Y. *Angew. Chem. Int. Ed.* **2006**, *45*, 3740–3747.

(7) Salameh, A.; Copéret, C.; Basset, J.-M.; Böhm, V. P. W.; Röper, M. *Adv. Synth. Catal.* **2007**, *349*, 238–242.

(8) Chauvin, Y.; Commereuc, D. *J. Chem. Soc., Chem. Commun.* **1992**, 462–464.

(9) Mol, J. *J. Mol. Catal. A: Chem.* **2004**, *213*, 39–45.

(10) Debecker, D. P.; Stoyanova, M.; Colbeau-Justin, F.; Rodemerck, U.; Boissière, C.; Gaigneaux, E. M.; Sanchez, C. *Angew. Chem. Int. Ed.* **2012**, *51*, 2129–2131.

(11) Debecker, D. P.; Bouchmella, K.; Stoyanova, M.; Rodemerck, U.; Gaigneaux, E. M.; Mutin, P. H. *Catal. Sci. Technol.* **2011**.

(12) Debecker, D. P.; Schimmoeller, B.; Stoyanova, M.; Poleunis, C.; Bertrand, P.; Rodemerck, U.; Gaigneaux, E. M. *J. Catal.* **2011**, *277*, 154–163.

(13) Debecker, D. P.; Stoyanova, M.; Rodemerck, U.; Gaigneaux, E. M. *J. Mol. Catal. A: Chem.* **2011**, *340*, 65–76.

(14) Debecker, D.; Bouchmella, K.; Poleunis, C.; Eloy, P.; Bertrand, P.; Gaigneaux, E.; Mutin, P. *Chem. Mater.* **2009**, *21*, 2817–2824.

(15) Iwasawa, Y.; Hamamura, H. *J. Chem. Soc., Chem. Commun.* **1983**, 130–132.

(16) Iwasawa, Y.; Kubo, H.; Hamamura, H. *J. Mol. Catal.* **1985**, *28*, 191–208.

(17) McCoy, J. R.; Farona, M. F. *J. Mol. Catal.* **1991**, *66*, 51–58.

(18) Farona, M. F.; Tucker, R. L. *J. Mol. Catal.* **1980**, *8*, 85–90.

(19) Grubbs, R. H.; Swetnick, S. J. *J. Mol. Catal.* **1980**, *8*, 25–36.

(20) Laverty, D. T.; Rooney, J. J.; Stewart, A. *J. Catal.* **1976**, *45*, 110–113.

(21) Rappe, A. K.; Goddard, W. A. *J. Am. Chem. Soc.* **1982**, *104*, 448–456.

(22) Grünert, W.; Stakheev, A. Y.; Feldhaus, R.; Anders, K.; Shpiro, E. S.; Minachev, K. M. *J. Catal.* **1992**, *135*, 287–299.

(23) Chen, X.; Zhang, X.; Chen, P. *Angew. Chem. Int. Ed.* **2003**, *42*, 3798–3801.

(24) Basrur, A. G.; Patwardhan, S. R.; Was, S. N. *J. Catal.* **1991**, *127*, 86–95.

(25) Howman, E. J.; Mgcrath, B. P.; Williams, K. V. Catalyst regeneration process. British Patent 1,144,085, March 5, **1969**.

(26) Zhao, D.; Feng, J.; Huo, Q.; Melosh, N.; Fredrickson, G. H.; Chmelka, B. F.; Stucky, G. D. *Science* **1998**, *279*, 548 –552.

(27) Thielemann, J. P.; Weinberg, G.; Hess, C. *ChemCatChem* **2011**, *3*, 1814–1821.

(28) Tian, H.; Roberts, C. A.; Wachs, I. E. *J. Phys. Chem. C* **2010**, *114*, 14110–14120.

(29) Hu, H.; Wachs, I. E.; Bare, S. R. *J. Phys. Chem.* **1995**, *99*, 10897–10910.

(30) Vuurman, M. A.; Wachs, I. E. *J. Mol. Catal.* **1992**, *77*, 29–39.

(31) Lee, E. L.; Wachs, I. E. *J. Phys. Chem. C* **2007**, *111*, 14410–14425.

(32) Dieterle, M.; Weinberg, G.; Mestl, G. *Phys. Chem. Chem. Phys.* **2002**, *4*, 812–821.

(33) Davydov, A. *Molecular spectroscopy of oxide catalyst surface*; John Wiley & Sons Ltd.: Chichester, 2003.

(34) Zhang, B.; Li, Y.; Lin, Q.; Jin, D. *J. Mol. Catal.* **1988**, *46*, 229–241.

(35) Langmuir, I. *J. Am. Chem. Soc.* **1916**, *38*, 2221–2295.

(36) Grabowski, R.; Efremov, A.; Davydov, A.; Haber, E. *Kinet. Catal.* **1981**, *22*, 794–797.

(37) Efremov, A.; Lokhov, Y.; Davydov, A. *Kinet. Catal.* **1981**, *22*, 969–975.
(38) Martín, C.; Rives, V.; Sánchez-Escribano, V.; Busca, G.; Lorenzelli, V.; Ramis, G. *Surf. Sci.* **1991**, *251-252*, 825–830.
(39) Finocchio, E.; Busca, G.; Lorenzelli, V.; Willey, R. J. *J. Chem. Soc., Faraday Trans.* **1994**, *90*, 3347.
(40) Goncharova, O.; Davydov, A. *React. Kinet. Catal. Lett.* **1983**, *23*, 285–289.
(41) Davydov, A.; Efremov, A. *Kinet. Catal.* **1983**, *24*, 1214–1220.
(42) Efremov, A.; Davydov, A. *React. Kinet. Catal. Lett.* **1981**, *18*, 363–366.
(43) Goncharova, O.; Davydov, A.; Yureva, T. *Kinet. Catal.* **1984**, *25*, 124–129.
(44) Sanchez Escribano, V.; Busca, G.; Lorenzelli, V. *J. Chem. Phys.* **1991**, *95*, 5541–5545.
(45) Efremov, A. A.; Davydov, A. A. *React. Kinet. Catal. Lett.* **1981**, *18*, 353–356.
(46) Vikulov, K. A.; Shelimov, B. N.; Kazansky, V. B. *J. Mol. Catal.* **1991**, *65*, 393–402.
(47) Vikulov, K. A.; Elev, I. V.; Shelimov, B. N.; Kazansky, V. B. *J. Mol. Catal.* **1989**, *55*, 126–145.
(48) Blanc, F.; Rendon, N.; Berthoud, R.; Basset, J.-M.; Coperet, C.; Tonzetich, Z. J.; Schrock, R. R. *Dalton Trans.* **2008**, 3156–3158.
(49) Rendón, N.; Berthoud, R.; Blanc, F.; Gajan, D.; Maishal, T.; Basset, J.-M.; Copéret, C.; Lesage, A.; Emsley, L.; Marinescu, S. C.; Singh, R.; Schrock, R. R. *Chem.—Eur. J.* **2009**, *15*, 5083–5089.
(50) Handzlik, J. *J. Phys. Chem. B* **2005**, *109*, 20794–20804.
(51) Handzlik, J. *J. Catal.* **2003**, *220*, 23–34.
(52) Handzlik, J. *Surf. Sci.* **2007**, *601*, 2054–2065.
(53) Handzlik, J.; Ogonowski, J.; Tokarz-Sobieraj, R. *Catal. Today* **2005**, *101*, 163–173.
(54) Handzlik, J. *Surf. Sci.* **2004**, *562*, 101–112.
(55) Handzlik, J.; Sautet, P. *J. Catal.* **2008**, *256*, 1–14.
(56) Li, X.; Guan, J.; Zheng, A.; Zhou, D.; Han, X.; Zhang, W.; Bao, X. *J. Mol. Catal. A: Chem.* **2010**, *330*, 99–106.
(57) Guan, J.; Yang, G.; Zhou, D.; Zhang, W.; Liu, X.; Han, X.; Bao, X. *Catal. Commun.* **2008**, *9*, 2213–2216.
(58) Li, X.; Zheng, A.; Guan, J.; Han, X.; Zhang, W.; Bao, X. *Catal. Lett.* **2010**, *138*, 116–123.
(59) Campbell, K. A.; Janik, M. J.; Davis, R. J.; Neurock, M. *Langmuir* **2005**, *21*, 4738–4745.
(60) Kazansky, V. B. *Catal. Today* **1999**, *51*, 419–434.
(61) Engelhardt, J.; Hall, W. K. *J. Catal.* **1995**, *151*, 1–9.
(62) Moro-oka, Y. *Appl. Catal., A* **1999**, *181*, 323–329.
(63) Iwasawa, Y.; Ichinose, H.; Ogasawara, S.; Soma, M. *J. Chem. Soc., Faraday Trans. 1* **1981**, *77*, 1763–1777.
(64) Shelimov, B. N.; Elev, I. V.; Kazansky, V. B. *J. Mol. Catal.* **1988**, *46*, 187–200.
(65) Elev, I.; Shelimov, B.; Kazansky, V. *Kinet. Catal.* **1989**, *30*, 787–792.
(66) Schrock, R. R.; Hoveyda, A. H. *Angew. Chem. Int. Ed.* **2003**, *42*, 4592–4633.
(67) Handzlik, J.; Ogonowski, J.; Stoch, J.; Mikolajczyk, M.; Michorczyk, P. *Appl. Catal., A* **2006**, *312*, 213–219.
(68) Aritani, H.; Fukuda, O.; Yamamoto, T.; Tanaka, T.; Imamura, S. *Chem. Lett.* **2000**, 66–67.
(69) Debecker, D. P.; Hauwaert, D.; Stoyanova, M.; Barkschat, A.; Rodemerck, U.; Gaigneaux, E. M. *Appl. Catal., A* **2011**, *391*, 78–85.
(70) Thomas, R.; Moulijn, J. A. *J. Mol. Catal.* **1982**, *15*, 157–172.
(71) Mol, J. C.; Leeuwen, P. W. N. M. *Metathesis of Alkens in "Handbook of Heterogeneous Catalysis"*; 2nd ed.; Wiley-VCH,: Weinheim, 2008.
(72) Dinger, M. B.; Mol, J. C. *Organometallics* **2003**, *22*, 1089–1095.
(73) Boer, M.; Dillen, A. J.; Koningsberger, D. C.; Geus, J. W.; Vuurman, M. A.; Wachs, I. E. *Catal. Lett.* **1991**, *11*, 227–239.
(74) Crocellà, V.; Cerrato, G.; Magnacca, G.; Morterra, C. *J. Phys. Chem. C* **2009**, *113*, 16517–16529.
(75) Lee, E. L.; Wachs, I. E. *J. Phys. Chem. C* **2008**, *112*, 6487–6498.

(76) Chempath, S.; Zhang, Y.; Bell, A. T. *J. Phys. Chem. C* **2007**, *111*, 1291–1298.
(77) Guo, C. S.; Hermann, K.; Hävecker, M.; Thielemann, J. P.; Kube, P.; Gregoriades, L. J.; Trunschke, A.; Sauer, J.; Schlögl, R. *J. Phys. Chem. C* **2011**, *115*, 15449–15458.
(78) Thielemann, J. P.; Kröhnert, J.; Hess, C. *J. Phys. Chem. C* **2010**, *114*, 17092–17098.
(79) Thielemann, J. P.; Ressler, T.; Walter, A.; Tzolova-Müller, G.; Hess, C. *Appl. Catal., A* **2011**, *399*, 28–34.
(80) Handzlik, J. *J. Phys. Chem. C* **2007**, *111*, 9337–9348.

Chapter 3: Impact of the Strain of Surface Metal Oxide Molecules in Supported Catalysts

Kazuhiko Amakawa, Lili Sun, Chunsheng Guo, Michael Hävecker, Israel E. Wachs, Soe Lwin, Anatoly I. Frenkel, Anitha Patlolla, Klaus Hermann, Robert Schlögl and Annette Trunschke

Abstract

The structure of MoO_x/SBA-15 having the surface Mo density of 0.2~2.5 atoms/nm^2 was investigated by N_2 physisorption, XRD, XRF, SEM-EDX, IR, visible- and UV-Raman, UV—vis, O K-edge NEXAFS, Mo K-edge EXAFS/XANES and DFT calculations, while the reactivity was evaluated by temperature programmed reduction by hydrogen (H_2-TPR). The spectroscopic data show that tetrahedral di-oxo Mo(VI) structures are predominantly formed by consuming surface silanol groups irrespective the Mo loadings, whereas the H_2-TPR evidences a remarkable increase of the reactivity at high Mo loading. It is suggested that surface metal oxide molecules are forced to be anchored in frustrated configurations at high coverage where available anchoring surface hydroxyl sites are limited, leading to an increased reactivity. The concept explains the sometimes observed non-linear coverage dependence in monolayer-type supported metal oxide catalysts.

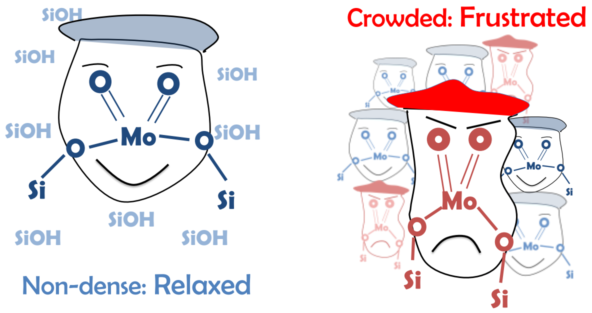

Acknowledgement

We thank G. Weinberg, Dr. T. Cotter, M. Hashagen, G. Lorenz, Dr. F. Girgsdies, E. Kitzelmann, A. Klein-Hoffmann, C.V.T. Nguyen, the NSLS staff, and the HZB staff for their professional assistance. Prof. Dr. I.E. Wachs thanks the Alexander von Humboldt Foundation, Germany, for the Humboldt Research Award. . Prof. Dr. A. I. Frenkel acknowledges the U.S. DOE Grant No. DE-FG02-05ER15688 for supporting X18B beamline operations. K. Amakawa is grateful to Mitsubishi Gas Chemical Co. Inc. for a fellowship.

3.1 Introduction

In 1925, Sir H.S. Taylor proposed that special active sites in a non-balanced state (*e.g.* low-coordinated species), which represent only a fraction of the surface atoms, are responsible for heterogeneous catalysis.[1] It took decades until the concept earned experimental and theoretical confirmation. Surface science proved that low-coordinated atoms at the edge of steps are indeed most active in metal catalysts.[2] Recent advances in materials characterization revealed that Sir Taylor's concept is even applicable to high-performing, multi-component catalysts, e.g. nanostructured Cu/ZnO for methanol synthesis[3] and supported gold nanoparticles[4], wherein ensemble sites formed at surface defects or at the metal-oxide interface play a crucial role for catalytic behavior.

Monolayer-type supported metal oxides represent another important class of heterogeneous catalysts. It has been observed that surface metal oxide species are not evenly active in general. In olefin metathesis over molybdena supported on silica, it was shown that only 1.5% of the molybdenum atoms are active sites,[5] recalling Sir Taylor's concept. The catalytic performance of supported metal oxides sometimes shows a non-linear dependence on the metal oxide loading where the activity develops steeply above a certain level of metal oxide coverage.[6–10] Reasons for this general observation remain, however, elusive.

The present study is devoted to unscramble the relations between reactivity and structure of monolayer-type oxide catalysts. Based on spectroscopic evidence, we propose that molecular surface metal oxide species become more frustrated with increased loading owing to the limited availability of anchoring sites at the support surface that, consequently, leads to enhanced reactivity of the metal oxide species formed at high coverage. This implies that Sir Taylor's concept is also applicable to surface metal oxides.

3.2 Results and Discussion

Silica-supported molybdena, which represents a model for oxidation[8] and metathesis[5,9] catalysts, was chosen to exemplify the impact of metal oxide coverage on reactivity. The reactivity of dehydrated[11] surface molybdena supported on mesoporous silica SBA-15 (MoO_x/SBA-15) was assessed by temperature-programmed reduction with hydrogen (H_2-TPR), which is of high relevance to catalysis.[9,10] The H_2-TPR profiles (Figure 3-1) reveal enhanced reducibility with increasing Mo loading. The sample of lowest loading (2.1% Mo) shows a single, sharp reduction peak at 1158 K. By increasing the Mo loading, a new distinct low temperature peak at 856 K occurs in addition to the progressive broadening of the high temperature peak, indicating extended appearance of surface molybdena species exhibiting higher reducibility.

The effect of coverage on the reactivity of monolayer oxides has been discussed with regard to the polymerization degree of surface metal oxides species (*e.g.* monomeric, polymeric and nano-crystalline domains).[7] In the present case, however, spectroscopy reveals only modest structural modification with increasing surface coverage. The very similar fingerprints in the Mo K-edge x-ray absorption near edge structure (XANES) and UV-vis spectroscopy (Figure 3-2 a and b) indicate little change in the connectivity of surface molybdena[12] and in the coordination geometry, featuring a predominantly tetrahedral coordination similar to the reference $Al_2(MoO_4)_3$ as suggested by the intense pre-edge peak at 20006 eV (Figure 3-2b). Fourier-transformed Mo K-edge extended x-ray absorption fine structure (EXAFS) spectra (Figure 3-2c) show two distinct distances at $R < 2$Å, which are assigned to Mo═O double and Mo—O single bonds referring to the observed vibrational bands in the Raman/IR analysis[13–16] (Supporting Information; Figure S6, 980—997 cm^{-1} for Mo═O, and 926—943 cm^{-1} for Mo—O). Conclusive structural assignment is provided by near edge x-ray absorption fine structure (NEXAFS) analysis at the O K-edge combined with DFT calculations. The double-peak absorption at the O

1s edge (Figure 3-2d; peaks at 530.2 and 532.5 eV) observed at low loadings is well reproduced by DFT calculations[17] considering models having two-fold anchored di-oxo (Si—O—)$_2$Mo(═O)$_2$ structures characterized by a Si—Si distance of 4.6-4.7 Å (Supporting Information; clusters **a** and **b** in Figure S3-1, Figure S3-5A, Table S3-1). In accordance with this result, the fitting of the first coordination sphere of Mo in the K-edge EXAFS using a di-oxo (O—)$_2$Mo(═O)$_2$ model reproduces the experimental spectra well, yielding Mo—O path lengths consistent with the theoretical prediction (Supporting Information; Figures S3-1, S3-4, Tables S3-1, S3-3). Moreover, the calculated IR spectra of the di-oxo models are in agreement with the experimental IR spectra (Supporting Information; Figures S3-6D, S3-7). All the results indicate that the two-fold anchored tetrahedral di-oxo (Si—O—)$_2$Mo(═O)$_2$ unit represents the major surface molybdena species, which is also in agreement with previous reports.[13–17]

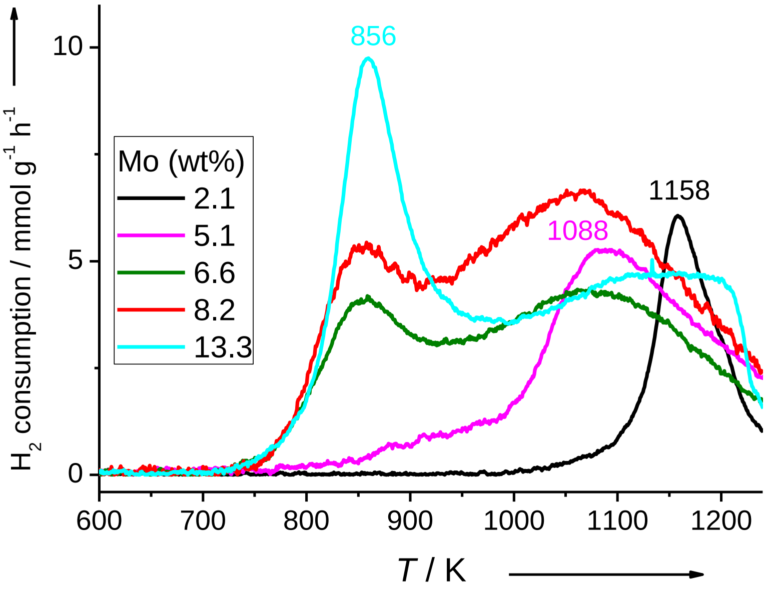

Figure 3-1. Temperature-programmed reduction (H_2-TPR) of supported MoO_x/SBA-15 measured at a heating rate of 10 K min^{-1} in 2% H_2 in Ar after pretreatment in 20% O_2 in Ar at 823 K for 0.5 h.

While the bond lengths obtained by EXAFS fitting are independent of the Mo loading (Supporting Information; Table S3-3), subtle structural variations are clearly imprinted in the O K-edge NEXAFS data. The O K-edge NEXAFS feature due to molybdena (528—534 eV) gradually loses the well-separated double peak structure by broadening of the peaks and occurrence of a new component at 531 eV (Figure 3-2d). The peak broadening and the occurrence of the new peak seem to be linked to the changes in the H_2-TPR profiles (Figure 3-1; broadening of the high temperature peak and the occurrence of the low temperature peak at 856 K). The broad NEXAFS feature is in clear contrast to the well separated double peak corresponding to crystalline Na_2MoO_4 (Figure 3-2d) that consists of uniform isolated MoO_4 units, implying changes in the bond angles due to variations in the Mo-Si distance with increasing loading. The Fourier transform of the Mo K-edge EXAFS at longer *R* (Figure 3-2c) shows neither distinct peaks nor systematic changes upon increasing the Mo loading, which indicates the absence of a well-defined geometrical order beyond the first coordination sphere and suggests, in turn, a broad distribution of the Mo—Si distance of anchoring Mo—O—Si motifs. The various Mo—Si distances originate from the amorphous nature of the silica surface that provides a distribution in the Si—Si distance of silanol pairs used for anchoring of the di-oxo structures.[13,18,19] This leads to variations in the Mo—O—Si angle and O—Si length. In addition, four-fold coordinated pentahedral mono-oxo (Si—O—)$_4$Mo═O structures may occur as a minority when four silanol sites are suitably arranged.[13] In fact, we observe additional vibrational bands assigned to the mono-oxo species[13,14] in the resonance Raman analysis that possibly detects minority species that are invisible in non-resonant Raman (Supporting Information; Figure S3-8).

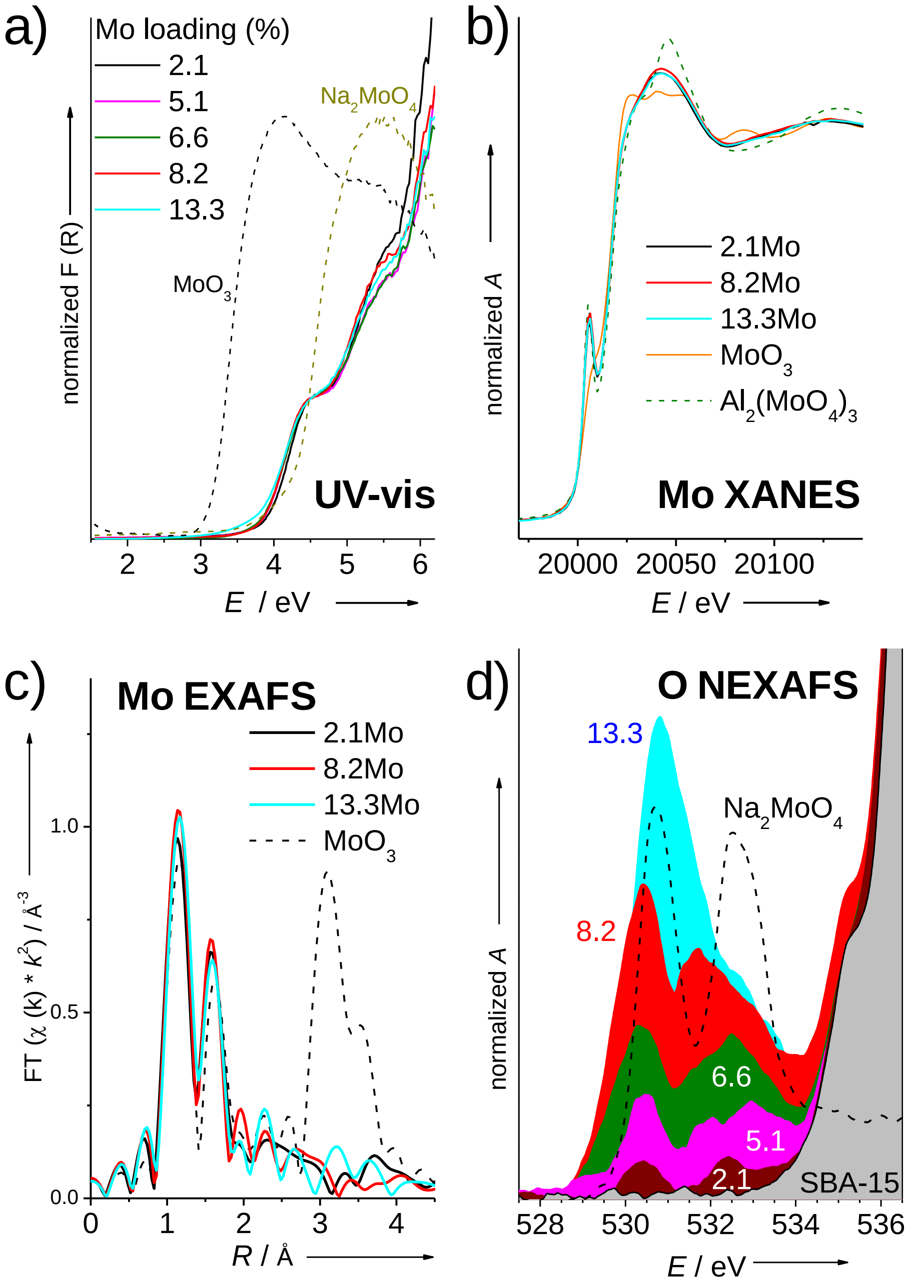

Figure 3-2. (a) UV-vis, (b) Mo K-edge XANES, (c) Fourier-transformed phase-uncorrected Mo K-edge EXAFS, and (d) O K-edge NEXAFS spectra of dehydrated MoO$_x$/SBA-15.

Surface silanol groups are consumed by forming Mo—O—Si bridging bonds. The density of isolated silanol sites drops from 1.6 (bare SBA-15) to 0.07 (13.3% Mo) sites per square nanometer (Supporting Information; Table S3-2, Figure S3-6C), revealing a highly "silanol deficient" state at high Mo coverage. Given the limited availability of silanol groups at high coverage, the formation of surface molybdena species having plural anchoring bonds (e.g. two-fold anchored di-oxo structure) involves the impact of strain. The models in Figure 3-3 illustrate the idea schematically. The two-dimensional (x—y axes) description in Figure 3-3a shows a network of siloxane rings comprising various ring sizes,[18,20] while another two dimensional description in Figure 3-3b reminds us that there is also a variation in the third axis z in real 3D space. In Figure 3-3a, the di-oxo MoO_4 units are anchored on less strained configurations at low molybdenum coverage, whereas the decrease of silanol sites forces the di-oxo MoO_4 structures to form more strained configurations. The distribution of species is most likely governed by the thermodynamic stability[21] due to the high mobility of molybdena.[11,22] In the 2D description, the geometric constraint may be approximated by the size of the smallest molybdosiloxane ring that belongs to the di-oxo MoO_4 unit as illustrated in Figure 3-3a. Extending the 2D model into the real 3D space further increases the variation of combinations of available silanol sites (even within the same size of a molybdosiloxane ring).

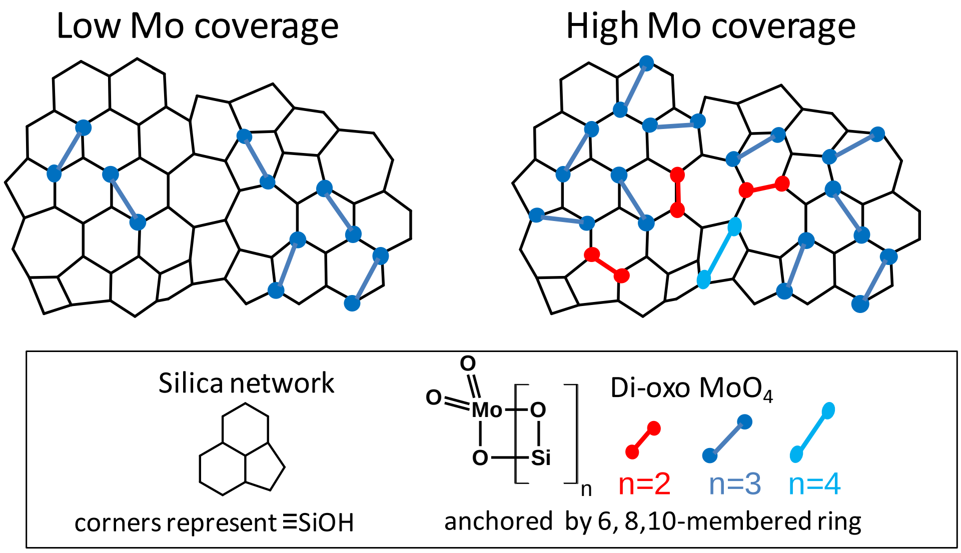
a) top view

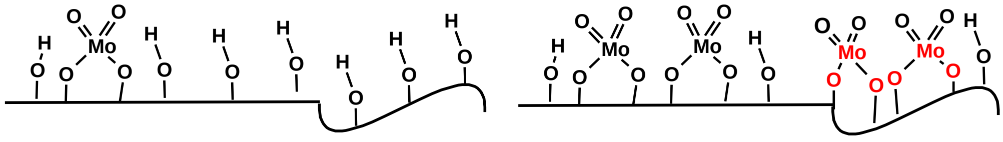
b) side view

Figure 3-3. Schematic illustration of the suggested anchoring patterns of di-oxo $(—Si—O—)_2Mo(=O)_2$ structures on a 2D silica surface at different surface molybdenum densities. Two 2D models (a, b) are shown to illustrate the real 3D space. The differently colored dots-terminated lines in "a) top view" represent the di-oxo species having different anchoring geometries.

Strain at the anchoring bonds leads also to a high potential energy at the location, which very likely enhances the reactivity considering the Brønsted−Evans−Polanyi relation,[23,24] which seems also applicable to metal oxides.[25] Accordingly, the increased reducibility at high Mo oxide coverage (Figure 3-1) is explained by the increased strain of surface molybdena species predominantly consisting of di-oxo MoO_4 structures. The occurrence of a distinct low temperature peak at 856 K in the H_2-TPR profile may reflect the presence of a discrete Si—Si distance (which may be related to a specific molybdosiloxane ring size) that accommodates a surface molybdena species, which is particularly reactive towards hydrogen. This is plausible because the flexibility of the siloxane network is not infinite.

As the availability of the anchoring surface hydroxyl sites is closely related to the impact of the strain, tuning the silanol population by thermal treatments (i.e. variation in the dehydration temperature) instead of changing the metal loading would also allow controlling of the frustration, leading to the change in the reactivity. In fact, the activity of silica-supported chromia catalysts used in ethylene polymerization (known as industrial Phillips catalysts) goes up with increasing the activation temperature up to 1198 K where progressive dehydroxylation takes places,[26–28] which may be rationalized in terms of the increased strain of the surface chromate species.[27–30]

To investigate the influence of the anchoring geometry on the O K-edge NEXAFS feature, we modeled a highly strained di-oxo $(Si—O—)_2Mo({=}O)_2$ structure (Supporting Information; cluster **c** in Figure S3-1) anchored on a silanol pair exhibiting a Si—Si distance of 3.07 Å, which is much shorter than that of other cluster models (4.6—4.7 Å) (Supporting Information; Figure S3-1, Table S3-1). The geometric constraint results in significant modification of the O═Mo═O angle and the Mo═O bond lengths, which drastically affects the NEXAFS feature (Supporting Information; Table S3-1, Figure S3-5A). Modification of the cluster model by changing the O═Mo═O bond angle while freezing other geometric parameters results in a strong systematic change in the calculated O K-edge NEXAFS spectra (data not shown). It was found that some of the angle-modified di-oxo clusters show intense absorption at 531 eV (Supporting Information; Figure S3-5B), which may account for the increased absorption at around 531 eV observed in the experimental spectra of the high-coverage samples (Figure 3-2d). As MoO_x/SBA-15 has a distribution of species as evidenced by H_2-TPR, the observed O K-edge NEXAFS spectra are a convoluted integral of all the species present, which cannot be readily simulated by the limited number of model clusters considered here. Nevertheless, these theoretical observations suggest that an increased distortion of the tetrahedral geometry of the $(Si—O—)_2Mo(=O)_2$ units due to limitations in space on the silica surface may be the reason for the observed changes in the O K-edge NEXAFS spectra. The stronger structure sensitivity of the O K-edge NEXAFS versus UV-vis and Mo K-edge XANES may be related to the fact that the O K-edge NEXAFS probes the excitation of electrons in the isotropic (i.e. spherical) O 1s core orbitals of all the O atoms coordinated to the Mo center into the unoccupied Mo 4d—O 2p orbitals that are anisotropic.

In addition to the strain imposed by the Mo—O—Si anchoring bonds, lateral interactions between vicinal surface molybdena species come into play at higher coverage, which can influence spectroscopic features and reactivity as well. The DFT calculations clearly reveal a repulsive interaction of two adjacent tetrahedral di-oxo MoO_4 units (Supporting Information; cluster **b** in Figure S3-1). Increasing the surface density of MoO_x species may induce O—O interactions, resulting in a modification of the O═Mo═O angle or other geometric parameters. Likewise, structural perturbations due to the hydrogen bonding between surface silanol groups and surface molybdena species may also influence the reactivity. In fact, the occurrence of hydrogen bonding is clearly visible in the IR/Raman spectra where the stretching vibrations due to hydroxyl and molybdenum—oxygen exhibit a red shift when Si-OH and surface molybdena coexist (Supporting Information; Figure S3-6B,C).

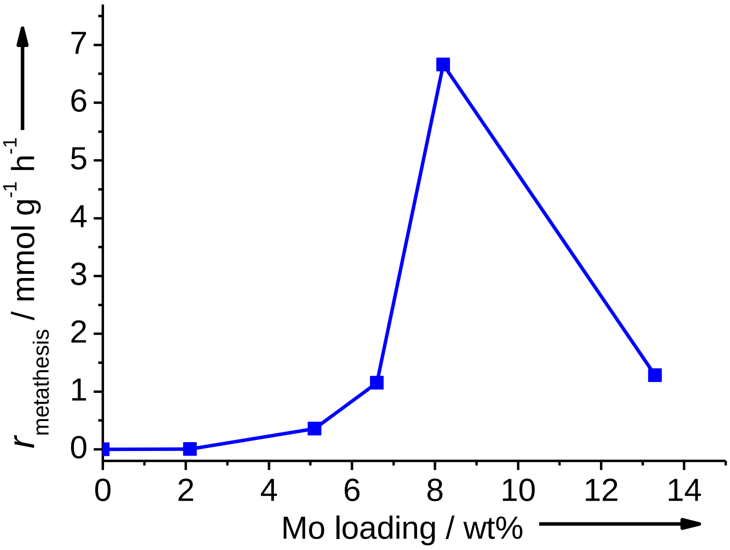

Figure 3-4. Catalytic performance of MoO_x/SBA-15. Propene metathesis at 323 K and at 15 h of time on stream. The catalysts were pretreated in 20% O_2 in Ar at 823 K for 0.5 h.

The H_2-TPR (Figure 3-1) probes the distribution of surface molybdena species and provides information on all the molybdena species present. In catalysis, it is expected that only fractional "high energy sites" formed at high coverage are reactive enough to perform catalytic turnovers at given conditions, which in detail depend on the chemistry of the catalytic reaction. Propene metathesis over MoO_x/SBA-15 uses at most only 1 % of total Mo atoms present, in which ensembles consisting of frustrated molybdena and adjacent silanol groups are required for the activity.[5,31] The steep development of the metathesis activity with increasing metal loading (Figure 3-4) is in accordance with the H_2-TPR data (Figure 3-1) that presumably represents the increased strain of the molybdena, whereas the decreased activity at the highest metal loading is due to the lack of silanol groups surrounding the strained molybdena necessary for the active sites.

As exemplified above, the frustration of surface metal oxide molecules is an important but not the sole factor in catalysis; a catalytic turn over consisting of multiple elementary reactions typically involves multiple chemical functions, rendering structure—performance relationships more complicated than in the case of H_2-TPR.

3.3 Summary and Conclusions

In summary, the remarkable increase of the reactivity of silica supported molybdena species at high Mo oxide coverage is related to an increased frustration of the surface molybdena species, which originates from geometric constraints of the anchoring bonds and additional lateral interactions of surface species. Given the similarity in the molecular structures of supported metal oxides,[14] the same scenario is likely to occur in monolayer-type oxides in general, especially for SiO_2 supports that tend to form isolated metal oxide sites.[14] Variation in the support material (e.g. alumina, titania, zirconia etc.) changes the nature of supported metal oxide species with respect to both the distribution of suitable geometric arrangements[32] and the electronic property.[33] Even given the complexity, strain-induced “high energy sites“ would locally occur at the metal-oxide—support interface whenever a distribution of the suitability of the anchoring exists, which is likely always the case.

We propose the frustration of the surface metal oxide species as an important and novel descriptor for catalysis over supported metal oxides to complement other structural classifications have been considered (e.g. degree of polymerization, coordination patterns). Based on these insights, we argue that theoretical and experimental efforts in heterogeneous catalysis should focus more on metastable configurations that are usually less acknowledged due to their instability or rareness. Furthermore, applying the mechanistic concept of the formation of “high energy sites” presented here, a rational catalyst design would be feasible by choosing strategies that artificially increase the probability of the formation of “high energy sites”, for example, the use of promoter elements or tuning the surface structure of the support by physicochemical treatments (e.g. activation temperature as in the case of Phillips catalysts).

3.4 Experimental Section

The structure of MoO_x/SBA-15 (Mo loading of 2.1~13.3 wt% / 0.2~2.5 Mo_atoms nm^{-2}) prepared by an ion-exchange approach was analyzed by vibrational (Raman, IR) and electronic (UV—vis, x-ray absorption at the O K-edge and the Mo K-edge) spectroscopy in conjunction with density functional theory (DFT) calculations. The reducibility was tested by temperature-programmed reduction with hydrogen (H_2-TPR). Prior to the spectroscopic and H_2-TPR measurements, the samples were pretreated in O_2 at 823 K for 0.5h. Details of the methods and the characterization results are summarized in the Supporting Information.

3.5 Supporting Information

3.5.1 Experimental and Theoretical Methods

3.5.1.1 Preparation of Supported MoO_x/SBA-15

To obtain highly dispersed molybdenum oxide species on mesoporous silica SBA-15, an anion exchange procedure was employed.[34] The preparation details have been described elsewhere.[5] In brief, freshly synthesized metal-free SBA-15 (internal sample ID 8233) was functionalized with propylammonium chloride using (3-aminopropyl)trimethoxysilane followed by treatment with hydrochloric acid. Then, the functionalized SBA-15 powder was stirred in an aqueous solution containing the desired amount of ammonium heptamolybdate to perform anion exchange. After washing with water and filtration, the material was dried and calcined at 823 K in air, yielding supported MoO_x/SBA-15 with the actual loadings of 2.1, 5.1, 6.6, 8.2 and 13.3 Mo% (internal sample ID 8442, 8440, 11054, 11055 and 8441, respectively). The sample labels are given in Table S3-2.

3.5.1.2 General Characterization

Nitrogen adsorption was carried out at 77 K on a Quantachrome Autosorb-6B analyzer. Prior to the measurement, the samples were outgassed in vacuum at 393 K for 16 h. The data were processed on Autosorb software (Quantachrome). The specific surface area A_s was calculated according to the multipoint Brunauer-Emmett-Teller method (BET) in the pressure range p/p_0 = 0.05-0.15 assuming a N_2 cross sectional area of 16.2 Å^2. The micropore surface area A_μ and micropore volume V_μ were estimated using the *t*-plot method in the statistical thickness t = 4.5-6.5 Å range. The total pore volume V_p was estimated by using the amount of physisorbed nitrogen at a relative pressure $P/P_0 = 0.95$. The pore size distribution was determined by NLDFT method using a model based on equilibrated adsorption of N_2 on silica assuming cylindrical pores at 77 K.

For chemical analysis, the samples and corresponding MoO_3 standards were mixed with boric acid flux (BM-0001-1, Fluxana) and fused in a Vulcan Fusion Machine (HD Electronic & Elektrotechnik GmBH) under formation of flat molten glass discs, which were analyzed by X-Ray Fluorescence spectroscopy using the spectrometer Pioneer S4 (Bruker AXS GmbH).

Powder X-ray Diffraction (XRD) analysis was performed using a STOE STADI-P transmission diffractometer equipped with Cu$K_{\alpha1}$ radiation.

The concentration of surface silanol groups of SBA-15 was determined by thermogravimetry (TG) using a Netzsch STA449 Jupiter thermoanalyzer. After the dehydration at 823 K for 1 h under argon stream, the temperature was raised with 10 K min^{-1} to 1473 K and held for 0.5 h. The concentration of surface hydroxyl groups was calculated based on the mass loss between 823 K and 1473 K assuming that one water molecule is formed by condensation of two hydroxyl groups.[35]

The morphology and local content of molybdenum was studied by scanning electron microscopy (SEM) coupled with energy-dispersive X-ray analysis (EDX) using a Hitachi S-4800 electron microscope operating at 2 kV in secondary electron (SE) mode and backscattering electron (BSE) mode.

3.5.1.3 Temperature-Programmed Reduction with Hydrogen (H_2-TPR)

Temperature-programmed reduction with hydrogen (H_2-TPR) was performed for supported MoO_x/SBA-15 in the dehydrated state using a using a quartz-made tubular gas flow reactor operating at atmospheric pressure. After the pretreatment at 823 K (heating rate 10 K·min^{-1}) for 0.5 h in a dehydrated 20 % O_2 in Ar flow, consumption of hydrogen during heating in 2 % H_2 in argon (20 ml min^{-1}, 323 to 1253 K, heating rate 10 K min^{-1}) was monitored with a quadrupole mass spectrometer (QMS200, Balzer) using argon as internal standard. The sample weight was varied to keep the amount of molybdenum at about 50 µmol.

3.5.1.4 Spectroscopy

Prior to spectroscopic measurements, unless stated, the samples were calcined in dry oxygen (20 kPa, neat or diluted with a dry inert gas) at 823 K (heating rate 10 K·min^{-1}) for 0.5 h, then cooled to room temperatures in the presence of oxygen in order to achieve the fully oxidized and dehydrated state of the catalyst (referred to as “the dehydrated state”).

UV—vis. The UV-visible (UV−vis) diffuse reflectance spectra were taken at room temperature with a PerkinElmer Lambda 650 instrument equipped with an in situ cell (Harrick Praying Mantis™ diffuse reflectance attachment DRP-P72 in combination with a HVC-VUV reaction chamber). The dehydrated SBA-15 was used as the white standard. To assure good spectral quality, the maximum value of Kubelka-Munk function F(R) was kept below 1 by diluting the sample with the SBA-15 white standard. The spectra were normalized at 4.51 eV.

Mo K-edge XAS. Mo K-edge X-ray absorption spectroscopy (XAS) was performed in transmission mode at the beam line X18B at the National Synchrotron Light Source (NSLS) at the Brookhaven National Laboratory, using ionization chamber detectors for measuring incident and transmitted beam intensities. In addition, a third ionization chamber was used to detect the beam through a reference Mo foil, for energy calibration and alignment purposes. A quartz capillary cell (I.D./O.D. = 0.8 / 1.0 mm) was used for in-situ measurements. Data processing and analysis were performed using Athena and Artemis softwares.[36]

O K-edge NEXAFS. In situ O K-edge near edge X-ray absorption fine structure spectroscopy (NEXAFS) was performed in the presence of 0.5 mbar O_2 at 623 K in the Auger electron yield mode at the synchrotron radiation facility BESSY II of the Helmholtz-Zentrum Berlin, Germany (HZB), using monochromatic radiation of the ISISS (Innovative Station for In Situ Spectroscopy) beamline as a tunable X-ray source. O K-edge spectra of the sample surface have been corrected for the remaining effects of O_2 gas phase absorption. Details of the setup, metrology and data treatment are presented elsewhere.[17,37,38]

Raman. Confocal Raman spectra were collected at room temperature using a Horiba-Jobin Ybon LabRam instrument equipped with a red laser excitation (633 nm / 1.96 eV, 1.5 mW at the sample position) and a Horiba-Jobin Ybon LabRam HR instrument equipped with a UV laser excitation (325 nm / 3.82 eV, laser power of 5 mW at the sample position). Spectral resolutions were better than 2 cm^{-1}. In situ cells (a home-made quartz cell and a Linkam CCR1000) were used to measure the dehydrated state.

FTIR. Diffuse reflectance FT infrared (IR) spectra were collected at room temperature on a Bruker IFS66 spectrometer equipped with a liquid nitrogen-cooled MCT detector at a spectral resolution of 4 cm^{-1} and accumulation of 1024 scans. An in situ cell (Harrick Praying Mantis™ diffuse reflectance attachment DRP-P72 in combination with a HVC-VUV reaction chamber) was used. KBr was used as reference material. The spectra were normalized using the silica band at 1865 cm^{-1}.

3.5.1.5 Theoretical Studies

Cluster Models. The silica-supported monomeric molybdena structures are modeled by polyhedral oligomeric silsesquioxane-based clusters.[17] The model clusters **a—c** contain tetrahedral di-oxo (Si—O—)$_2$Mo(=O)$_2$ units. Figure S3-1 shows the optimized geometric structures of the clusters.

The tetrahedral MoO$_4$ units in cluster **a** and **b** are anchored on silica to form 8-membered Mo—Si—O rings, while cluster **c** comprises a 6-membered Mo—Si—O ring. The difference between **a** and **b** is that **a** represents a di-oxo structure in the neighborhood of a silanol species, and **b** models two adjacent Mo di-oxo species.

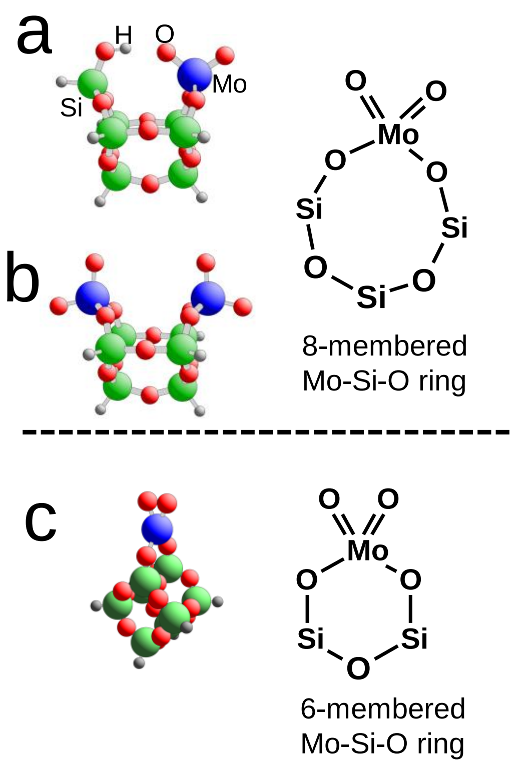

Figure S 3-1. Geometric structure of the molybdena—silica model clusters having tetrahedral di-oxo units in a stick-ball representation: (a) MO$_4$—Si$_7$O$_{10}$H$_8$, (b) (MoO$_4$)$_2$—Si$_6$O$_7$H$_6$, (c) MO$_4$—Si$_8$O$_{12}$H$_6$

Table S 3-1. Bond distances and angles in the Mo—Si—O clusters having tetrahedral di-oxo MoO$_4$ structures (Figure S3-1).

Cluster	distance (Å)			angle (°)
	Mo=O[a]	Mo—O[b]	Si—Si[c]	O=Mo=O[a]
a : MoO$_4$—Si$_7$O$_{10}$H$_8$	1.70—1.71	1.87	4.6	108.1
b : (MoO$_4$)$_2$—Si$_6$O$_7$H$_6$	1.70	1.89	4.7	107.7
c : MoO$_4$—Si$_8$O$_{12}$H$_6$	1.92—1.93	2.02	3.07	43.9

[a] terminal molybdenum—oxygen bonds, [b] at the bridging Mo—O—Si bonds, [c] the Si atoms at the two bridging Mo—O—Si bonds.

Calculations of O K-edge NEXAFS and FTIR Spectra. Theoretical O 1s X-ray absorption spectra of the model clusters were calculated by density-functional theory (DFT) using the transition potential approach and applying the StoBe cluster code.[39] Further details of NEXAFS spectra calculation are described elsewhere.[17] Theoretical IR spectra of selected clusters were calculated by DFT at BLYP level using DZP basis set employing deMon2k software.[40]

3.5.1.6 Catalytic Test

Propane Metathesis The catalytic activity for the self metathesis of propene to ethene and 2-butenes was measured using a fixed-bed tube flow reactor at atmospheric pressure. All the gases were thoroughly dehydrated and deoxygenated (except oxygen) using trapping filters. The catalysts were pressed under ~135 MPa, crushed and sieved to a particle size of 250-355 μm. Then, 100 mg of the catalyst was loaded into a U-shaped quartz reactor with an inner diameter of 4 mm. Guard beds consisting of silica gel (BET surface area = 428 m^2 g^{-1}) were placed both immediately above (100 mg) and below (50 mg) the catalyst bed in order to protect the catalyst bed from possible contamination by water. The use of the silica guard beds is essential to obtain a good catalytic performance. A blank test using bare SBA-15 with silica beds confirmed inertness of the apparatus and the guard beds. The catalyst was activated at 823 K (heating rate 10 K·min^{-1}) for 0.5 h, cooled to 323K in a 20 % O_2 in Ar (20 ml min^{-1}), and then flushed with a flow of Ar (20 ml min^{-1}) before reaction. A neat propene flow of 8 ml min^{-1} was fed to start the reaction. Inlet and outlet gases were analyzed by on-line gas chromatography using an Agilent Technologies 6890A GC system equipped with a flame ionization detector. The conversion of propene was kept below 5 % to stay in a differential regime. The selectivity to the metathesis products (ethane, cis- and trans-butene) was above 99.5 %, while trace amounts of 1-butene and higher hydrocarbons were detected. The activity is presented as formation rate of the metathesis products (i.e. sum of ethane, cis- and trans-butene) normalized by the weight of the catalyst.

3.5.2 Extended Characterization of MoO_x/SBA-15

3.5.2.1 Texture and Dispersion

The N_2 physisorption shows that the cylindrical mesoporous structure of SBA-15 (~ 7nm) prevails after introduction of MoO_x, as can be seen in the characteristic type-IV isotherms with H1-type hysteresis patterns (Figure S3-2) and derived pore diameters (d_p, in Table S3-2). Surface area (A_s) and pore volume (V_p) are significantly decreased in the Mo containing catalysts (Table S3-2) largely due to preferential filling of the micropores in the course of Mo deposition (Table S3-2).

Table S 3-2. Properties of MoO_x/SBA-15

sample name	Mo loading [a]	Surface density		A_s	A_μ [e]		V_p [g]	d_p [h]
	(wt%)	Mo [b] (nm^{-2})	SiOH [c, d] (nm^{-2})	(m^2/g)	(m^2/g)	(%)[f]	(ml/g)	(nm)
SBA-15	0	0	1.6 [c]	859	261	36	1	7.5
2.1M	2.1	0.21	1.1 [d]	637	164	31	0.79	7.1
5.1Mo	5.1	0.58	0.88[d]	554	127	28	0.71	7.1
6.6Mo	6.6	0.85	0.68 [d]	490	135	28	0.61	7.1
8.2Mo	8.2	1.13	0.51 [d]	457	147	31	0.58	7.0
13.3Mo	13.3	2.51	0.07 [d]	332	36	13	0.55	7.4

[a] by XRF, [b] Mo loading (at%) divided by A_s, [c] by TG, [d] by IR at the dehydrated state using relative heights of the silanol peak at $3745 cm^{-1}$, [e] micropore (< ~0.9 nm of width) surface estimated by *t*-plot method, [f] A_μ divided by A_S, [g] at $P/P_0 = 0.95$, [g] at the dehydrated state; [h] estimated by NLDFT approach.

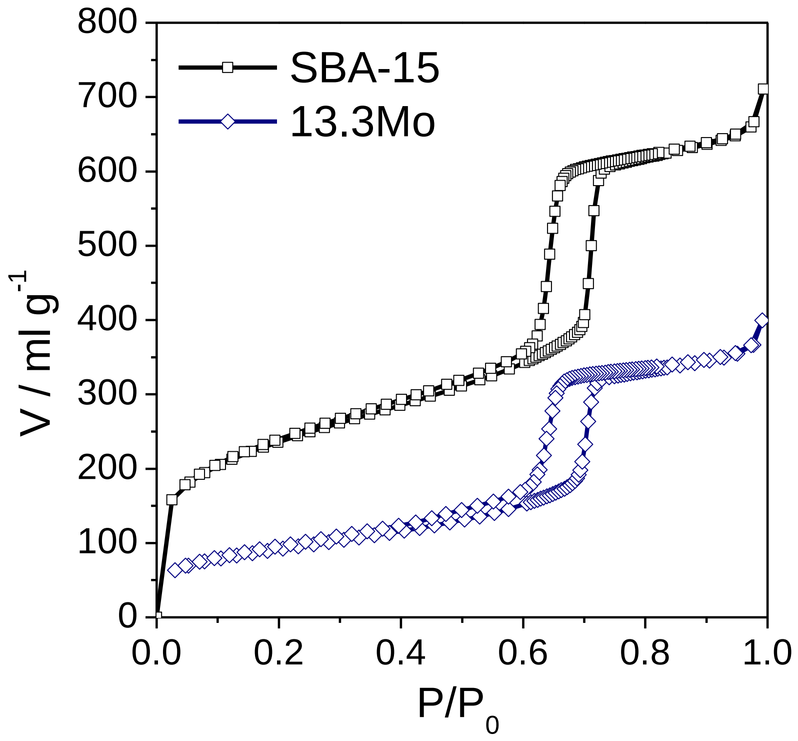

Figure S 3-2. Selected adsorption/desorption isotherms of nitrogen on supported MoO_x/SBA-15 (13.3wt%_Mo) and SBA-15 measured at 77 K. Note that all the supported MoO_x/SBA-15 samples show similar Type-IV isotherms with H1 type hysteresis patterns at P/P_0 = ~0.65.

SEM-EDX confirmed a homogeneous distribution of Mo (data not shown) except in case of the catalyst 13.3Mo. In 13.3Mo, a minor amount of plate-like particles was found in the SEM image (Figure S3-3b). These particles are identified as crystalline MoO_3 by the characteristic plate-like morphology, the local Mo content determined by EDX (ca. 60%; the theoretical content of MoO_3 is 67%), the occurrence of characteristic bands due to MoO_3 (e.g. 993, 817 and 665 cm^{-1})[41] in the Raman spectrum (Figure S3-6A) and by XRD that exhibits very weak MoO_3 reflection peaks (not shown). The regions free of crystalline MoO_3 possess a loading of 12.9±0.5 wt% Mo that is close to the overall content determined by XRF (13.3 wt%), which suggests that the vast majority (~97%, estimated by the comparison of XRF and EDX) of the supported molybdena is present as surface MoO_x species that are not detectable in the SEM images because of their non-crystalline nature. It is noted that the Raman spectrum of 13.3Mo (Figure S3-6A) shows intense bands due to crystalline MoO_3 (e.g. 993, 817 and 665 cm^{-1})[41] owing to the very high Raman scattering cross section of MoO_3.[42,43] However, the corresponding IR spectrum does not show detectable features of MoO_3 as the relative concentration of this phase is very low as revealed by SEM-EDX. Neither Raman spectroscopy nor XRD show any sign of segregated MoO_3 nanoparticles in the Mo catalysts with loadings lower than 13.3% Mo.

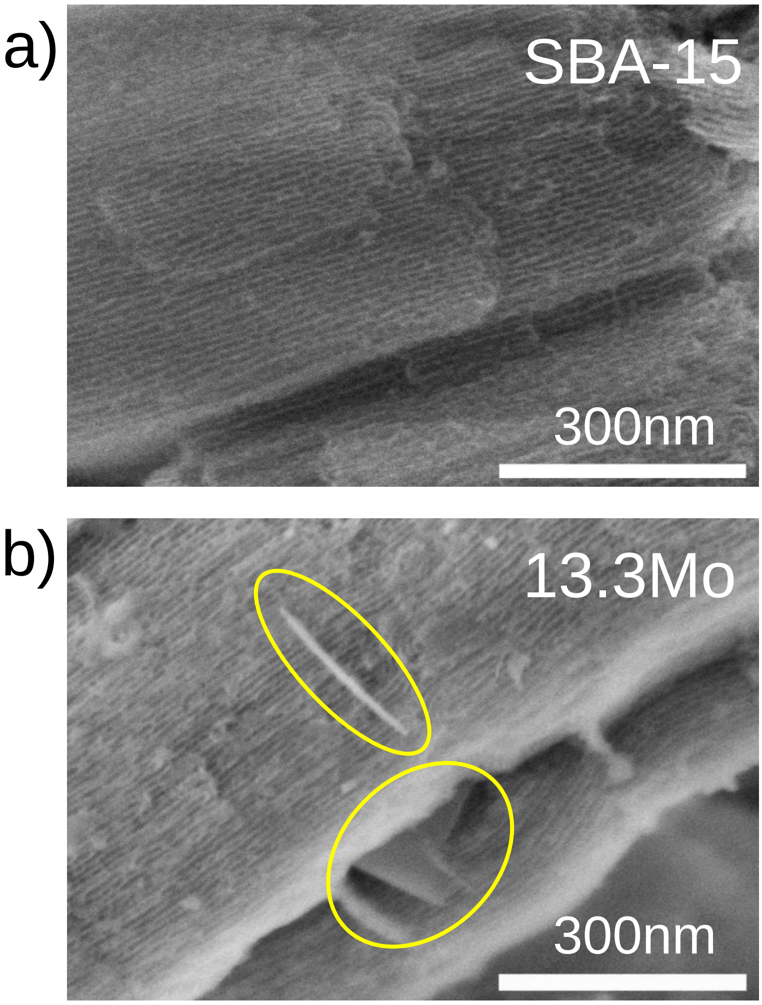
a)
SBA-15
300nm
b)
13.3Mo
300nm

Figure S 3-3. High resolution SEM images of SBA-15 (a) and 13.3Mo (b). Plate-like crystalline MoO_3 particles are highlighted by the yellow circles in (b).

3.5.2.2 Mo K-edge XAS

XANES The Mo K-edge X-ray absorption near-edge structure (XANES) spectra show a pronounced pre-edge peak at 20006 eV (Figure 3-2b) that is mainly due to the dipole transitions from Mo 1s to the p components in Mo 4d – Mo 5p hybridized orbitals, where the deviation from the perfect centrosymmetry (i.e. octahedral without distortion) governs the peak intensity.[44] MoO_3 shows a modest pre-edge intensity (Figure 3-2b) reflecting the distorted octahedral symmetry of Mo atoms.

EXAFS Figure S3-4 shows the extended X-ray absorption fine structure (EXAFS) fit for the tetrahedral-dioxo structure and the pentahedral mono-oxo structure in catalysts with different loadings. The obtained bond lengths are 1.70—1.71 and 1.91—1.92 Å (Table S3-3). Minor contributions of pentahedral mono-oxo structures cannot be excluded, because the EXAFS fit for 2.1Mo assuming a pentahedral coordination, where the coordination numbers are constrained as $N = 1$ and $N = 4$, results in similar, however, less perfect agreement with the experimental spectrum (Figure S3-4A).

Table S 3-3. Curve fit parameters for the single-scattering refinements[a] of the EXAFS spectra of the dehydrated MoO_x/SBA-15 for the tetrahedral di-oxo $(O{=})_2Mo({-}O{-}Si)_2$ model (Figure S3-5). Uncertainties in the last significant digits are given in parentheses.

Sample	path	assignment	N^b	R^c (Å)	$\sigma^{2\,d}$ (Å^2)
2.1Mo	Mo─O	Mo═O	2	1.71(2)	0.0016(15)
	Mo─O	Mo─O─Si	2	1.92(3)	0.0014(18)
8.2Mo	Mo─O	Mo═O	2	1.70(2)	0.0005(12)
	Mo─O	Mo─O─Si	2	1.91(2)	0.0007(16)
13.3Mo	Mo─O	Mo═O	2	1.71(2)	0.0011(12)
	Mo─O	Mo─O─Si	2	1.92(3)	0.0019(19)

[a] k range = 2~12 Å, R range = 1~2.09 Å, [b] coordination number, [c] distance, [d] EXAFS Debye-Waller factor.

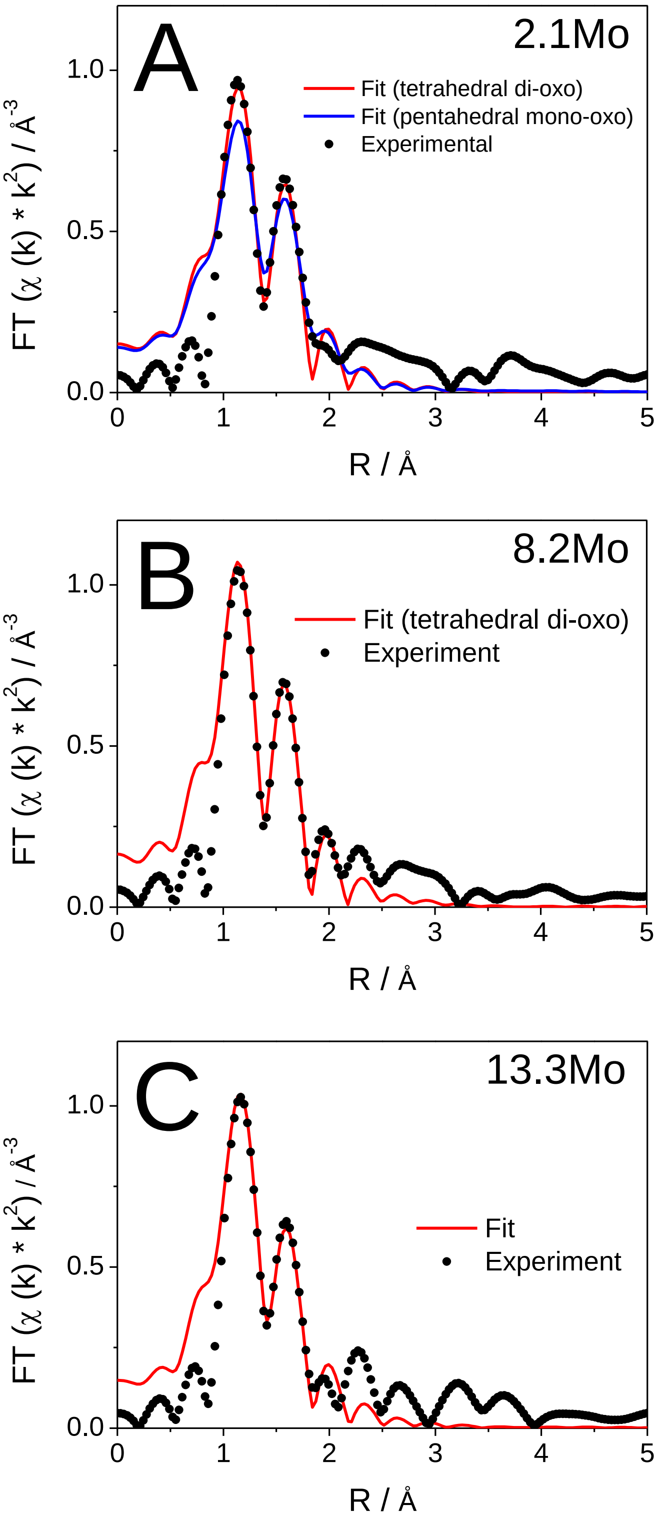

Figure S 3-4. Magnitudes of Fourier-transformed k^2-weighted Mo K-edge EXAFS spectra in non-phase-corrected *R* space for the dehydrated MoO_x/SBA-15 (dot) with curve fits to the single-scattering models for the tetrahedral-dioxo structure (red line) and the pentahedral mono-oxo structure (blue line, only for 2.1Mo): (A) 2.1Mo, (B) 8.2Mo, and (C) 13.3Mo. The fits were performed for the *R* range of 1~2.09 Å.

3.5.2.3 O K-edge NEXAFS

Theoretical O 1s excitation spectra were calculated for cluster **a**—**c** (Figure S3-1). The calculated spectra of clusters **a** and **b** that possess isolated di-oxo MoO_4 structures anchored by 8-membered molybdosiloxane rings show a distinct double-peak structure, reproducing the experimental spectra of these low-loaded samples 2.1Mo, 5.1Mo and 6.6Mo (Figure S3-5A).

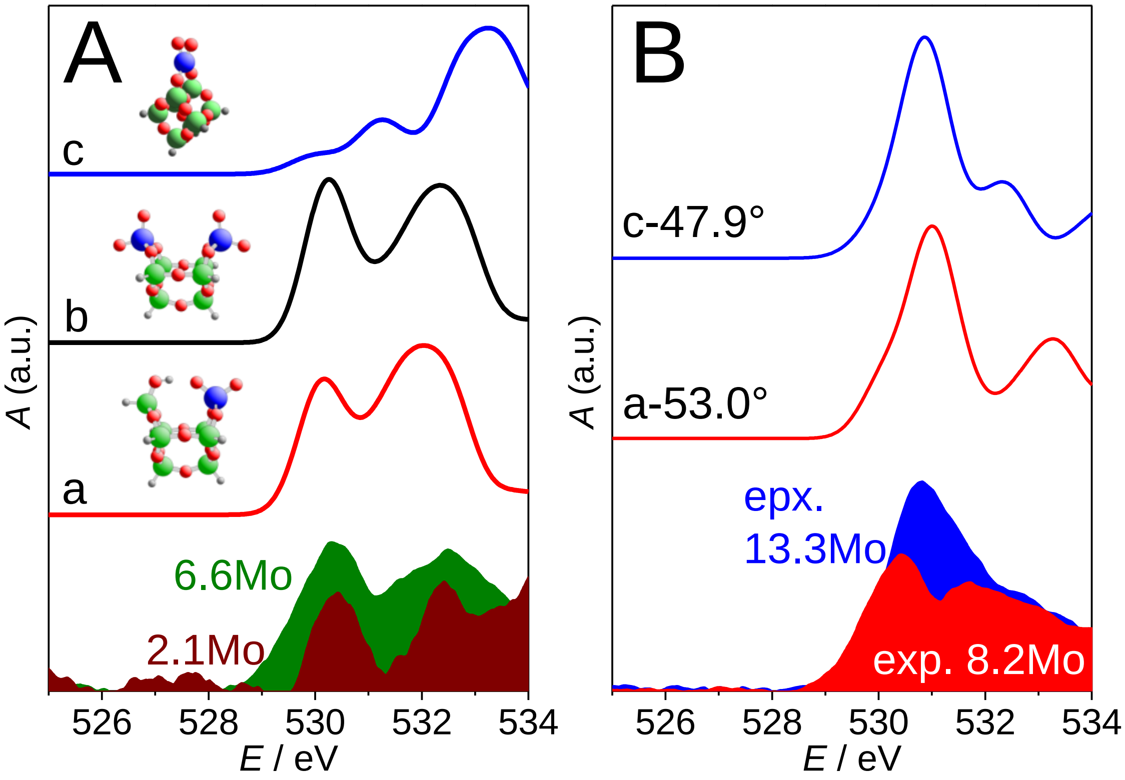

Figure S 3-5. Theoretical and experimental O K-edge NEXAFS spectra. (A) Theoretical spectra for clusters **a**—**c** and experimental spectra of 2.1Mo and 6.6Mo. (B) Experimental spectra of 8.2Mo and 13.3Mo and theoretical spectra of modified cluster **a** and **c** where the O═Mo═O angle is changed to 53 and 47.9°, respectively. The spectra are arbitrary offset and scaled for clarity. Note that the absorption due to silica above 533 eV makes a large contribution in 2.1Mo due to the high Si/Mo ratio.

The theoretical O K-edge NEXAFS spectrum of cluster **c** (Figure S3-5A) is characterized by main absorption at 533.2 eV and weaker absorption at lower energy, which is totally different from any of the experimental spectra.

The structure of clusters **a** and **c** was modified by changing the O=Mo=O angle while freezing other geometric parameters. Figure S3-5B shows the experimental spectra of 8.2Mo and 13.3Mo and the theoretical spectra of angle-modified cluster **a** and **c** where the O=Mo=O angle is changed to 53 and 47.9°, respectively.

3.5.2.4 Raman and FTIR

The IR spectra of MoO_x/SBA-15 (Figure S3-6C) show the evolution of a new and broad band at 3620 cm^{-1}, indicating the occurrence of hydrogen bonding of the Si-OH groups to the surface MoO_x species. Consistent with the change in the OH stretching, modifications of the ν(Mo=O) and ν(Mo—O—Si) bands are visible in the Raman and IR spectra. With increasing molybdenum loading, the ν_s(Mo=O) Raman band at 980—997 cm^{-1} becomes sharper and is blue-shifted (Figure S3-6B), which is also observed in IR (Figure S3-6D). The blue shift is also observed for the ν(Mo—O—Si) band at 926—943 cm^{-1} in IR (Figure S3-6D).

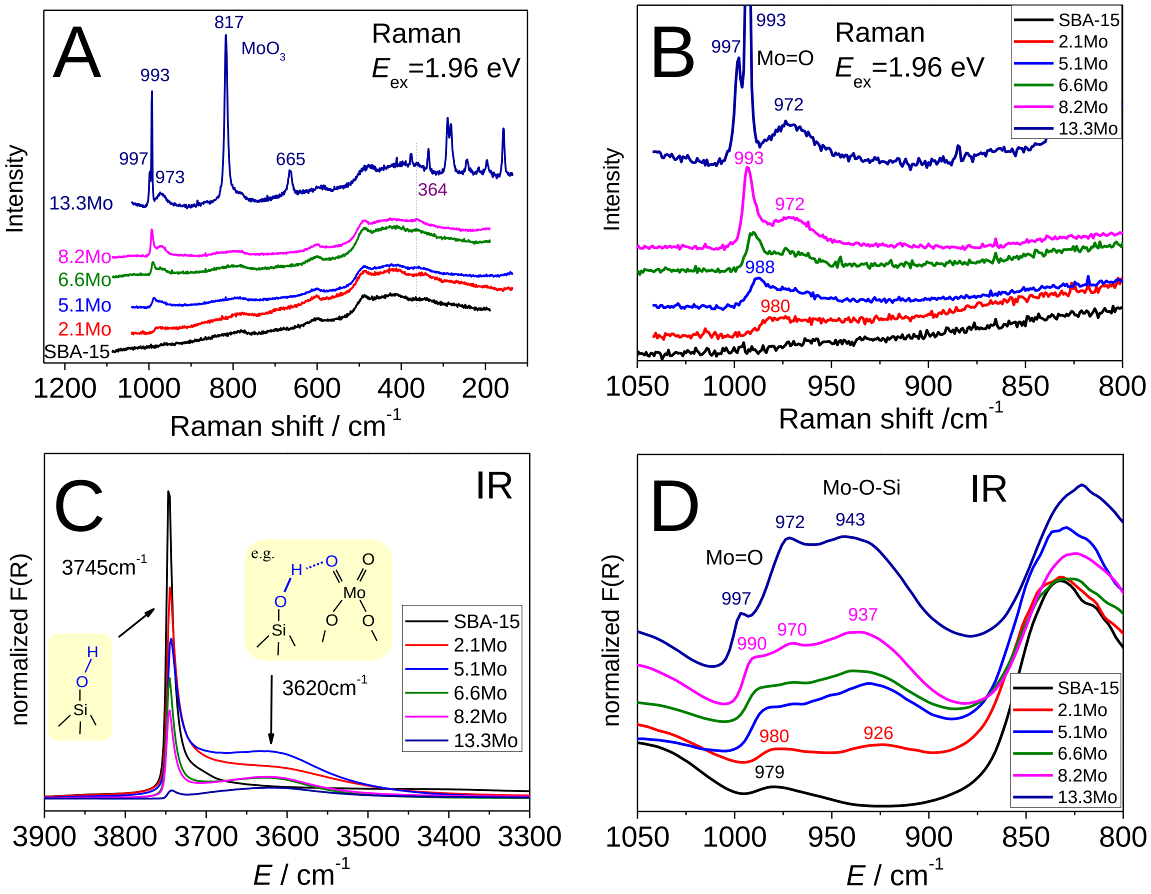

Figure S 3-6. In situ Raman and FTIR spectra of supported MoO_x/SBA-15 at the dehydrated state (pretreated in 20% O_2 at 823 K for 0.5 h) measured at room temperature: overview Raman spectra upon 1.96 eV (633 nm) excitation (A), a magnification of panel A (B), IR spectra in the OH stretching region (C), and IR spectra in the Mo=O and Mo—O—Si stretching region (D). The IR spectra were normalized by the SBA-15 intensity at 1865 cm^{-1}. The Raman spectra were vertically offset for clarity.

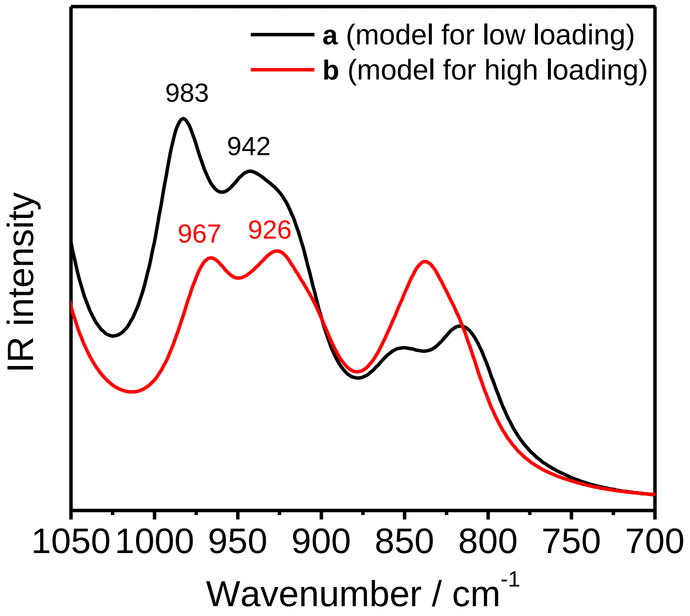

Figure S 3-7. Calculated IR spectra for clusters **a** ((Si—O—)$_2$Mo(=O)$_2$ with a Si—O—H in the vicinity) and **b** (two adjacent (Si—O—)$_2$Mo(=O)$_2$ units).

The calculated spectrum of cluster **b** (Figure 3-1) presents blue-shifted peak positions comparing to cluster **a** in the range between 900—1000 cm^{-1} (Figure S3-7), qualitatively reproducing the experimentally observed progressive blue shift along the increase of the molybdenum loading (Figure S3-6B and D).

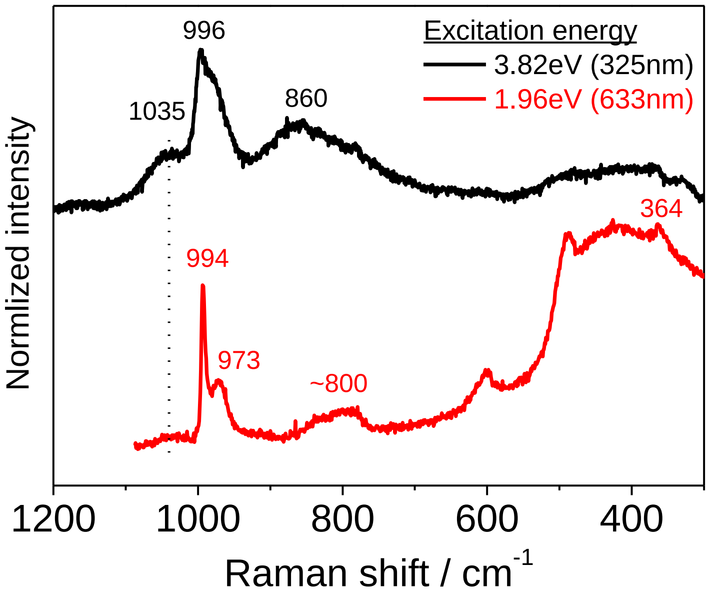

Figure S 3-8. In situ Raman spectra of the dehydrated 8.2Mo measured at room temperature using excitation energies of 3.82 and 1.96 eV. The intensity was normalized at the Mo=O band at 994—996 cm^{-1}. The spectra were vertically offset for clarity.

Figure S3-8 displays Raman spectra of 8.2Mo upon two different excitation energies. The use of the near-resonant UV excitation results in the occurrence of new bands at 1035 and ~860 cm^{-1}. These bands are not due to silica.[45] The band at 1035 cm^{-1} has been assigned to the stretching vibration of pentahedral mono-oxo O═Mo(─O─Si)$_4$ species,[13–15,46] suggesting that the pentahedral mono-oxo species in minor concentration show a strong resonance enhancement at the excitation energy used (3.82 eV). The selective enhancement of pentahedral O═Mo(─O─Si)$_4$ species over tetrahedral (Si—O—)$_2$Mo(=O)$_2$ species (bands at 994, 973 and 364 cm^{-1}) is reasonable, because the optical absorption edge energy of pentahedral species is generally higher than tetrahedral species.[47] Among the spectroscopic methods used, only the UV Raman was able to detect pentahedral mono-oxo species, strongly indicating that the relative concentration of the mono-oxo species is rather low. This observation is indeed in agreement with the recent theoretical study by Handzlik and Ogonowski in which the authors showed that a minor fraction of the surface of amorphous silica prefers the formation of the mono-oxo species besides a predominant fraction of di-oxo species.[13] The broad band at 860 cm^{-1} maybe related to Mo—O—Si (as indicated in the theoretical spectra in Figure S3-7) or Mo—O—Mo stretch[48] of minority polymeric species. The increased relative intensity of the band at ~970 cm^{-1} may be due to Mo—O—Si stretch of the mono-oxo species and/or the Si—OH vibration[45] that is enhanced at this excitation condition.

3.6 References

(1) Taylor, H. S. *Proc. R. Soc. Lond. A* **1925**, *108*, 105–111.
(2) Zambelli, T.; Wintterlin, J.; Trost, J.; Ertl, G. *Science* **1996**, *273*, 1688–1690.
(3) Behrens, M.; Studt, F.; Kasatkin, I.; Kühl, S.; Hävecker, M.; Abild-Pedersen, F.; Zander, S.; Girgsdies, F.; Kurr, P.; Kniep, B.-L.; Tovar, M.; Fischer, R. W.; Nørskov, J. K.; Schlögl, R. *Science* **2012**, *336*, 893–897.
(4) Green, I. X.; Tang, W.; Neurock, M.; Yates, J. T. *Science* **2011**, *333*, 736–739.
(5) Amakawa, K.; Wrabetz, S.; Kröhnert, J.; Tzolova-Müller, G.; Schlögl, R.; Trunschke, A. *J. Am. Chem. Soc.* **2012**, *134*, 11462–11473.
(6) Chen, K.; Bell, A. T.; Iglesia, E. *J. Catal.* **2002**, *209*, 35–42.
(7) Wachs, I. E. *Catal. Today* **2005**, *100*, 79–94.
(8) Liu, T.-C.; Forissier, M.; Coudurier, G.; Védrine, J. C. *J. Chem. Soc., Faraday Trans. 1* **1989**, *85*, 1607–1618.
(9) Thomas, R.; Moulijn, J. A. *J. Mol. Catal.* **1982**, *15*, 157–172.
(10) Lou, Y.; Wang, H.; Zhang, Q.; Wang, Y. *J. Catal.* **2007**, *247*, 245–255.
(11) Boer, M.; Dillen, A. J.; Koningsberger, D. C.; Geus, J. W.; Vuurman, M. A.; Wachs, I. E. *Catal. Lett.* **1991**, *11*, 227–239.
(12) Weber, R. S. *J. Catal.* **1995**, *151*, 470–474.
(13) Handzlik, J.; Ogonowski, J. *J. Phys. Chem. C* **2012**, *116*, 5571–5584.
(14) Lee, E. L.; Wachs, I. E. *J. Phys. Chem. C* **2007**, *111*, 14410–14425.
(15) Chempath, S.; Zhang, Y.; Bell, A. T. *J. Phys. Chem. C* **2007**, *111*, 1291–1298.
(16) Gregoriades, L. J.; Döbler, J.; Sauer, J. *J. Phys. Chem. C* **2010**, *114*, 2967–2979.
(17) Guo, C. S.; Hermann, K.; Hävecker, M.; Thielemann, J. P.; Kube, P.; Gregoriades, L. J.; Trunschke, A.; Sauer, J.; Schlögl, R. *J. Phys. Chem. C* **2011**, *115*, 15449–15458.
(18) Lichtenstein, L.; Büchner, C.; Yang, B.; Shaikhutdinov, S.; Heyde, M.; Sierka, M.; Włodarczyk, R.; Sauer, J.; Freund, H.-J. *Angew. Chem. Int. Ed.* **2012**, *51*, 404–407.
(19) Bordiga, S.; Bertarione, S.; Damin, A.; Prestipino, C.; Spoto, G.; Lamberti, C.; Zecchina, A. *J. Mol. Catal. A: Chem.* **2003**, *204–205*, 527–534.
(20) Tielens, F.; Gervais, C.; Lambert, J. F.; Mauri, F.; Costa, D. *Chem. Mater.* **2008**, *20*, 3336–3344.
(21) Banares, M. A.; Hu, H. C.; Wachs, I. E. *J. Catal.* **1994**, *150*, 407–420.
(22) Braun, S.; Appel, L. G.; Camorim, V. L.; Schmal, M. *J. Phys. Chem. B* **2000**, *104*, 6584–6590.
(23) Bronsted, J. N. *Chem. Rev.* **1928**, *5*, 231–338.
(24) Evans, M. G.; Polanyi, M. *Trans. Faraday Soc.* **1938**, *34*, 11–24.
(25) Vojvodic, A.; Calle-Vallejo, F.; Guo, W.; Wang, S.; Toftelund, A.; Studt, F.; Martínez, J. I.; Shen, J.; Man, I. C.; Rossmeisl, J.; Bligaard, T.; Nørskov, J. K.; Abild-Pedersen, F. *J. Chem. Phys.* **2011**, *134*, 244509–244509–8.
(26) Weckhuysen, B. M.; Wachs, I. E.; Schoonheydt, R. A. *Chem. Rev.* **1996**, *96*, 3327–3350.
(27) McDaniel, M. P.; Welch, M. B. *J. Catal.* **1983**, *82*, 98–109.
(28) McDaniel, M. P. In *Handbook of Heterogeneous Catalysis*; Wiley-VCH Verlag GmbH & Co. KGaA, 2008.
(29) Groppo, E.; Lamberti, C.; Bordiga, S.; Spoto, G.; Zecchina, A. *Chem. Rev.* **2005**, *105*, 115–184.
(30) Demmelmaier, C. A.; White, R. E.; Van Bokhoven, J. A.; Scott, S. L. *J. Catal.* **2009**, *262*, 44–56.
(31) Amakawa, K et al. *submitted*
(32) Tsilomelekis, G.; Boghosian, S. *Catal. Sci. Technol.* **2013**.
(33) Fievez, T.; Geerlings, P.; Weckhuysen, B. M.; De Proft, F. *ChemPhysChem* **2011**, *12*, 3281–3290.
(34) Thielemann, J. P.; Weinberg, G.; Hess, C. *ChemCatChem* **2011**, *3*, 1814–1821.
(35) Ek, S.; Root, A.; Peussa, M.; Niinistö, L. *Thermochim. Acta* **2001**, *379*, 201–212.
(36) Ravel, B.; Newville, M. *J. Synchrotron Rad.* **2005**, *12*, 537–541.

(37) Knop-Gericke, A.; Kleimenov, E.; Hävecker, M.; Blume, R.; Teschner, D.; Zafeiratos, S.; Schlögl, R.; Bukhtiyarov, V. I.; Kaichev, V. V.; Prosvirin, I. P.; Nizovskii, A. I.; Bluhm, H.; Barinov, A.; Dudin, P.; Kiskinova, M. *Adv. Catal.* **2009**, *52*, 213–272.
(38) Hävecker, M.; Cavalleri, M.; Herbert, R.; Follath, R.; Knop-Gericke, A.; Hess, C.; Hermann, K.; Schlögl, R. *Phys. Status Solidi B* **2009**, *246*, 1459–1469.
(39) Hermann, K.; Pettersson, L. G. M.; deMon developers group *StoBe software V. 3.6, 2011; see http://www.fhi-berlin.mpg.de/KHsoftware/ StoBe/*.
(40) Geudtner, G.; Calaminici, P.; Carmona-Espíndola, J.; Del Campo, J. M.; Domínguez-Soria, V. D.; Moreno, R. F.; Gamboa, G. U.; Goursot, A.; Köster, A. M.; Reveles, J. U.; Mineva, T.; Vásquez-Pérez, J. M.; Vela, A.; Zúñinga-Gutierrez, B.; Salahub, D. R. *WIREs. Comput. Mol. Sci.* **2012**, *2*, 548–555.
(41) Mestl, G.; Srinivasan, T. K. K. *Catal. Rev. Sci. Technol.* **1998**, *40*, 451.
(42) Baltrus, J. P.; Makovsky, L. E.; Stencel, J. M.; Hercules, D. M. *Anal. Chem.* **1985**, *57*, 2500–2503.
(43) Kakuta, N.; Tohji, K.; Udagawa, Y. *J. Phys. Chem.* **1988**, *92*, 2583–2587.
(44) Yamamoto, T. *X-Ray Spectrom.* **2008**, *37*, 572–584.
(45) Galeener, F. L.; Mikkelsen, J. C. *Phys. Rev. B* **1981**, *23*, 5527–5530.
(46) Lee, E. L.; Wachs, I. E. *J. Phys. Chem. C* **2008**, *112*, 6487–6498.
(47) Jarupatrakorn, J.; Coles, M. P.; Tilley, T. D. *Chem. Mater.* **2005**, *17*, 1818–1828.
(48) Xiong, G.; Li, C.; Feng, Z.; Ying, P.; Xin, Q.; Liu, J. *J. Catal.* **1999**, *186*, 234–237.

Chapter 4: Active Sites for Olefin Metathesis in Supported Molybdena Catalysts

Kazuhiko Amakawa, Jutta Kröhnert, Sabine Wrabetz, Benjamin Frank, Felix Hemmann, Christian Jäger, Robert Schlögl and Annette Trunschke

Abstract

In the propene metathesis over supported molybdenum oxides catalysts, only about 1% of total Mo atoms represent active carbene sites. In this work, the structure of relevant catalyst precursor species in molybdenum oxides supported on mesoporous silica SBA-15 (MoO_x/SBA-15) is disclosed. The surface Mo density shows great impact on the propene metathesis activity, where the highest activity was observed at an intermediate density (1.1 Mo/nm^2). Propene adsorption study by IR and microcalorimetry suggests that protonation of propene to isopropoxide species and subsequent oxidation to acetone are relevant to the genesis of the active sites, where the Mo(IV) sites formed by the reduction by propene are considered to be the precursor of the active carbene sites. The acidity characterization by ammonia adsorption, IR and ^{1}H-NMR suggests that the surface silanol groups in the vicinity of surface molybdena serve as Brønsted acid site that provide the protonation function. It is suggested that the subsequent oxidation to acetone is facilitated at the frustrated surface molybdena species exhibiting a high strain at the bridging Mo—O—Si formed at high Mo density, where the migration of the isopropoxide intermediate onto the Mo(VI) sites allows oxidation of the intermediate. The exposure of Mo(IV) sites needs the desorption of the formed acetone, which requires another silanol site in the vicinity of the molybdena site. It is proposed that the relevant catalyst precursor features a $(Si—O—)_2Mo(=O)_2$ structure exhibiting high strain at Mo—O—Si bonds surrounded by at least two adjacent silanol sites that equip the Brønsted acidity and the trapping function for by-product acetone. Applying the gained insights, a debottlenecking of the carbene generation was achieved by a methanol pretreatment procedure where the creation of Mo(IV) sites does not require Brønsted acid sites, increasing the initial metathesis activity by factor of 800.

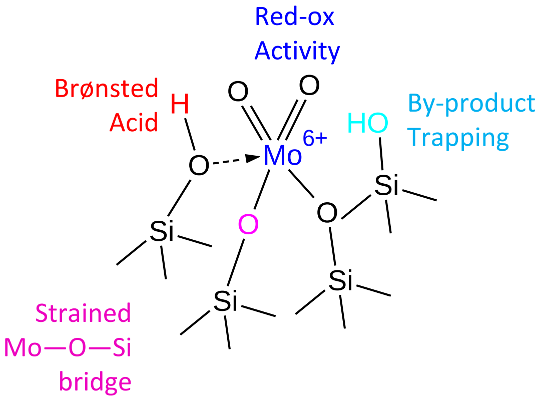

Acknowledgement

We thank M. Hashagen, G. Lorenz and A. Klein-Hoffmann for their professional assistance. P. K. Nielsen is acknowledged for providing a MoO_x/SBA-15 sample. K. Amakawa is grateful to Mitsubishi Gas Chemical Co. Inc. for a fellowship.

4.1 Introduction

C2-C4 olefins are produced over 200 million tons yearly. Propene production by cross-metathesis of ethene and butenes has become an important option to satisfy the increasing propene demand,[1] where silica-supported W oxides catalysts are currently employed at high temperature (>573 K).[2] It has been considered to substitute the W-based catalysts by more active and regenerable Mo oxides catalysts operating at mild conditions. Recent studies showed that Mo oxides supported on acidic materials (e.g. silica-alumina) give best results.[3,4]

Metal-carbene sites (M═CHR) are the active site for olefin metathesis.[5] Olefin metathesis over supported metal oxide catalysts requires in situ generation of M═CHR species through surface reactions between metal oxide species and reactant olefin itself, where only a small fraction of metal atoms (ca. 1% in supported molybdena catalysts[6,7]) represents the active sites. Recently, we proposed a mechanism of the formation of the Mo═CHR sites in supported molybdena,[7] wherein a Mo(VI) site is reduced by propene to a Mo(IV) site, which is followed by the oxidative addition of another propene molecule to yield a Mo(VI)═CHR site (as exemplified in Scheme 1a). Though the general route of the carbene generation was clarified, structural identification of the relevant surface molybdena species remains an elusive challenge, as it demands discrimination of small minority (ca. 1%) from the spectator species. Here, we analyze the structure—reactivity relationships in olefin metathesis over regenerable supported molybdena catalysts to specify the structure of the active sites.

4.2 Results and Discussion

Propene self-metathesis at 323 K over monolayer-type molybdena supported on mesoporous silica SBA-15 (MoO_x/SBA-15) was studied as a model for the desired reverse reaction (i.e. propene production). To identify the relevant pre-catalyst species that can yield active carbene (Mo═CHR), the surface Mo density was varied by changing the Mo content (Supporting Information; Table S1). The surface Mo density shows a great impact on the propene metathesis activity (Figures 4-1a and S4-1). The density of the active carbene sites (Mo═CHR) determined by post-reaction titrative ethene-d_4 metathesis[7] are at most 1% of all the surface Mo atoms (Figure 4-1a). The density of Mo═CHR sites coarsely follows the trend of the activity (Figure 4-1a), indicating that the number of the active sites is a strong factor governing the activity. Dividing the rate by the active site density yields turn over frequency (TOF; Figure 1b), which shows a significant increase with increasing the Mo density.

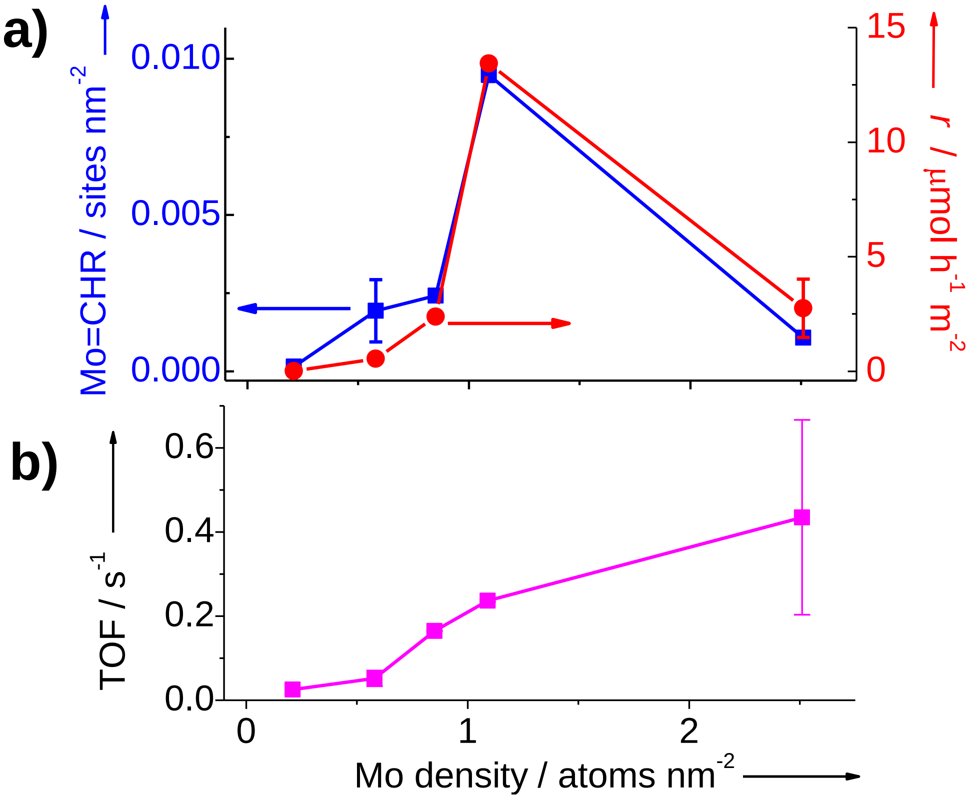

Figure 4-1. Propene metathesis performance of MoO_x/SBA-15 at 323 K and at 15~21 h of time on stream: (a) metathesis rate and active carbene site (Mo=CHR) density, (b) turn over frequency (TOF). The catalysts were pretreated in 20%O_2 at 823 K for 0.5 h. Error bars are estimated by two repeated measurements.

The Mo density affects both the probability of the active site formation and the intrinsic metathesis activity (i.e. TOF) of resulting Mo═CHR sites (Figure 4-1). To find an explanation for the variation, representative three Mo densities were compared in propene adsorption studies. Tracing the carbene generation process upon propene adsorption by in situ IR (Figure 4-2a) reveals protonation of propene to isopropoxide and subsequent oxidation to acetone, where Brønsted acidity and oxidation ability due to surface molybdena are involved (Scheme 4-1a 1 to 4). The quantity and strength of the propene adsorption sites were evaluated by microcalorimetry (Figure 4-2b), revealing a positive correlation between the density of Mo═CHR sites in the catalysis and the density as well as the strength (i.e. heat of adsorption) of propene adsorption sites (Figures 4-1a 4-2b S4-2), manifesting the involvement of these sites in the generation of the active sites.[7] The densities of Mo═CHR sites are significantly lower than that of propene adsorption sites (Figure S4-2b), suggesting that only a fraction of the adsorbed propene yields the active sites.

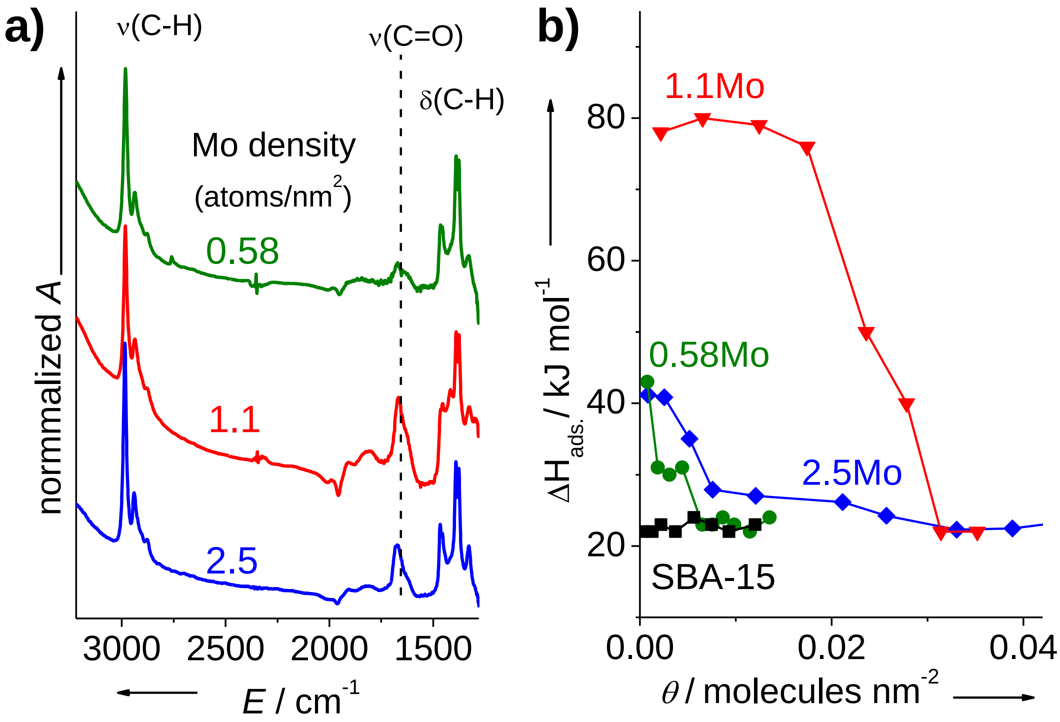

Figure 4-2. Propene adsorption onto MoO$_x$/SBA-15 at 323 K. **(a):** IR spectra collected after propene dosing at 3 hPa for 18 h and subsequent evacuation. The C—H vibrations (stretching : 2983, 2939, 2880 cm^{-1}; deformation: 1465, 1455, 1389, 1375 cm^{-1}) and ν(C═O) at 1668 cm^{-1} are assigned to isopropoxide and acetone, respectively.[7] **(b):** Differential heat of propene adsorption as a function of coverage determined by microcalorimetry. Surface Mo density (Mo_atoms nm^{-2}) is indicated close to the data.

Accordingly, Brønsted acidity and oxidation ability that transform propene to acetone are considered to be prerequisites for the carbene generation.[7]

To identify the structure of the Brønsted acid sites, hydrogen species was characterized by ^{1}H-NMR (Figure 4-3). While bare SBA-15 possesses virtually isolated silanol[8] (Figure 4-3a, 1.75 ppm) only, the loading of molybdena leads to an occurrence of hydrogen-bonded silanol groups[8] (Figure 4-3a, broad band at 2-5 ppm) and a perturbation of the isolated silanol (i.e. shift to 1.93 ppm). In agreement with these observations, the corresponding IR spectra (Figure S4-3) show a decrease of isolated silanol groups and the occurrence of a hydrogen-bonded silanol species by the Mo loading. The results are consistent with the structural analysis by Raman, IR, UV-Vis, Mo K-edge XANES/EXFAS, O K-edge NEXAFS and DFT calculations,[9] which shows the formation of two-fold anchored tetrahedral di-oxo (Si—O—)$_2$Mo(═O)$_2$ structures at the expense of surface silanol groups where a fraction of surface silanol groups are in hydrogen bonding with the molybdena species. Probing the acid sites by ammonia adsorption monitored by IR reveals a monotonous increase of both Brønsted and Lewis acid (coordinatively unsaturated Mo(VI) centers) sites with increasing the Mo density, where at most 10% of total Mo atoms serve as Brønsted acid sites (Figure 4-3b). Provided no indication for the presence of molybdenol groups by ^{1}H-NMR (Figure 3a; Mo—OH likely occurs below 1 ppm[10]) and by other spectroscopic characterization,[9] silanol sites in the vicinity of surface molybdena species are likely and only possible source of the Brønsted acid sites. Analogously to the Brønsted acid sites in silica-alumina materials,[11] the silanol sites likely become Brønsted acidic by the stabilization of the conjugated Brønsted base by the adjacent Lewis acidic Mo(VI) and by the terminal oxygen (as illustrated in Figure 4-3c). It is noted that only a fraction Brønsted acid sites can protonate propene, though the overall (i.e. including the Lewis sites) acid strength estimated by the ammonia desorption temperature (Figure S4-5) appears similar for all the catalysts. While the ammonia uptake increases monotonously with the Mo density (Figure 4-3b), the propene uptake represents at most 3% of total Mo atoms and shows a non-linear dependence to the Mo density (Figure 2b; ~0.03 C_3H_6 molecules nm^{-2} for 1.1 Mo_atoms nm^{-2}). At present, origin for the decrease of propene uptake at the highest Mo density is unclear.

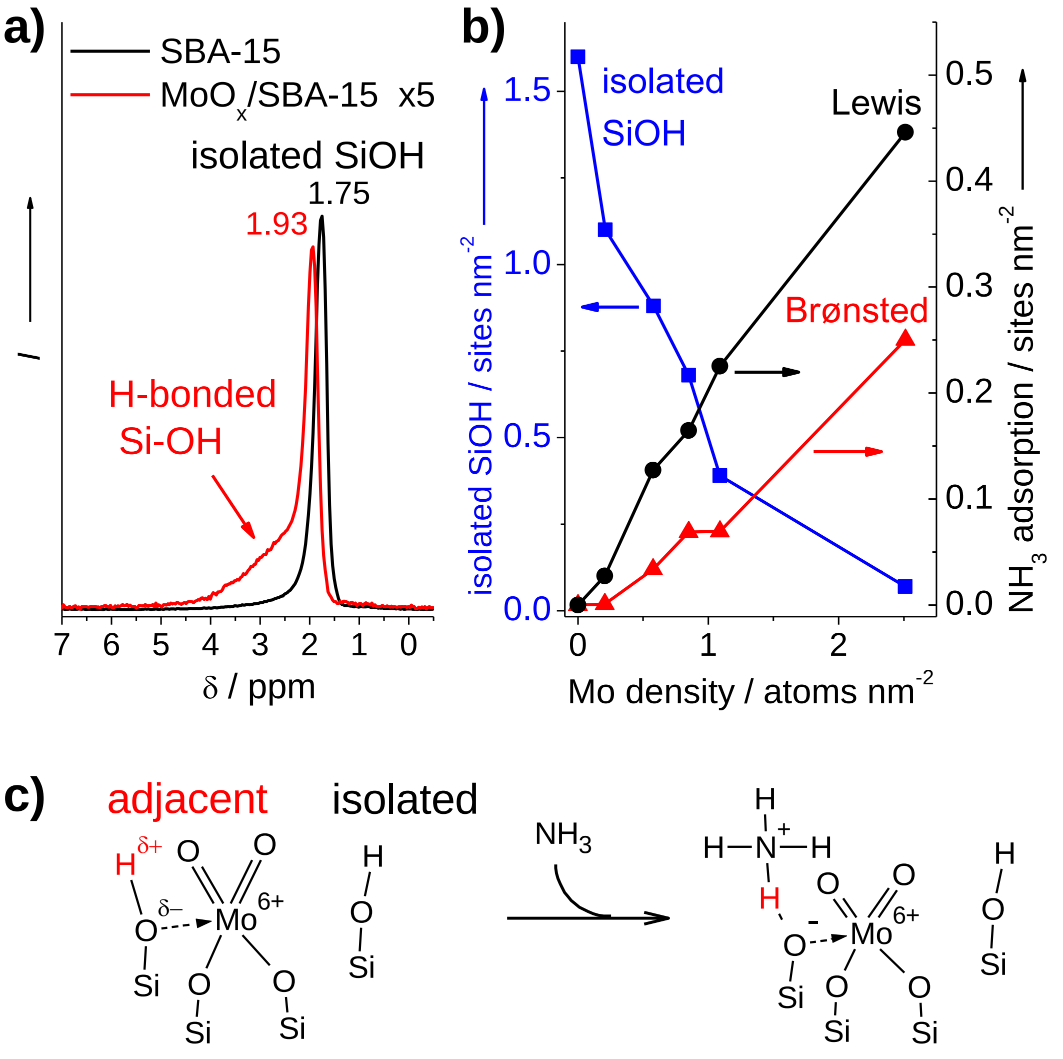

Figure 4-3. Study on acidity and hydroxyl groups in MoO$_x$/SBA-15. **(a):** ^{1}H-MAS-NMR spectra of SBA-15 and MoO$_x$/SBA-15 (1.27 Mo_atoms nm^{-2}). The spectrum of MoO$_x$/SBA-15 is magnified by factor of 5. **(b):** Density of isolated silanol and ammonia adsorption sites estimated by IR. **(c):** Schematic illustration of the suggested model for Brønsted acid sites. The IR spectra and the quantification procedure are presented in the Supporting Information (Figures S4-2 and S4-3). The catalysts were pretreated in O_2 at 823 for 0.5 h

To transform propene to acetone, the isopropoxide species formed at a Brønsted acidic silanol site needs to migrate to a Mo(VI) center that exhibits oxidation ability. Such migration of surface alkoxide species across silanol sites and molybdena sites was observed by in situ IR using isotope labeling;[12] however, its mechanism remains unclear. The IR data show an increased acetone formation at high Mo density (Figure 4-2a; ν(C═O) at 1668 cm^{-1}), suggesting a higher probability of the migration, which is in line with the increased reactivity of the surface molybdena due to the increased strain at the anchoring Mo—O—Si bonds (reported elsewhere[9]). Based on the IR observation and the structural characterization,[9] we propose that the migration involves a breaking of a Mo—O—Si bond and concurrent formation of a Si—O—Si bond (Scheme 4-1a 2 to 3), wherein a high strain at Mo—O—Si emerging at high Mo density is expected to be a key driving force of the rearrangement event.

The formed acetone needs to desorb to allow access of another propene molecule to the Mo(IV) center that leads to the formation of Mo(VI)═CHR (Scheme 4-1a 4 to 5). The desorption of acetone upon heating after the catalysis (Figure S4-6) evidences formation and preservation of acetone, suggesting a reversible capture of acetone at silanol groups[13] in the vicinity to the molybdena sites.[7] The low activity at the highest Mo density (Figure 4-1a) may be related to the low silanol density due to the extensive coverage by Mo (Figure 4-3b).

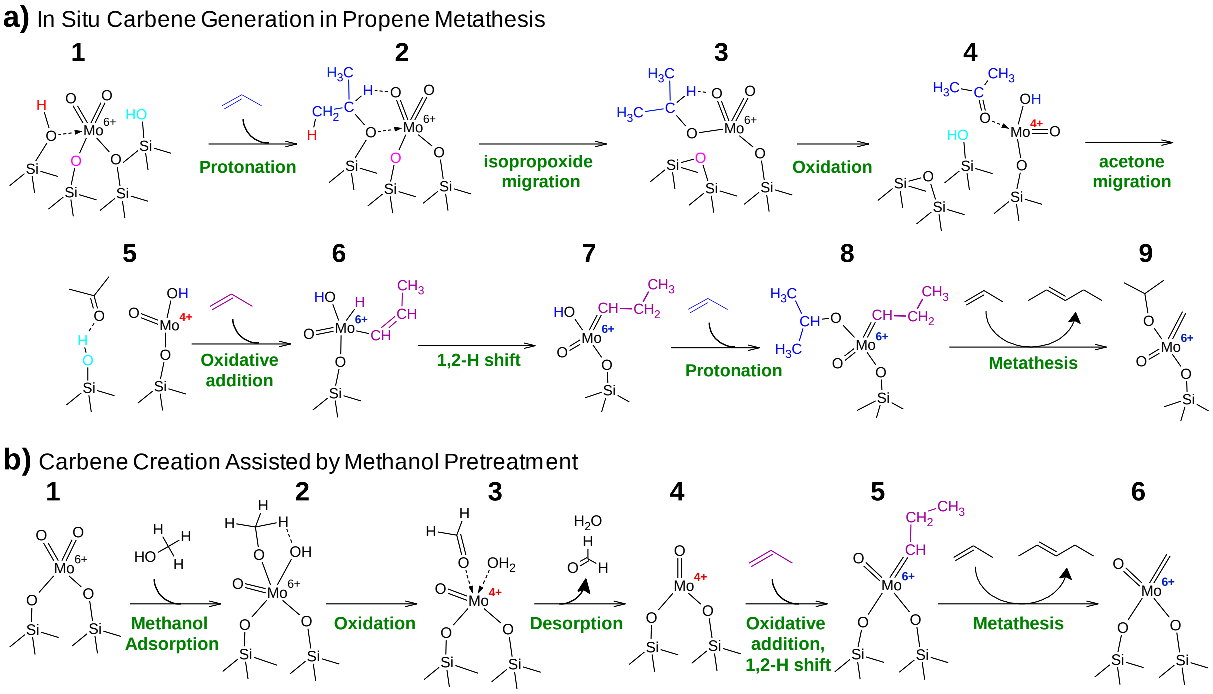
a) In Situ Carbene Generation in Propene Metathesis

b) Carbene Creation Assisted by Methanol Pretreatment

Scheme 4-1. Suggested mechanisms for the generation of a Mo(IV)—carbene site in propene metathesis: in the cases without **(a)** and with **(b)** methanol pretreatment.

Summarizing the structural assignments for the required functions for the carbene generation, a model for the catalyst precursor is envisaged. The model (Scheme 4-1a 1) is characterized by a (Si—O—)$_2$Mo(═O)$_2$ structure exhibiting high strain at Mo—O—Si bonds surrounded by at least two adjacent silanol sites that equip the Brønsted acidity and the trapping function for by-product acetone. Following the sequential reactions discussed above, a mono-anchored tetrahedral Mo(VI)—propylidene is expected to occur (Scheme 4-1a 7), which may further undergo the alkoxide formation (Scheme 4-1a 8) and transformation to Mo(VI)—methylidene by propene metathesis (Scheme 4-1a 9). The strained molybdena species occur at relatively high Mo density,[9] while it needs still adjacent silanol sites to form the active sites, which accounts for the presence of an optimum Mo density (Figure 4-1a). The low intrinsic activity at low Mo density (Figure 4-1b) may be due the increased steric hindrances by abundant silanol groups surrounding the carbene center blocking the access of propene[14] and/or subtle variation in the geometric configuration (e.g. bond lengths and angles),[15,16] as suggested by theoretical studies

Having the understanding into the mechanism of carbene generation, a debottlenecking of the active site creation is feasible. To enhance the formation of coordinatively unsaturated Mo(IV) sites, the catalyst was first treated with methanol at 523 K followed by a heat treatment in Ar at 823 K. The reduction of the abundant di-oxo $(Si—O—)_2Mo({=}O)_2$ species by methanol does not require Brønsted acidity,[17] leaving coordinatively unsaturated Mo(IV) sites after the desorption of by-products in the post-treatment in Ar (Scheme 4-1b 1 to 4). This procedure increases the initial catalytic activity by a factor of 800 (Figure 4-4). The high initial activity allows detection of the temporal formation of pentene at the initial period of the reaction (Figure 4-4 inset), which indicates the occurrence of Mo(VI)—propylidene species (Scheme 4-1b 5) thus corroborates the suggested mechanism for the carbene formation. A continuous deactivation was observed in the case of the methanol pretreatment, implying that the anticipated two-fold anchored Mo(VI)—carbene (Scheme 4-1b 6) is less stable than the mono-anchored structure (Scheme 4-1a 9). Indeed, the gradual deactivation of the two-fold anchored tetrahedral Mo(VI)—carbene was reported previously,[18] whereas mono-anchored Schrock-type Mo(VI)—alkylidene on dehydroxylated silica, which is similar to the anticipated structure in the case of the standard pretreatment (Scheme 4-1a 9), exhibit a stable activity.[19]

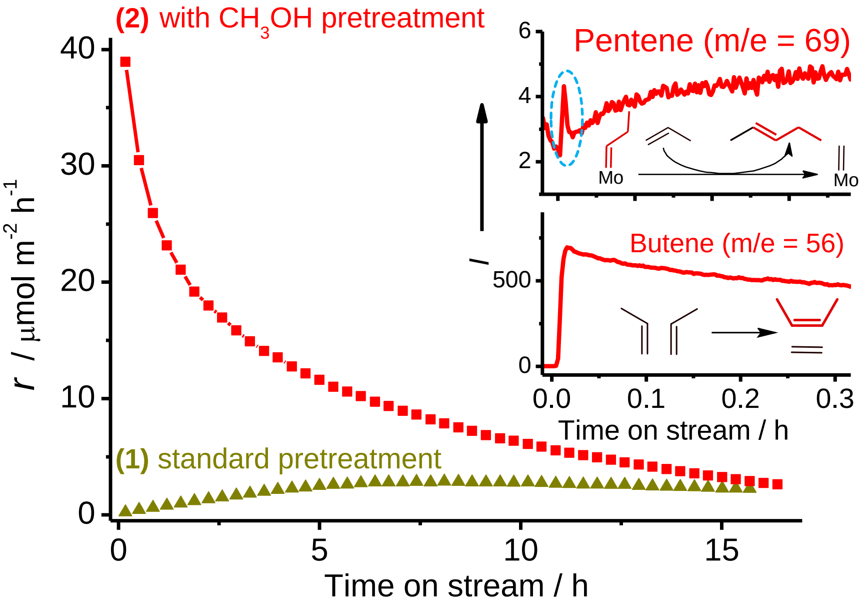

Figure 4-4. Propene metathesis activity of of MoO_x/SBA-15 (0.85 Mo_atoms nm^{-2}) after different pretreatment procedures. (1) Standard pretreatment (20% O_2, 823 K, 0.5 h). (2) Methanol pretreatment (4% CH_3OH-Ar, 523 K, 0.5h) and subsequent desorption (Ar, 823 K, 0.5h) after the standard pretreatment. The inset shows signal of mass spectrometer for m/e=69 (pentene) and m/e=56 (butenes) at initial period of the reaction with the methanol pretreatment.

4.3 Summary and Conclusion

In summary, we specified the structures of the active sites for propene metathesis in MoO_x/SBA-15 by integrating the inputs from the active site quantification, probe molecule adsorption and structural characterization. We propose that ensembles of a strained molybdena and adjacent silanol groups represent the precursor of the carbene sites. The suggested prominent roles of the adjacent silanol sites here may help understanding the beneficial effect of use of acidic supports.[3,4] The obtained insights pave the way for evolution of metathesis catalysts by rational approaches, as has been exemplified in Figure 4-4.

4.4 Experimental Section

Propene metathesis over MoO_x/SBA-15 was tested at 323 K. Adsorption of propene and ammonia was studied by IR and microcalorimetry. ^{1}H-NMR and IR were measured to investigate H species. Experimental details are summarized in the Supporting Information.

4.5 Supporting Information

4.5.1 Supplemental Figures

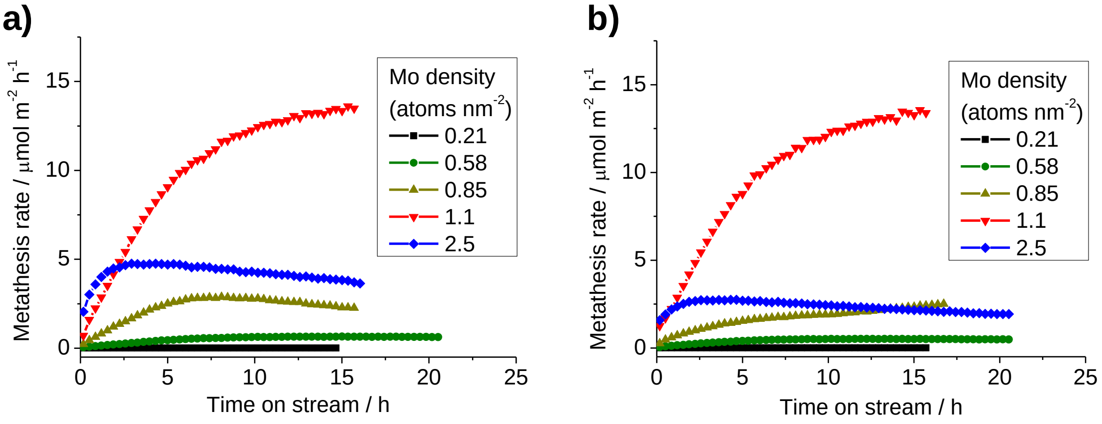

Figure S 4-1. Time trend of the propene metathesis activity of MoO_x/SBA-15 normalized by BET surface area: (a) Fresh catalysts, and (b) regenerated catalysts. Reaction conditions: T = 323 K, contact time = 0.75 s g ml^{-1}, p = 0.1 MPa, neat propene. Pretreatment or regeneration: T = 823 K, 0.5 h in 20% O_2-Ar, subsequent purge with pure Ar at 323 K.

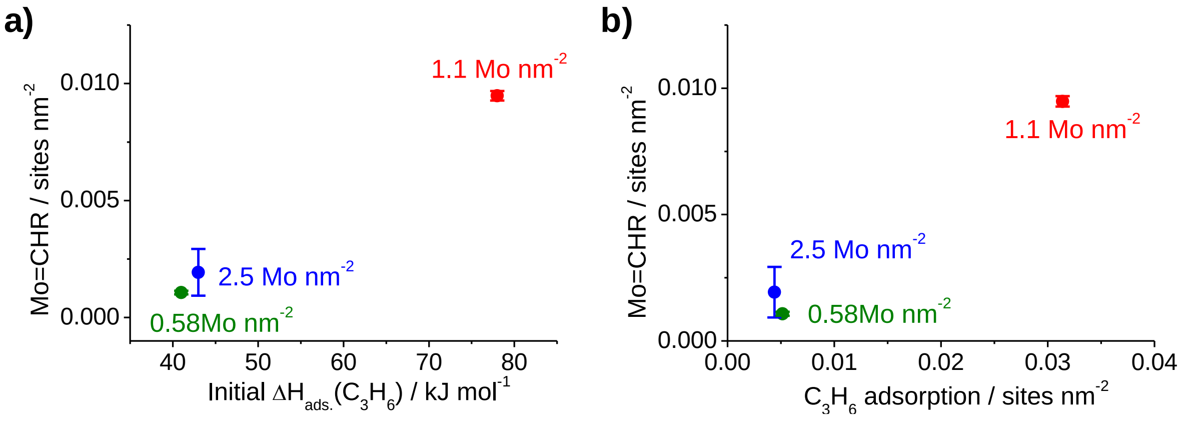

Figure S 4-2. Relationship between the propene adsorption microcalorimetry data and the density of active carbene (Mo=CHR) sites found after propene metathesis. a) Density of the Mo=CHR sites as a function of the initial heat of propene adsorption, and b) density of the Mo=CHR sites as a function of the density of propene adsorption sites exhibiting heat of adsorption higher than 30 kJ mol^{-1}. See also Figures 4-1 4-2b in the main text.

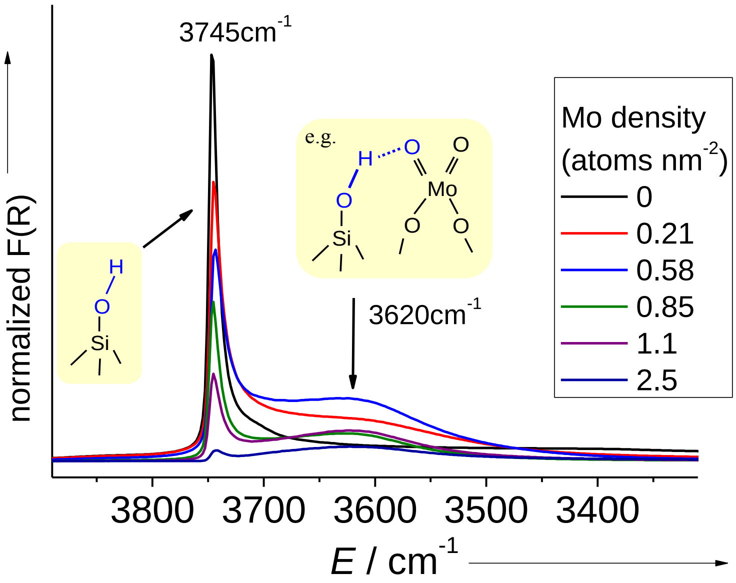

Figure S 4-3. IR spectra of MoO_x/SBA-15 measured at RT after pretreatment in 20% oxygen at 823 K for 0.5 h. The sharp band at 3745 cm^{-1} due to isolated silanol groups decrease with increasing the Mo density. The broad band due to hydrogen-bonded silanol groups occurs at 3745 cm^{-1} upon introduction of surface molybdena.

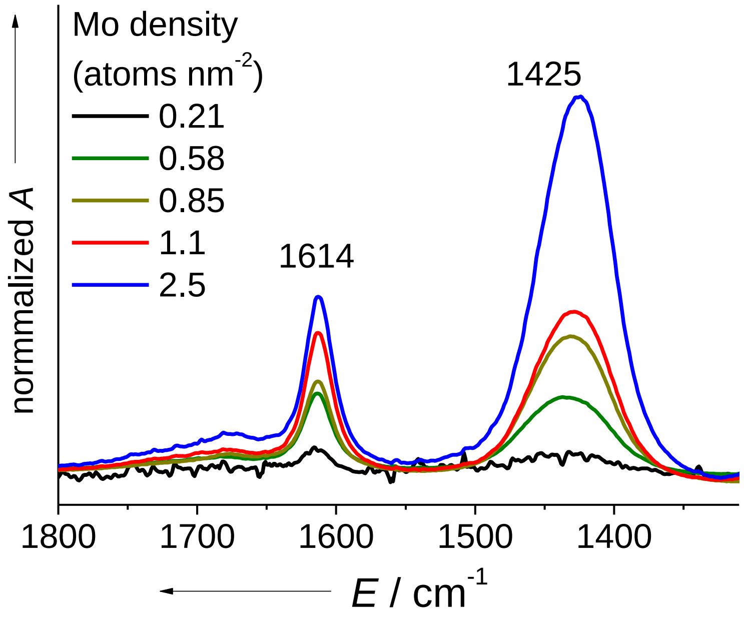

Figure S 4-4. IR spectra of MoO_x/SBA-15 recorded after ammonia dosing (7 hPa, 353 K) and subsequent evacuation for 1h. The catalysts were pretreated in O_2 at 823 K and at 20 kPa for 0.5 h. Spectra before ammonia dosing were used as reference. The catalysts were pretreated in O_2 at 823 K and at 20 kPa for 0.5 h.

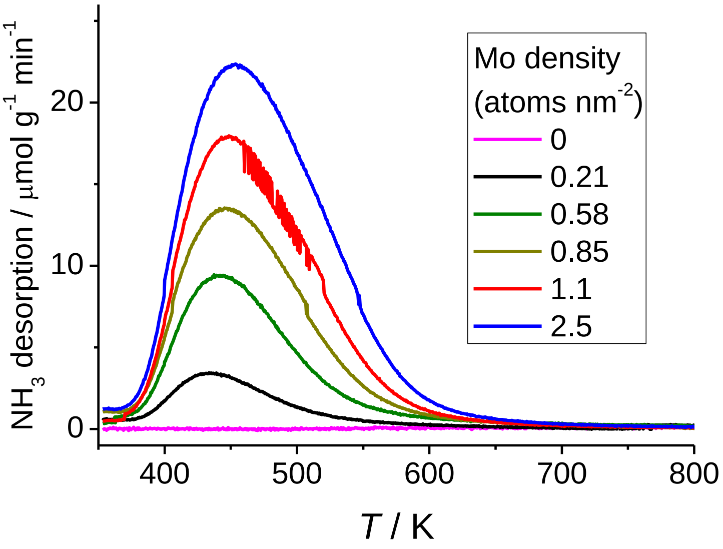

Figure S 4-5. Profiles of temperature programmed desorption of ammonia (NH_3-TPD) from MoO_x/SBA-15 at a ramp rate of 10 K min^{-1}. The similar profiles suggest no significant variation in average acid strength. The catalysts were pretreated in 20% O_2 in Ar at 823 K for 0.5 h, which was followed by ammonia adsorption at 353 K by feeding 1% NH_3 in Ar and subsequent purge in a He stream at 353 K for 0.5h.

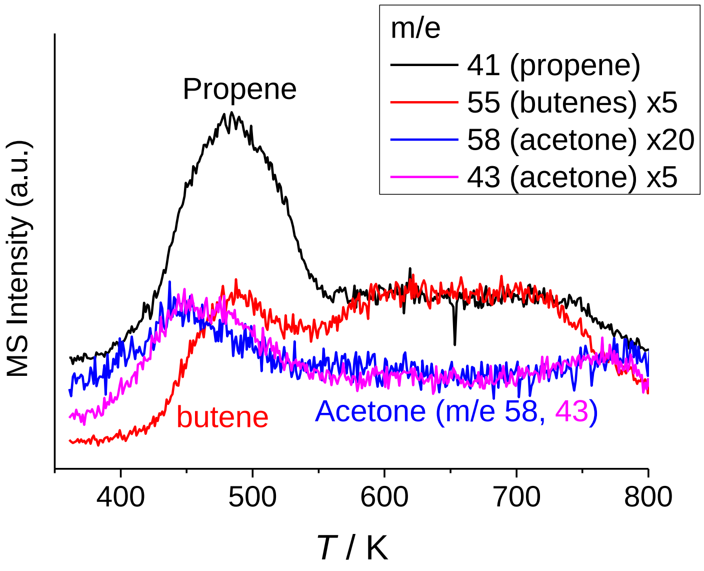

Figure S 4-6. Temperature programmed desorption (TPD) profile after propene metathesis over MoO_x/SBA-15 (1.1 Mo atoms nm^{-2}). The concurrent occurrence of m/e = 58 and 43 with an intensity ratio of approximately 1:4 indicates desorption of acetone. Besides, desorption of propene (m/e 41) and butenes (m/e 55) was observed. Metathesis reaction conditions: T = 323 K, contact time = 0.75 s g ml^{-1}, p = 0.1 MPa, neat propene, 16 h of reaction time. Pretreatment: T = 823 K, 0.5 h in 20% O_2-Ar, subsequent purge with pure Ar at 323 K. Post-reaction TPD: ramp rate of 10 K min^{-1} in Ar.

4.5.2 Experimental Details

4.5.2.1 Preparation of supported MoO_x/SBA-15

The MoO_x/SBA-15 catalysts (molybdena supported on mesoporous silica SBA-15; Mo loading 2.1~13.3 wt%) were prepared by an ion exchange protocol [20]. The details of the preparation were described elsewhere [7]. In brief, freshly synthesized metal-free SBA-15 (internal sample ID 8233) was functionalized with propylammonium chloride using (3-aminopropyl)trimethoxysilane followed by treatment with hydrochloric acid. Then, the functionalized SBA-15 powder was stirred in an aqueous solution containing desired amount of ammonium to perform anion exchange. After washing with water and filtration, the material was dried and calcined at 823 K in air, yielding supported MoO_x/SBA-15 with the actual Mo loadings of 2.1, 5.1, 6.6, 9.7 and 13.3 % (internal sample ID 8442, 8440, 11054, 8438, 8441, respectively). The properties of the catalysts are summarized in Table 1. Additionally, a SBA-15 (BET surface are = 833 m^2/g, internal ID 8261) and a MoO_x/SBA-15 (BET surface are = 532 m^2/g, 10.8 Mo%, 1.27 Mo/nm^2, internal ID 13578) were prepared using the same procedure but in different batches for the ^{1}H-NMR study.

4.5.2.2 Structural Characterization of MoO_x/SBA-15

A detailed structural characterization by N_2 physisorption, XRF, XRD, SEM-EDX, IR, Raman, UV—vis, O K-edge NEXAFS, Mo K-edge XANES/EXAFS and DFT calculations was reported elsewhere.[9] Table S1 summarizes textural property of MoO_x/SBA-15. The introduction of surface molybdena species at the expense of silanol sites while preserving the large mesopore (ca. 7 nm) of SBA-15. Decrease of micropore suggests a preferential formation of surface molybdena at micropore.

^{1}H-NMR Solid-state magic angle spinning (MAS) NMR experiments were performed on a Bruker Avance 600 spectrometer (600.2 MHz, 14.1 T) at room temperature. Measurements were run with rotor-synchronized echo detection for suppressing probe background signals using a MAS frequency of 12.5 kHz. The ^{1}H background signal of the probe was corrected by subtracting the ^{1}H MAS NMR spectrum of an empty rotor. ^{1}H chemical shifts were referenced versus TMS. The pretreated samples were transferred into an air-tight rotor in a glove box to avoid exposure to air. Approximately the same amount of sample was charged into the rotor for every experiment.

FTIR Diffuse reflectance FT infrared (IR) spectra were collected at room temperature on a Bruker IFS66 spectrometer equipped with a liquid nitrogen-cooled MCT detector at a spectral resolution of 4 cm^{-1} and accumulation of 1024 scans. An in situ cell (Harrick Praying Mantis™ diffuse reflectance attachment DRP-P72 in combination with a HVC-VUV reaction chamber) was used. KBr was used as reference material. The spectra were normalized using the silica band at 1865 cm^{-1}.

Prior to spectroscopic measurements, the samples were pretreated in dry oxygen (20 kPa, neat or diluted with a dry inert gas) at 823 K (heating rate 10 $K\cdot min^{-1}$) for 0.5 h, then cooled to room temperatures in the presence of oxygen in order to achieve the fully oxidized and dehydrated state of the catalyst.

Table S 4-1. Properties of MoO_x/SBA-15

Mo loading [a]	Surface Mo density (nm^{-2})		A_s	A_μ [e]		V_p [g]	d_p [h]
(wt%)	Mo [b] (nm^{-2})	Isolated SiOH [c, d] (nm^{-2})	(m^2/g)	(m^2/g)	(%)[f]	(ml/g)	(nm)
0	0	1.6 [c]	859	261	36	1	7.5
2.1	0.21	1.1 [d]	637	164	31	0.79	7.1
5.1	0.58	0.88[d]	554	127	28	0.71	7.1
6.6	0.85	0.68 [d]	490	135	28	0.61	7.1
9.7	1.09	0.39 [d]	556	96	21	0.78	7.2
13.3	2.51	0.07 [d]	332	36	13	0.55	7.4

[a] by XRF, [b] Mo loading (at%) divided by A_s, [c] by TG, [d] by IR at the dehydrated state using relative heights of the silanol peak at 3745cm^{-1}, [e] micropore (< ~0.9 nm of width) surface estimated by *t*-plot method, [f] A_μ divided by A_S, [g] at $P/P_0 = 0.95$, [g] at the dehydrated state; [h] estimated by NLDFT approach.

4.5.2.3 Adsorption of Probe Molecules

Prior to the adsorption, the samples were pretreated in dry oxygen (20 kPa, neat or diluted with a dry inert gas) at 823 K (heating rate 10 K·min^{-1}) for 0.5 h, then cooled to room temperatures in the presence of oxygen in order to achieve the fully oxidized and dehydrated state of the catalyst.

Microcalorimetry of Propene Adsorption Differential heats of propene adsorption were determined at 323 K using a MS70 Calvet Calorimeter (SETRAM). The calorimeter was combined with a custom-designed high vacuum and gas dosing apparatus. Propene was stepwise introduced into the initially evacuated cell ($p < 3·10^{-6}$ Pa), and the pressure evolution and the heat signal were recorded for each dosing step. Though the propene was dosed at the reaction temperature for propene metathesis, possible thermal and volumetric contribution of the metathesis reaction can be neglected owing to the thermo- and stoichiometric-neutral nature of the reaction.[7]

In situ IR for Adsorption of Propene and Ammonia Adsorption of propene and ammonia was studied by in-situ IR spectroscopy. The IR experiments were carried out in transmission mode using a Perkin Elmer 100 FTIR spectrometer equipped with a DTGS detector at a spectral resolution of 4 cm^{-1} and accumulation of 64 scans. The samples were pressed (125 MPa) into self-supporting wafers, which were placed in an in-situ IR cell. The IR cell was directly connected to a vacuum system (residual pressure of 3 10^{-6} Pa) equipped with a gas dosing line. Propene was dosed at 323 K at the pressure up to 3 hPa. Ammonia was dosed at 353 K at the pressure up to 7 hPa. In each experiment, the spectrum taken before probe dosing was used as background. Contribution of gas phase species was corrected by subtracting the spectrum without sample wafer. The spectra shown were normalized by the areal weight density of the wafer. The concentration of ammonia adsorption sites were estimated using the band at 1614 and ~1430 cm^{-1} for Lewis acid sites and Brønsted acid sites, respectively. Extinction coefficients of 16 cm μmol^{-1} (Brønsted acid sites) and 1.46 cm μmol^{-1} (Lewis acid sites) were used. [21]

4.5.2.4 Propene Metathesis and Post-reaction Active Site Counting

Propane metathesis The catalytic activity for the self metathesis of propene to ethene and 2-butenes was measured using a fixed-bed tube flow reactor at atmospheric pressure. All the gases were thoroughly dehydrated and deoxygenated (except oxygen) using trapping filters. The catalysts were pressed under ~135 MPa, crushed and sieved to a particle size of 250-355 μm. Then, 100 mg of the catalyst was loaded into a U-shaped quartz reactor with an inner diameter of 4 mm. Guard beds consisting of silica gel (BET surface area = 428 m^2 g^{-1}) were placed both immediately above (100 mg) and below (50 mg) the catalyst bed in order to protect the catalyst bed from possible contamination by water. The use of the silica guard beds is essential to obtain a good catalytic performance. A blank test using bare SBA-15 with silica beds confirmed inertness of the apparatus and the guard beds. The catalyst was activated at 823 K (heating rate 10 K·min^{-1}) for 0.5 h, cooled to 323K in a 20 % O_2 in Ar (20 ml min^{-1}), and then flushed with a flow of Ar (20 ml min^{-1}) before reaction. A neat propene flow of 8 ml min^{-1} was fed to start the reaction. Inlet and outlet gases were analyzed by on-line gas chromatography using an Agilent Technologies 6890A GC system equipped with a flame ionization detector. The conversion of propene was kept below 5 % to stay in a differential regime. The selectivity to the metathesis products (ethane, cis- and trans-butene) was above 99.5 %, while trace amounts of 1-butene and higher hydrocarbons were detected. The activity is presented as formation rate of the metathesis products (i.e. sum of ethane, cis- and trans-butene) normalized by the BET surface area of the catalyst. The catalytic test was repeated after a regeneration procedure. The regeneration procedure is the same as the initial activation (823 K (heating rate 10 K·min^{-1}) for 0.5 h and cooled to 323 K in a dehydrated 20 % O_2 in Ar, then flushed with Ar before starting the reaction).

Active Site Counting by Post-reaction Ethene-d_4 Metathesis After the metathesis reaction, the reactor was flushed with flowing Ar (20 ml min^{-1} for 10 min, then 5 ml min^{-1} for 20 min), then the feed gas was switched to 5 ml min^{-1} of 1%C_2D_4 in Ar. The formation of propene-1,1-d_2 was monitored and quantified with a quadrupole mass spectrometer (QMS200, Balzer) using the signal of m/z = 43. The formation of propene-1,1-d_2 was also confirmed by the simultaneous detection of the molecular ion (m/z = 44). The two-fold amount of the liberated amount of propene-1,1-d_2 normalized by the BET surface are of the catalyst was assumed as the active site density.

4.6 References

(1) Ding, J.; Hua, W. *Chem. Eng. Technol.* **2013**, *36*, 83–90.
(2) Mol, J. *J. Mol. Catal. A: Chem.* **2004**, *213*, 39–45.
(3) Zhu, X.; Li, X.; Xie, S.; Liu, S.; Xu, G.; Xin, W.; Huang, S.; Xu, L. *Catal Surv Asia* **2009**, *13*, 1–8.
(4) Debecker, D. P.; Stoyanova, M.; Colbeau-Justin, F.; Rodemerck, U.; Boissière, C.; Gaigneaux, E. M.; Sanchez, C. *Angew. Chem. Int. Ed.* **2012**, *51*, 2129–2131.
(5) Chauvin, Y. *Angew. Chem. Int. Ed.* **2006**, *45*, 3740–3747.
(6) Handzlik, J.; Ogonowski, J. *Catal. Lett.* **2003**, *88*, 119–122.
(7) Amakawa, K.; Wrabetz, S.; Kröhnert, J.; Tzolova-Müller, G.; Schlögl, R.; Trunschke, A. *J. Am. Chem. Soc.* **2012**, *134*, 11462–11473.
(8) Trébosc, J.; Wiench, J. W.; Huh, S.; Lin, V. S.-Y.; Pruski, M. *J. Am. Chem. Soc.* **2005**, *127*, 3057–3068.
(9) Amakawa, K et al. *submitted*.
(10) Herrera, J. E.; Kwak, J. H.; Hu, J. Z.; Wang, Y.; Peden, C. H. F. *Top. Catal.* **2006**, *39*, 245–255.
(11) Leydier, F.; Chizallet, C.; Chaumonnot, A.; Digne, M.; Soyer, E.; Quoineaud, A.-A.; Costa, D.; Raybaud, P. *J. Catal.* **2011**, *284*, 215–229.
(12) Seman, M.; Kondo, J. N.; Domen, K.; Oyama, S. T. *Chem. Lett.* **2002**, *31*, 1082–1083.
(13) Crocellà, V.; Cerrato, G.; Magnacca, G.; Morterra, C. *J. Phys. Chem. C* **2009**, *113*, 16517–16529.
(14) Cao, X.; Cheng, R.; Liu, Z.; Wang, L.; Dong, Q.; He, X.; Liu, B. *J. Mol. Catal. A: Chem.* **2010**, *321*, 50–60.
(15) Handzlik, J. *J. Phys. Chem. B* **2005**, *109*, 20794–20804.
(16) Handzlik, J. *J. Phys. Chem. C* **2007**, *111*, 9337–9348.
(17) Gregoriades, L. J.; Döbler, J.; Sauer, J. *J. Phys. Chem. C* **2010**, *114*, 2967–2979.
(18) Vikulov, K. A.; Shelimov, B. N.; Kazansky, V. B.; Mol, J. C. *J. Mol. Catal.* **1994**, *90*, 61–67.
(19) Blanc, F.; Rendon, N.; Berthoud, R.; Basset, J.-M.; Coperet, C.; Tonzetich, Z. J.; Schrock, R. R. *Dalton Trans.* **2008**, 3156–3158.
(20) Thielemann, J. P.; Weinberg, G.; Hess, C. *ChemCatChem* **2011**, *3*, 1814–1821.
(21) Matyshak, V. A.; Krylov, O. V. *Kinet. Catal.* **2002**, *43*, 391–407.

Chapter 5: Conclusion

This work contributes to the understanding in heterogeneous metathesis over silica-supported molybdena catalysts through structural identification of the active sites at a quantitative level.

The genesis of the active sites is a demanding *in situ* and *one-pot* synthesis of metal carbene species from surface metal oxides, which involves Brønsted acid-base chemistry, oxidation-reduction processes, by-product capture and oxidative addition. The multiple functional requirements account for why only ca. 1% of total Mo atoms are the active sites. The thorough structural characterization of the silica-supported molybdena provides a structural assignment for the function required in the carbene generation, rationalizing the effect of the surface Mo density. A part of the discussion remains speculative, which would be addressed in future. Nonetheless, the gained insights will indicate proper directions for catalyst improvement. We exemplified the enhancement of the catalytic performance using the simple procedures developed by rational approaches.

The mechanistic insights combined with the quantification of the active sites open the opportunity to quantitatively compare with the homogeneous metathesis catalysts, contributing to bridge the gap between homogeneous and heterogeneous catalysis.

We hope that the work serves as a worthwhile example in heterogeneous catalysis research providing an integration of a strict quantification of active sites, an elucidation of mechanism of the active site formation, a comprehensive structural characterization of catalytic materials, and applications of gained insights. We showed how to correlate the structure and catalytic performance and identify minor fraction of species that are truly relevant to the catalysis. It has been observed in a number of catalytic systems that a minor fraction of a catalyst surface may represent the active site. In this context, we hope that the present work will be of significance for heterogeneous catalysis research in general.

Appendix: List of publication

Scientific Papers

11. K. Amakawa, Y. V. Kolen'ko, A. Villa, M. Schuster, L. I. Csepei, G. Weinberg, S. Wrabetz, R. Naumann d'Alnoncourt, F. Girgsdies, L. Prati, R. Schlögl, A. Trunschke, Multifunctionality of Crystalline M1 MoV(TeNb) Oxide Catalysts in Selective Oxidation of Propane and Benzyl Alcohol,
    ACS Catal. **2013,** 3, 1103-1113
10. K. Amakawa, S. Wrabetz, J. Kröhnert, G. Tzolova-Müller, R. Schlögl, A. Trunschke, In Situ Generation of Active Sites in Olefin Metathesis,
    J. Am. Chem. Soc. **2012**, 134, 11462–11473.
9. Y. V. Kolen'ko, K. Amakawa, R. Naumann d'Alnoncourt, F. Girgsdies, G. Weinberg, R. Schlögl, A. Trunschke,
   Unusual Phase Evolution in MoVTeNb Oxide Catalysts Prepared by a Novel Acrylamide-Gelation Route,
   ChemCatChem **2012**, *4*, 495–503. (selected as **Cover Article**)
8. K. Amakawa, L. Sun, C. S. Guo, M. Hävecker, I. E. Wachs, S. Lwin, A. I. Frenkel, A. Patlolla, K. Hermann, R. Schlögl, A. Trunschke,
   Why Do Surface Metal Oxide Monolayers Become Reactive at High Coverage?,
   2013, *submitted to Angew. Chem. Int. Ed.*
7. K. Amakawa, J. Kröhnert, S. Wrabetz, F. Hemmann, C. Jäger, R. Schlögl, A. Trunschke,
   Active Sites for Olefin Metathesis in Supported Molybdena Catalysts,
   2013, *to be submitted to Angew. Chem. Int. Ed.*
6. K. Amakawa, O. Khavryuchenko, J. Kröhnert, R. Schlögl, A. Trunschke,
   Acidity of Silica-Supported Molybdena Probed by Ammonia Adsorption: Experiment and Theory,
   2013, *to be submitted to J. Phys. Chem. C*
5. R. Arrigo, M. E. Schuster, S. Abate, K. Amakawa, S. Wrabetz, D. Teschner, M. Freni, G. Centi,
   S. Perathoner, M. Hävecker, A. Knop-Gericke, R. Schlögl,
   Insight into the reactivity of the Pd species in the H_2O_2 direct synthesis and the role of the surface chemistry,
   2013, *to be submitted to ChemSusChem*
4. K. Amakawa, S. Wrabetz, J. Kröhnert, N.G. Hamilton, R. Schlögl, A. Trunschke,
   Propene Metathesis over Molybdenum Oxide Supported on Silica, Alumina and Silica-Alumina,
   2013, *in preparation*
3. K. Amakawa, I. E. Wachs, S. Lwin, R. Schlögl, A. Trunschke,
   Electronic Structure of Surface Molybdenum Oxide Species on Silica Studied by Photoluminescence, UV—vis and Multi-wavelength Raman spectroscopy,
   2013, *in preparation*
2. K. Amakawa,
   Recent progresses and future prospects of researches on copper based methanol synthesis catalysts,
   Catalysts and Catalysis (Shokubai) **2008**, 50, 384-386.

1. K. Otsuka, R. Takahashi, K. Amakawa, I. Yamanaka,
   Partial oxidation of light alkanes by NO_x in the gas phase,
   Catal. Today **1998**, 45, 23–28.

Presentations (since 2008, as principal presenter)

23rd North American Catalysis Society Meeting, Louisville, USA, **2013**
Talk: " The Active Site for Propene Metathesis in MoO_x/SBA-15”,
K. Amakawa, S. Wrabetz, J. Kröhnert, M. Hävecker, C. S. Guo, L. Sun, K. Hermann, I. E. Wachs, S. Lwin, A. I. Frenkel, A. Patlolla**,** R. Schlögl, A. Trunschke

15th International Congress on Catalysis, Munich, Germany, **2012**
Poster (selected for Poster Symposia): "Structure and Catalysis of Silica-Supported Molybdenum Oxide”,
K. Amakawa, J. Kröhnert, M. Hävecker, R. Schlögl, A. Trunschke

15th International Symposium on Relations between Homogeneous and Heterogeneous Catalysis (ISHHC-XV), Berlin, Germany, **2011**
Talk: "Origin of active sites for propene metathesis in MoO_x/SBA-15”,
K. Amakawa, S. Wrabetz, J. Kröhnert, R. Schlögl, A. Trunschke

Europacat X, Glasgow, Scotland, **2011**
Talk: "Insight into the active site of MoO_x/SBA-15 in propene metathesis”,
K. Amakawa, S. Wrabetz, J. Kröhnert, G. Tzolova-Müller, R. Schlögl, A. Trunschke

44th Annual German Catalysis Meeting, Weimar, Germany, **2011**
Poster: “In-situ Spectroscopy and Active Site Quantification on Propylene Metathesis over MoO_x/SBA-15”,
K. Amakawa, S. Wrabetz, J. Kröhnert, R. Schlögl, A. Trunschke

43th Annual German Catalysis Meeting, Weimar, Germany, **2010**
Poster: “MoO_3/SBA-15 via ion exchange and thermal spreading”,
K. Amakawa, A. Trunschke, R. Schlögl

Catalysis for Society, Krakow, Poland, 2008
Poster: "Effect of precipitation sequence on the precursor formation of Cu-Zn-Al methanol synthesis catalysts",
K. Amakawa, H. Yamada, T. Watanabe, H. Shimizu, S. Ebata, J. Yoshihara